# A torque calculation of the multi-pole permanent magnet stepping motor

Suurmeyer, B.M.

*Award date:*
1969

technische hogeschool eindhoven
afdeling der elektrotechniek - groep elektromechanica





# A torque calculation of the multi-pole permanent magnet stepping motor.

EM 69-13 B.M. Suurmeyer.

9 oktober 1969

Leader of the section elektromechanics;
Prof.dr.ir. J.G. Niesten.
Mentor: Ir. A.J.C. Bakhuizen.

Contents.

List of symbols

| | | dimension |
|---|---|---|
| $\underline{T}$ | = electromechanical torque | Nm |
| $\Theta$ | = relative position of stator to rotor in radians | |
| $\xi$ | = relative position of stator to rotor in two-dimensional model | m |
| $W'_m$ | = magnetic coenergy | joule |
| A | = surface area | $m^2$ |
| dA | = surface element | $m^2$ |
| V | = Volume | $m^3$ |
| V | = Volume element | $m^3$ |
| $\phi$ | = magnetic flux | V sec. |
| $\underline{B}$ | = magnetic induction | V sec/$m^2$ |
| $\underline{H}$ | = magnetic field strength | A/m |
| $\underline{n}$ | = normal unit vector | |
| $\underline{t}$ | = tangential unit vector | |
| $\underline{J}$ | = conduction current density | A/$m^2$ |
| $u_o$ | = permeability of vacuum | H/m |
| $\underline{M}$ | = intensity of magnetization | A/m |
| p | = number of pole-pairs | |
| I,i | = conduction current | A |
| n | = number of turns | |
| $d\underline{l}$ | = vectorial element of length | m |
| w | = tooth pitch | m |
| g | = airgap width | m |
| $b_p$ | = pole-width | m |
| R | = radius | m |
| $U,U_m$ | = scalar magnetic potential | A |
| $\varphi$ | = scalar electric potential | V |
| $\sigma$ | = normal tension | N/$m^2$ |
| $\tau$ | = shear tension | N/$m^2$ |
| $M_r$ | = value for the remanence of magnetization | A/m |
| $B_r$ | = value for the remanence of magnetic induction | V sec/$m^2$ |
| $\rho^*$ | = "magnetic charge" density | Am/$m^3$ |
| $\sigma^*$ | = "magnetic surface charge" density | Am/$m^2$ |

Summary

This work is directed to an existing industrial stepping motor, but it is sufficiently generalised to apply the results to other types.
For the calculations of the torque the field in the air-gap has been analysed, using a number of simplifications.
To check the calculations a test-machine has been designed and built.
The calculations show a fair agreement with the measurements; the existing deviations indicate a field of further investigation.

## 1. Introduction.

1.1. The present subject is one in a series of investigations on the properties of stepping-motors.
These motors can be divided in the following classes:

a) The types with a reactive rotor, usually called "variable reluctance stepping-motors"; where the slotted surfaces of the highly permeable stator and rotor makes the airgap-reluctance to depend on the rotorposition relative to the stator. Driving power is derived from this system's preference for positions of maximum field energy, due to the excitation of the stator.

b) The types with an active rotor. Here the rotor is magnetically polarised, either by a coil or by a part of it being permanently magnetised and the driving power is derived from the mutual force-action between the poles of the rotor and the excited stator.
A variety of constructions has been designed with differences in stator structure and rotor shape.

One succesful type from the second class of stepping-motors is that of Philips Gloeilampenfabrieken N.V. no. AU 5105/80.
Figure 1 shows the exploded view; figures 2 and 3 give further information. In chapter 2 there will be occasion to go into more detail about this motor.
The aim of this paper is to derive expressions or design formulae for this type of motor indicating the quasi-static torque depending on rotor position, in its relation to size, material and excitation.

1.2. There are two ways of approach, strongly interrelated, to attain expressions for torque or force between rotor and stator.

a. find the total magnetic coenergy $W_m'$ and its dependence on rotor position $\theta$. The torque follows from (L1) *

$$\underline{T} = \frac{\partial}{\partial \theta} W_m' \qquad (1.1)$$

b. evaluate "Maxwell's stresses" (L2) and make a summation for the whole surface A of the rotor (or stator)

$$\underline{T} = \frac{1}{\mu_0} \int_A \underline{r} \times \left\{ (\underline{B} \cdot \underline{n}) \underline{B} - \tfrac{1}{2} B^2 \underline{n} \right\} dA \qquad (1.2)$$

Both ways require an extensive information regarding the magnetic field in stator, rotor and airgap, possibly even also of the adjacent space.
As the configuration is rather complicated it will be necessary to have resource to a number of simplifications to obtain a workable model that allows analysis of the magnetic field, by mathematical methods.
This analysis must be based on Maxwell's equations for the magnetostatic field (L2)

$$\text{rot } \underline{H} = \underline{J} \qquad (1.3)$$

$$\text{div } \underline{B} = 0 \qquad (1.4)$$

$$\underline{B} = \mu_0 (\underline{H} + \underline{M}) \qquad (1.5)$$

These equations must be completed with relevant boundary conditions and information on the relation of $\underline{M}$ to $\underline{H}$ or $\underline{B}$.
The problem, even in its simplest form, remains such that only numerical methods employing a digital computer are able to supply adequate solutions.
The details of this method will be explained first, after which results will be submitted to a cheque with experiments.
Finally there will be comment on the results and conclusions regarding possibillities of optimalisation of this type of stepping-motor.

* (L....) refers to list of publications.

## 2. Methods of calculation.

### 2.I. Some details of stepping-motor.

From fig.1 it is easy to recognize that the motor consists of two equal parts, viz. two stators and two rotors; the latter mounted on one shaft.
Each stator carries 2p teeth alternatively connected to an inner and an outer disk.
The magnetic circuit is completed with a barrel between the two disks. The remaining space between the disks is occupied by a coil. The rotor consists of a ring of permanently magnetised ceramic material with 2p uniformly spaced poles on the cilindrical outer surface.
When the motor is assembled the two stators are mutually shifted over exactly half a circular pitch.
If excited by a coil the teeth of the highly permeable stator acquire an alternating magnetic polarity.
Fig.2 shows in more detail the structure of one stator and one rotor with p=2.
The operation of the motor will further be explained with the aid of fig.3a and 3b, they show a cross-section of the two stators, one excited and the other unexcited.

Changing of the excitation results in the rotation of the rotor, such that a new position with maximum magnetic energy is obtained.

The following commutation scheme shows the successive positions.

| stator current | | |
|---|---|---|
| left | right | rotor-position(ccw) |
| + | 0 | $0^{\circ}$ |
| 0 | + | $45^{\circ}$ |
| - | 0 | $90^{\circ}$ |
| 0 | - | $135^{\circ}$ |
| + | 0 | $180^{\circ}$ |

One complete cycle of excitations involves a rotation over half a revolution in 4 steps.
Thus one step is here equal to $\pi/4$ radians = 45 degrees.
General with 2p teeth (or poles) the

$$\text{stepangle} = \frac{360}{4xp} \text{ degrees.}$$

Some applications allow or require simultaneous excitation of both stators, in that case the following scheme applies.

| stator current | | |
|---|---|---|
| left | right | rotor-position(ccw) |
| + | + | 22.5° |
| + | - | 67.5° |
| - | - | 112.5° |
| - | + | 157.5° |
| + | + | 202.5° |

The stepangle remains unchanged.
If however, both ways are applied alternatively then the number of steps is doubled, for the stepangle then becomes $\frac{360}{4xpx2}$ degrees.
It is well to remember here that this type of stepping-motor exhibits a holding torque, even if the power source is interrupted, as the rotor will try to remain in a position of minimum energy.

## 2.2. Calculation of the quasi-static torque.

### 2.2.1. Simplified model of the stepping-motor.

The calculation requires a thorough analysis of the magnetic field, especially in the surroundings of the teeth or the rotor surface as "Maxwell's stresses" will be applied to compute the resulting force or torque.
The field analysis of the rather complicated rotor-stator assembly, if not impossible at all, leads to gigantic inconveniences; therefore a number of simplifications will be introduced.
Some of these simplifications are self-evident, others are of a more delicate nature; here they are presented in their natural sequence.

2.2.1.1. The magnetic coupling between both stators is neglected.
This is justified

- if the spatial distance between both stators is large compared to e.g. the airgap-width
- if the reluctance of the iron circuits of the stator teeth, disks and barrel is small, compared to that of the other parts of the magnetic circuit.
  In the final comment there will be occasion to scrutinize this effect in some detail.
  This simplification reduces further analysis to the field of one stator and rotor set only.

2.2.1.2. The axial length of rotor and stator is supposed to be large enough to consider the magnetic field to be independent of the axial direction.
It has to be shown that this simplification is justified

- either because the influence of end effects on the torque are neglectable compared to the "main" field torque
- or by introduction of a proper correction.

This also is a matter of examination in the final chapter.
The main problem is reduced to the analysis of a two-dimensional field, for which many a powerful method is available.

2.2.1.3. As the field is periodic on a double pole-pitch 2w it is sufficient to analyse only one such a region.(fig.4)

2.2.1.4. **The section of the annular stator-rotor system may be developed as shown in fig.5.**
This is the more justified as most motors have a considerable number of poles and the airgap g is usually small compared to the pitch w. It has the advantage of easier formulae; the difference with the real situation is neglectable.

2.2.2. The equations and boundary conditions for the magnetic field.

The simplified arrangement presents the problem to find a solution to Maxwell's equations for the magnetic field.

2.2.2.1. As there are no moving media and changing electric charges Maxwell's relations read here

$$\text{rot } \underline{H} = \underline{J} \qquad (2.1)$$

$$\text{div } \underline{B} = 0 \qquad (2.2)$$

The relation of $\underline{B}$ and $\underline{H}$ will be

$$\underline{B} = \mu_o ( \underline{H} + \underline{M} ) \qquad (2.3)$$

As everywhere in the two-dimensional array $\underline{J}$ due to free current is zero, it can be stated that

$$\underline{H} = -\text{grad } U \qquad (2.4)$$

Now it has to be realised that the coil is remote from the two-dimensional array and to evaluate its influence it is recommendable to follow one contour in the original system as shown in figure 2.
Such a line consists of 4 parts:i.e. that where it passes from a stator tooth through the airgap to the rotor, its path through the p.m. material, again the airgap to the first vicinal stator-tooth and back along the rather complex path through the stator teeth, disks and barrel.

Writing (2.1) by a line integral there applies for this contour:

$$\underset{\substack{\text{airgap}\\ \text{out-in}}}{\int \underline{H}.d\underline{l}} + \underset{\text{p.m}}{\int \underline{H}.d\underline{l}} + \underset{\substack{\text{airgap}\\ \text{in-out}}}{\int \underline{H}.d\underline{l}} = nI - \underset{\text{stator}}{\int \underline{H}.d\underline{l}} \qquad (2.5)$$

2.2.2.2. It is a realistic proposition that the excitation nI will be of a constant value; the stator material is now idealised such that in every stator stretch $\int \underline{H}.d\underline{l}$ may be considered to have a constant value such that the teeth may be attributed with a constant magnetic potential + $U_s$ respectively - $U_s$ from

$$nI - \int \underline{H}.d\underline{l} = 2U_s \qquad (2.6)$$

With saturation of parts of the stator circuit this condition becomes dubious.
This will also be a subject of discussion in a later chapter.

Some manipulation of the basic relations leads to

$$\text{div } \underline{B} = \mu_o \text{ div } (\underline{H} + \underline{M}) = 0$$

Hence it appears

$$\text{div } \underline{H} = - \text{ div } \underline{M}$$

With (2.4) it follows

$$\text{div grad } U = \text{div } \underline{M}$$

With an orthogonal coordinate system as applied in fig.5 and considering 2.2.2. wich implies $\frac{\partial U}{\partial z} = 0$ then

$$\frac{\partial^2 U}{\partial x^2} + \frac{\partial^2 U}{\partial y^2} = 0 \qquad \text{outside p.m. material} \qquad (2.7)$$

$$\frac{\partial^2 U}{\partial x^2} + \frac{\partial^2 U}{\partial y^2} = \text{div } \underline{M} \qquad \text{inside p.m. material} \qquad (2.8)$$

The solution, U(x,y), of these partial differential equations has to comply with a set of boundary conditions.

2.2.2.3. On the surface of the teeth, according to (2.6) the potential will be fixed at value $+U_s$ or $-U_s$.

This implies that a zero potential is allocated to the central or neutral spaces, such as

- the motor shaft,
- the centre of the stator circuits, i.e. the barrel at least at its centre
- the outside shielding, if it consists of ferromagnetic material.

This is of little use to the developed motor of fig.5 as the shaft would map itself at a great value of -y
In appendix A it has been shown that for a system of alternating poles U reduces to a neglectable value at distances y = 2w below and above the teeth.
Therefore it is acceptable to state the following boundary conditions

$$y = +2w \qquad U = o \qquad (2.9)$$

$$y = -2w \qquad U = o \qquad (2.10)$$

2.2.2.4. Across boundaries at which there is a change in the material the normal component of $\underline{B}$ and the tangential component of $\underline{H}$ must be continuous.
According to (I.5) the boundary conditions which must be satisfied at the interface air-ferroxdure are:

$$(H_n)_{air} = (H_n + M_n)_{ferroxdure} \qquad (2.11)$$

$$(H_t)_{air} = (H_t)_{ferroxdure} \qquad (2.12)$$

where n denotes the normal direction to the interface and t denotes the direction of the tangent at a point on the interface.

2.2.2.5. As the stator-rotor arrangement is periodic over a double pole-pitch 2w the potential function, U(x,y), must be identic for x = o and x = 2w

$$U(+o,y) = U(2w,y) \qquad (2.13)$$

on account of the symmetry in fig.5 there applies

$$U(\ o,y) = -U(+w,y) \qquad (2.14)$$

2.2.3. Calculation of the torque.

It is the most right away to decide for finding the torque on a body of Volume V from the magnetic field by "Maxwell's stresses" defined as follows.
When the surface A in (1.2 ) is wholly situated in air it is usual to suppose $\underline{B} = \mu_0 \underline{H}$.
In that case ( 1.2 ) becomes

$$\underline{T} = \mu_0 \int_A \underline{r} \times \left\{ (\underline{H} \cdot \underline{n}) \underline{H} - \tfrac{1}{2} H^2 \underline{n} \right\} dA \qquad (2.15)$$

If in every point of A the field strength $\underline{H}$ is resolved in a normal component $\underline{H}_n$ and a tangential component $\underline{H}_t$ then (2.15) passes into

$$\underline{T} = \mu_0 \int_A \underline{r} \times \left\{ \tfrac{1}{2}(H_n^2 - H_t^2) \underline{n} + H_n \underline{H}_t \right\} dA \qquad (2.16)$$

as indicated in (L3).

Each part of the surface seems to be subject to a normal tension amounting to

$$\sigma = \tfrac{1}{2} \mu_0 (H_n^2 - H_t^2) \qquad (2.17)$$

and a shear tension of

$$\tau = \mu_0 H_n H_t \qquad (2.18)$$

Referring to fig.5 it appears reasonable to decide either for the volume ABCD, (with axial length 1) or for both teeth EFGH and E'F'G'H' as the base for further calculation; only force components in x direction are of importance for the computation of the torque.

2.2.3.1. If the rotor volume ABCD is used, only the tangential forces to the planes AB and CD count. The forces on AD and BC cancel due to symmetry. To find the torque the forces should be multiplied by the appropiate distance from the shaft centre.

2.2.3.2. On the stator teeth forces in x direction are only to be found on the sides faces FG, EH, F'G' and E'H'; because with the idealized iron of the teeth the field has only normal components at the metal surface.
In this case the extension to the shaft centre has to be properly accounted for. It must be clear that here appears one of the flaws of the method of transformation to the developed motor, the torque eventually found on stator and rotor will differ, depending on the relation of R to g and to tooth height.

## 3. The magnetic properties of the rotor.

These properties depend on the characteristics of the ceramic material and on the methods of magnetization. To find U(x,y) the value of div $\underline{M}$ in (2.5) must be known, and it can be necessary to examine $\underline{M}$ as it appears in every point within the rotor material.

### 3.I. The rotor material.

The active material is the ceramic material designated as 'ferroxdure -100'; it has the typical high coercive force and remanence value of oxide magnetic materials. It is essentially isotropic. Fig.6 shows the behaviour of the B-H curve and the relevant part of the hysteresis loop as taken from the makers publication (L4).
The part OA, the virgin curve, is important for the initial magnetization only; all those parts where the field intensity $\underline{H}$ has been at least of the value A have the common demagnetization curve A-$B_r$ and, its continuation $B_r$-$H_{cB}$ (in case the intensity H becomes negative).
The most attractive property of this material is indicated by the fact that A-$H_{cB}$ is for the greater part a straight line, and that the stability is such that minor hysteresis loops coincide with this curve.
From the B-H curve with (1.5) it is possible to draw also the M-H curve.
The linear part of the demagnetization curve can be represented by

$$M_t = H_t \tan\delta + M_r \qquad (3.1)$$

Here t refers to the vector components along the direction of magnetization. Perpendicular to this direction magnetization $M_n$ can be due to magnetic field intensity $H_n$ in that direction only.

The relation between $M_n$ en $H_n$ is not known, however one can suppose that it will have the value

$$M_n = H_n \tan\delta \qquad (3.2)$$

If necessary it makes further calculations much easier and it introduces no appreciable error.

In vector notation (3.1) and (3.2) combine to

$$\underline{M} = \underline{H} \tan\delta + \underline{M}_r \qquad (3.3)$$

After some manipulation (2.8) becomes

$$\frac{\partial^2 U_2}{\partial x^2} + \frac{\partial^2 U_2}{\partial y^2} = \frac{\text{div } \underline{M}_r}{1 + \tan\delta} \qquad (3.4)$$

3.2. The process of magnetization.

For this purpose a special jig as shown in fig.7 is employed. It is shaped to fit close around the rotor material and consists of laminated soft iron.
The number of slots equals the number of poles; the wiring in the slots is such that the current passes the slots in alternating direction. Proper magnetization requires a high value of excitation, the duration is less important.
Following a simple closed curve C as shown in fig.8 the Ampère line integral reads

$$\underset{\substack{\text{air}\\ \text{out-in}}}{\int} \underline{H}.d\underline{l} + \underset{\substack{\text{p.m.-}\\ \text{material}}}{\int} \underline{H}.d\underline{l} + \underset{\substack{\text{air}\\ \text{in-out}}}{\int} \underline{H}.d\underline{l} = ni - \underset{\text{jig}}{\int} \underline{H}.d\underline{l} \qquad (3.5)$$

Here ni denotes the m.m.f. of one slot.
If the jig fits properly to the rotor ring the "air-gap" contributions to (3.5) may be neglected.

It may further be assumed that the jig has a relatively small reluctance such that, actually (3.5) reduces to

$$\int \underline{H}.d\underline{l} = \begin{cases} ni & \text{under excitation} \\ 0 & \text{afterwards} \end{cases} \qquad (3.6)$$

The field $\underline{H}$ that appears during excitation can be found by an analysis that has been dealt with in appendix B. Considering the previous assumption, the isotropicity of the material and the B-H curve it is possible to make a reasonable guess about the pattern of magnetization.
In every part where the intensity of $\underline{H}$ has been above or at the saturation value A (fig.6), the $\underline{M}$ field will have the direction of $\underline{H}$ and the value of $M_r = B_r/\mu_o$ after magnetization.
In other parts where the material not has been saturated the value of $\underline{M}_r$ is lower because of inferior hysteresis loops.

3.3. The simplification of the magnetisation of the rotor.

Figure 8[a] shows an illustration of the probable pattern of the magnetisation of the ceramic material.
The vector, tangent to the field-lines indicates the remanent magnetisation.
The magnetic potential problem ressembles that of a static electric field; therefore it is usual to understand the sources of the magnetic field as the magnetic analoque of "bounded charge".
According to 2.2.2.2. the sources of the $\underline{H}$-field are opposite to the sources of the $\underline{M}$-field defined as

$$\operatorname{div} \underline{M} = \lim_{\Delta V \to 0} \frac{\int (\underline{M}.\underline{n})dA}{\Delta V} \qquad (3.7)$$

see L2 page 4 .

Thus for points inside the rotor material this leads to the introduction of "magnetic charge" density

$$\rho^* = -\nabla.\underline{M} \qquad (3.8)$$

and for points on the rotor surface the "magnetic surface charge" density

$$\sigma^* = \underline{M}.\underline{n} \qquad (3.9)$$

With a volume $\Delta V_1$, situated at the outside face of the rotor the sources are easily found if one can suppose that the material that was adjacent to the jig has been completely saturated during the process of magnetisation. It is reasonable to suppose that this is the case and the further calculation will be based on this assumption. As the iron jig even then is far from saturation, the field vector is perpendicular to the surface everywhere under the jig, except very close to the corners.
The "magnetic surface charge" density $\sigma^*$ is than according to (3.9)

$$\sigma^* = \pm M$$

A volume $\Delta V_2$ inside the material will in general also show a certain quantity of "magnetic charge" density $\rho^*$. In a first approximation of the torque calculation these contributions are ignored, whether this simplification is allowed is a subject of later discussion.
Appendix B gives a way to calculate the inside source-density, to be used for more complete calculations.
The rather complicated source distribution is with this simplification reduced to the simple surface-charge as shown in figure $8^b$ and 9.

The inner surface of the rotor-ring may be considered as not magnetised as the field intensity has been there verly low, any surface charge, if existent, may be disregarded.
The calculation of the magnetic field, in the air-gap-space, becomes now rather easy as everywhere the equation of Laplace holds,

$$\Delta U = 0 .$$

The rotor-surface is now a boundary where according to 2.2.2.4. the following conditions are to be fullfilled:

$$\frac{\partial U}{\partial n_{(air)}} = \frac{\partial U}{\partial n_{(ferroxdure)}} + \sigma^* \qquad (3.10)$$

$$\frac{\partial U}{\partial t_{(air)}} = \frac{\partial U}{\partial t_{(ferroxdure)}} \qquad (3.11)$$

Assuming that at those parts of the rotor that were not in touch with the jig no surface charge exists, the same boundary conditions remain but with $\sigma^* = 0$.
It has to be realised that $\sigma^*$ is not a constant value but depends on the field-intensity in the material; this $\sigma^*$ can be found from the demagnetisation-curve, see the graph in fig.10.

## 4. Measurements.

The results of the analysis and calculation of chapter 2 and 3 are to be compared to the measured torque of a real stator-rotor combination. A test-machine was built so that all required measuring facilities are available; its main features are given in the next section.

### 4.I. The test machine.

The machine ought only to have the same properties as one stator-rotor set of a real stepping-motor of the type under consideration, on the other hand it has to be provided with the possibility to take readings in more extreme circumstances than the real motor does work, e.g. with over-excitation of the stator coil.
The construction differs therefore clearly from the industrial type as may be conceived from the cross-section, see figure 11.
Its outer appearance is dominated by the facilities for positioning the rotor and those for the measurement of torque and position, see figure 12.

#### 4.I.I. The rotor.

The rotor has the annular shape and is magnetised in such a way that it has 8 poles on its outer cylindrical surface; this is the so called laterally magnetisation as it is mentioned in the technical data sheet of the makers, see fig.4. From the available range of rings the biggest one was choosen in order to obtain as great as possible independance from inaccuracies of, e.g. stator-bore, excentricity, and further imperfections of work and also to bring about as large as possible a torque, which has advantages that need no explanation.
The magnetic body is clamped on a brass jacket between a set of nylon disks by a nut; the jacket is fixed to a brass shaft.

The shaft is carried by a set of ball-bearings, these are fitted in two aluminum shields.

4.1.2. The stator.

The stator consists of two equal parts; the material is Armco-iron, a high-grade ferro-magnetic material.
Each part has a cylindrical shape see fig.13.
In the inside-leg is worked out a set of teeth, the outside-leg has provisions to fit the two parts together, assuring a proper positioning.
When fitted together the stator takes the coil in its inside, that, if excited provides for a magnetic field that shows alternating poles at the system of teeth.
The magnetic circuit is closed, on one side through the outside jacket of the stator body, and on the other side through the teeth, air-gap and rotor material, disregarding the leakage fields.
The stator is accurately fitted in the two shields; locked against rotation and held together by a set of bolts through the shields. The coil has 1000 windings of copper-wire of 1 mm. dia, for a short duration a current of 5 amps is allowable.

4.I.3. The positioning of the rotor.

On fig.14 one recognizes at the front shaft-end a body of annular shape provided with two radial arms.
One of them carries a segment; it serves as a guide for a string that carries the movable element of a position-transducer. The other arm is caught between two set-screws, these screws belong to a frame that can move concentrically with the shaft.
The movement of this frame is brought about by a hand-wheel with reduction-gear.
The set-screws are fastened so that the rotor is held in a position without play; care is taken to prevent undue stress to the steel arm.

4.I.4. The measurement of the torque.

On the arm caught between the set-screws there are glued two straingauges, connected to an appropriate instrument that provides for a reading of the bending torque in the arm; this torque is direct proportional to the force that the rotor applies to the positioning device, it is therefore a measure for the electromagnetic torque, assuming bearing friction may be ignored.
The scaling factor of the gauge-strain bridge is shown in fig.15.
The strain-gauge bridge also supplies the input signal for the X - Y recorder if torque-to-position curves are to be drawn.

4.I.5. Determination of the magnetic flux.

There are some arrangements to find the magnetic flux through certain parts of the stator circuit. This is necessary to calculate $\int \underline{H}.d\underline{l}$ in the iron parts of the stator, see appendix D.
To establish the proper magnetic potential on the surface of the teeth the m.m.f. of the coil has to be reduced by said amount.
One tooth of the stator carries a small coil and the excitation coil has some additional windings; both are suitable for connection to a flux-meter. When the excitation current is commutated the flux-meter reads the flux that is linked with the transducer-coils.
Also the course of the flux during the (slow) rotation of the rotor is registered as a function of the rotor-position by integrating the e.m.f. excited in the coils.
The movement is sufficiently slow to prevent errors due to eddy-currents.

4.I.6. The induction in the air-gap.

The induction in the air-gap, midway of a tooth is measured by a set of Hall-probes.
These are glued to the inside surface of the teeth.
The probes were beforehand checked against readings of a Gauss-meter.
To obtain information about the original magnetisation of the rotor-ring, a special iron jacket was made that replaces the stator. This jacket encompasses the rotor completely so that it can develop its own field within a constant air-gap and the very low reluctance of the jacket.(fig.26.)
With a Hall-probe it is easy to read the flux distribution, which gives important information about the distribution of the magnetisation, more in particular about the surface value of $\underline{M}$.

Baran (L5) analysed the field of permanent magnetisation by introduction of a bounded surface charge density $\sigma^*$ only.
He found satisfactory results in comparing his analysis to the real field.
From the readings of the Hall-probe, brought in connection with Baran's theory it must be possible to obtain proper information of the $\underline{M}$ distribution on the rotor surface, the intensity as well as the width of the "poles" are of utmost importance for the calculation of the torque.

4.2. Results of measurements.

With an x-y recorder there are drawn several torque-to-position curves for the two stator-rotor combinations viz. g/w= 0.05 and g/w=0.025, shown in the figures 16, 17, 18 and 19, the parameter is the current through the stator-coil.
As expected, the torque increases slightly with decreasing g/w; further it is clear that the maximum torque due to excitation only, is nearly proportional to the stator-current up to about 2 amps.

It may be an indication that the influence of saturation of the teeth is neglectable till 2 amps.
The flux through a tooth as well as the flux through the stator-body are measured, see fig.20, and show a fair agreement.
Above the value of 2 amps the iron of the stator becomes saturated; from then on there appears a considerable amount of leakage flux.
Further when the stator current becomes still higher, a part of the magnetisation is destroyed due to the extremely high field-strength.
In fig.21 and 22 two curves are drawn, that show the induction under a tooth. One of the curves fig.21 is drawn before the recording of the torque-to-positions curves the other after that. Qualitatively it may be considered as a good indication for the deterioration of the remanent magnetisation.
It clearly sets a limit to the admissable stator current.

## 5. Comments on the calculations and measurements.

### 5.1. The torque-calculation; test-run of the computer-programme.

The torque is calculated by solving the differential equations for the magnetic field with a numerical method, that makes use of finite-difference equations.
More details about this method are given in Appendix C.
For a restricted number of positions varying from $\xi = 0$ till $\xi = w$ the force between rotor and the teeth is calculated.
This provides a good knowledge about the behaviour of the torque of the stepping-motor for different rotor-positions.
In this way there are enough data on hand to compare the calculated torque to the measured torque; on the other hand it leads to a number of calculations that does not demand much computer-time.
The dimensions applied to the mathematical model are taken from the test-machine; the parameter is the fixed potential of the teeth $+U_s$ respectively $-U_s$.
It is clear that there is another parameter that must have influence on the force viz. the ratio between pole-width $b_p$ and tooth-pitch w, as well as the intensity of magnetisation M.
As the dimensions of the magnetizing jig are not known, the pole-width of the magnetisation $b_p$ has to be guessed; later an improved method will be considered.
With the guessed value of $b_p/w = 0{,}5$ the Algol-programme has been tested.
The forces calculated on a ELX8 of the mathematical department of the T.H. in Eindhoven are shown in graphical form for a stator-rotor combination with $g/w = 0.05$ in fig. 23 .
These results are a force per double pole-pitch per unit-length in the axial direction. To compare these figures to the real torque they must be multiplied by

a) the number of pole-pairs
b) the outside radius of the rotor
c) the axial length of the annular rotor.

of the test machine.

Especially because of the finite axial length an error can be introduced, for the magnetic field has axial components too on the edges of the annular rotor.
In accordance with the relevant conclusions in (LB1) these effects are neglected.
The curves of figure 23 show that the force (or torque) can be considered as the sum of two components,

a) the reluctance-torque by the permanent magnetisation

b) the torque by the polarised teeth.

for in the case with the permanent magnetised rotor it can be stated that (1.1.) must be rewritten by

$$T = \frac{\partial}{\partial\theta}\int_0^i \Phi \, di \quad - \quad \frac{d}{d\theta} W_{m_o}$$

with $\Phi = \Phi_o(\theta) + \Phi_c(i)$
and $W_{m_o}$ the magnetic field energy if i = 0. (26)
Here $\Phi_o$ is the magnetic flux due to the permanent magnetised annular rotor and $\Phi_c(i)$ that caused by the stator current i.
Hence

$$T = \underbrace{i\frac{\partial\Phi_o}{\partial\theta}}_{b} \quad - \quad \underbrace{\frac{d}{d\theta} W_{m_o}}_{a}$$

The component called under b) increases proportional to the value of $U_s$ which is apart from the saturation in the stator proportional to the stator-current i. This is born out by the calculations as may be seen from the curves of fig. 24.
These results are now to be compared to measurements.

5.2. Comparison with measurements.

Fig. 25 shows again the recorded torque-to-position curves of a real sator-rotor combination with g/w 0.05; in the same figure there are drawn the curves of the calculated torque with $b_p/w$= 0.5.
Assuming the material of the stator idealised it is allowed to transform the magnetic potentia $U_s$ of the teeth to the stator-current
with

$$U_s = \frac{ni}{2}$$

There is quite a difference between the calculated and measured curves; especially concerning their form. Even with i =0 the difference is such that it is reasonable to conclude that the ratio $b_p/w$= 0.5 is not the proper value to manifest the magnetisation in the annular rotor.

In the next section there will be discussed a method by which the ratio $b_p/w$ can be found through an additional investigation of the field caused by the magnetised ring in a uniform air-gap.

5.3. The field of the magnetised ring in a uniform air-gap.

The induction on the inside of the iron jacket, see fig 26, due to the permanent magnetised ring is measured with a Hall-probe, the recorded curve is shown in fig 27. In the same figure is also drawn the calculated curve according to the analysis of Mr.Baran (L5), who also assumed a periodic covering of magnetic "bounded" surface charge.
The curves show a considerable difference that explains the bad disagreement between the calculated and measured torques. Now it is even clear how to fit the theory with the facts viz. the ratio $b_p/w$ must be choosen greater than 0,5.
For different values of $b_p/w$ the induction curve is calculated and the best agreement appears with $b_p/w$=0,9, see fig. 28.

5.4. Torque calculation with improved pole-width.

The computer has been made to calculate the torque for $b_p/w$=0,9; the results for several excitations has been plotted in fig. 29.
These curves show a fair agreement with experiments.

# 6. Conclusions and suggestions.

## 6.1. Discussion of the calculations.

The calculation of the stationary torque as performed in this paper is simplified by the following assumptions

a) the unknown sources of the magnetisation in the annular rotor material is replaced by a virtual layer of magnetic charge at the cilindrical surface.
b) the magnetic properties of the stator now are idealized strongly as the relative permeability is fixed at infinitive, or, the surfaces of the teeth are considered to be planes of fixed and constant magnetic potential.

Even with these, more or less primitive, suppositions the calculated values of the torque compare well with the recordings of a measuring device, through there are a number of details yet to be cleared.

The method of calculation allows the designer to find

a) details about the geometry of the stator, e.g. the dimensions of an optimal rectangular tooth-form and air-gap.
b) the most profitable width of magnetised zone on the rotor, when aiming at a certain shape of the torque-to-position curve.
c) the value of the torque with a moderate accuracy if size and the stator-current of the machine are given.

## 6.2. Information from the experiment.

Apart from the verification of the calculation, the measurements lead to an indication of the limits of stator excitation. It is shown that at too high a value of the current the permanent magnetisation can be disturbed definitely, which is to be avoided under all circumstances.

The experiments are also most useful to obtain indications for urgence of refinements in the analysis.

6.3. Suggestions.

6.3.1. It has to be verified what is the influence of the simplified representation of the rotor magnetisation. In appendix B is given a preparatory calculation method concerning the distribution of the magnetisation inside the material.
It has to be checked whether this leads to a fair representation of the real distribution of M, and the method of calculation of the torque has to be extended to account property for this complexity.
The investigation would only then be complete if the magnetisation with certain magnetic material can be predicted from the shape of the jig and the current during the process of magnetisation.

6.3.2. The actual reluctance of the stator part of the magnetic circuit has to be accounted for. As the value of the line-integral of H depends on the flux-density the calculation will be considerably complicated and much more computer-time-consuming.

6.3.3. It is therefore worth-while to try to find a more direct approach to account for this complication in the analysis.

6.3.4. A comprehensive optimal-design method has yet to be formulated.

APPENDIX A

In section 2.2.2.3. the boundary-conditions of the potentialfield U (x,y) are established.
As shown in fig.5, no material boundaries exist parallel to and above or below the x-axis. The figure is therefore completed by two false boundaries parallel to the x-axis, at distance to be estimated as follows:
The field at large distances from the teeth, i.e. y>w, resembles an electrical field of a regular row of charged wires, situated at distances w at the x-axis, perpendicular to the paper,(fig. A 1a).
These lines are to be charged alternatively with positive and negative charges of $\lambda$ C/m.
According to Maxwell the static field is governed by

$$\text{rot } \underline{E} = \underline{0} \qquad \text{(A1)}$$

and

$$\text{div } \underline{E} = \rho/\varepsilon_0 \qquad \text{(A2)}$$

At any point of the field, except in the line-sources, the latter equation becomes

$$\text{div } \underline{E} = 0 \qquad \text{(A3)}$$

Because of (A1), the field must be a gradient field of a scalar potential and therefore

$$\underline{E} = -\text{grad } \varphi \qquad \text{(A4)}$$

According to (L1A) the field around this grid can be found from the complex potential

$$\chi = \frac{\lambda}{2\pi\varepsilon_0} \log \cot \frac{\pi z}{2w} \qquad \text{(A5)}$$

when z = x + jy

This is an analytic function $\chi = \varphi + j\psi$ in the entire x,jy plane except at x=kw. (k= $\pm$ 0,1,2...)
A well known property of analytic functions is that Re $\chi$ as well as Im $\chi$ satisfy the equations of Cauchy - Riemann, and therefore they are solutions of the equation of Laplace (LA2)

$$\Delta(\text{Re } \chi) = \Delta(\text{Im } \chi) = 0$$

As (A3) and (A4) yield

$$\Delta\varphi = 0 \tag{A6}$$

it is clear that $\varphi$ can be derived from (A5) as

$$\varphi = Re\,\chi = \frac{\lambda}{2\pi\varepsilon_0}\log\left|\sqrt{\frac{\cos^2\frac{\pi x}{2w}+\sinh^2\frac{\pi y}{2w}}{\sin^2\frac{\pi x}{2w}+\sinh^2\frac{\pi y}{2w}}}\right| \tag{A7}$$

A good impression of the field can be had by following the potential at the x-axis and at lines parallel to the y-axis.
The first gives the potential as follows

$$\varphi(x,0) = \frac{\lambda}{2\pi\varepsilon_0}\log\left|\cot\frac{\pi x}{2w}\right| \tag{A7$^a$}$$

For lines x= $\pm$ kw the potential appears as

$$\varphi(kw,y) = \frac{\lambda}{2\pi\varepsilon_0}\log\left|\coth\frac{\pi y}{2w}\right| \tag{A7$^b$}$$

The behaviour of these functions is shown in the graphs A1a and A1b, they are tabulated in tables A1 and A2.
In this particular case it is of more interest to find the region where the potential diminishes to a value close to zero.
Therefore the value of $\varphi(0,y)$ is compared to that at a distance of y = w/6 from the line source. This distance is of the order of magnitude of the size of the teeth.
See fig. A1b. For y=w/6, $\log\left|\coth\frac{\pi y}{2w}\right| = 1.36$
From the graph and the table A2 it is clear that a distance y = 2w, for which $\log\left|\coth\frac{\pi y}{2w}\right| = 0{,}0038$ the relative value is reduced to 0.2%
At places to the left or to the right of (x,y)=(0,2w) the potential must be still lower and therefore it is justified to draw the false boundaries at y= $\pm$ 2w, and attribute them with the potential zero. In appendix B a field is calculated making use of this approximation.
The results compare well with the corresponding experiment, which appears to be an additional justification.

Table AI

| x/w = | $\frac{\pi x}{2w} =$ | $\log \left\lvert \cot \frac{\pi x}{2w} \right\rvert =$ |
|---|---|---|
| 0 | 0 | |
| 0.01 | 0.01571 | 4.14 |
| 0.02 | 0.03142 | 3.47 |
| 0.03 | 0.04712 | 3.06 |
| 0.04 | 0.06283 | 2.77 |
| 0.05 | 0.07854 | 2.43 |
| 0.06 | 0.09425 | 2.35 |
| 0.07 | 0.10996 | 2.21 |
| 0.08 | 0.12566 | 2.07 |
| 0.09 | 0.14137 | 1.95 |
| 0.1 | 0.15708 | 1.85 |
| 0.2 | 0.31416 | 1.12 |
| 0.3 | 0.47124 | 0.67 |
| 0.4 | 0.62832 | 0.32 |
| 0.5 | 0.78540 | 0.00 |
| 0.6 | 0.94248 | -0.32 |
| 0.7 | 1.09956 | -0.67 |
| 0.8 | 1.22566 | -1.12 |
| 0.9 | 1.41372 | -1.85 |
| 0.91 | 1.42943 | -1.95 |
| 0.92 | 1.44514 | -2.07 |
| 0.93 | 1.46085 | -2.21 |
| 0.94 | 1.47656 | -2.35 |
| 0.95 | 1.49227 | -2.43 |
| 0.96 | 1.50797 | -2.77 |
| 0.97 | 1.52368 | -3.06 |
| 0.98 | 1.53939 | -3.47 |
| 0.99 | 1.55510 | -4.14 |
| 1.00 | 1.57086 | |

Table A2

| $\frac{\pi y}{2w} =$ | $\log \left\lvert \coth \frac{\pi y}{2w} \right\rvert =$ |
|---|---|
| 0 | |
| 0.01 | 4.61 |
| 0.02 | 3.88 |
| 0.03 | 3.51 |
| 0.04 | 3.22 |
| 0.05 | 3.00 |
| 0.06 | 2.83 |
| 0.07 | 2.66 |
| 0.08 | 2.53 |
| 0.09 | 2.41 |
| 0.1 | 2.30 |
| 0.2 | 1.72 |
| 0.3 | 1.23 |
| 0.4 | 0.96 |
| 0.5 | 0.77 |
| 0.6 | 0.62 |
| 0.7 | 0.50 |
| 0.8 | 0.41 |
| 0.9 | 0.33 |
| 1 | 0.27 |
| 2 | 0.036 |
| 3 | 0.005 |
| 4 | 0.0007 |
| 5 | 0.0001 |

APPENDIX B

The residual magnetism in the annular rotor.

Introduction.

The annular rotor of isotropic ferroxdure 100 is magnetised in a jig, see fig. B1, which shows a cross-section.
If the winding is excited with a current of i amps, the magnetic field intensity gets such values that at least in the vicinity of the teeth of the jig the material becomes saturated.
After the current is reduced to zero, the effect of hysteresis manifests itself as a residual magnetisation, even when the jig is removed, because of the high coercive force of this material.
To calculate the effects of this remanence in combination with the stator of the stepping-motor, a good knowledge of the magnetisation vektor $\underline{M}_r$ everywhere in the material is essential.
The subject of this appendix is a method to calculate this quantity.

B.I. Assumptions.

B.I.I. In the actual process of magnetisation a intense current of short duration is lead through the winding.
Because of the laminated iron jig and the high resisivity of ferroxdure 100 eddy currents may be neglected; for this calculation it is therefore supposed that in spite of the short duration of the current it is allowed to consider the field as if it were excited by d.c.

B.I.2. Consequently the maximum value of the current is considered to be decisive for the ultimate magnetisation.
According to (LB1) the necessary magnetic fieldenergy to magnetise ferroxdure 100 is about $6 \times 10^5$ joule/$m^3$.

For the 8-pole rotor of the test equipment, see chapter 3, this leads to an amplitude of 12000 Amps.
The calculations are based on this current.

B.I.3. As usual the field perpendicular to the motor shaft is considered to be independent of the axial direction, end-effects being neglected.

The calculation of the field may considered as a two-dimensional problem.

B.I.4. Owing to the periodicity the area of one double pole-pitch ought to be investigated only.

B.I.5. The curvature of jig and ring is abandonned therefore it has been developed as shown in fig.B2.
This in accordance with the method of torque calculation, where this simplification also was applied.

B.2. Analysis of the field.

The final magnetisation depends on the field distribution during excitation and the hysteresis of the rotor material. The first aim is to establish the field intensity during excitation.
In the area below the teeth ($y < o$)

$$\text{rot } \underline{H} = \underline{0}$$

and therefore

$$\underline{H} = -\text{grad } U_m$$

Considering that the material of the jig is nowhere saturated and has further excellent magnetic properties (high permeable), the iron surfaces may be seen as equipotentialplanes, having an alternating potential of $\pm U_{mo}$ when the line of symmetry of a slot has zero potential so that

$$U_{mo} = \frac{ni}{2}$$

with ni the m.m.f. of one slot.

This follows from the line-integral of the fieldintensity $\underline{H}$ along a contour c around a whole slot.
The slots can now thought to be extended to infinity, see fig. B3, which introduces no appreciable error in the field calculation outside the slot.
The complete determination of the field requires some boundary conditions

a) At the distance y = -2w the potential is fixed at zero, as was explained in appendix A.

b) In the slots the field becomes homogeneous for $y > w/2$ as was shown in (LB2).

B.3. The field in ferroxdure 100 if the relative permeability $\mu_r = 1$.

This section serves to justify the premisses and calculations.

With

$$\text{div } \underline{B} = 0$$

and

$$\underline{B} = \mu_o \underline{H}$$

there follows

$$\text{div grad } u_m = 0$$

This field was calculated by numerical methods given in detail in appendix C on a digital computer; the results are compared to an experimental estimate of an electrical analogon on conductive paper and are found to correspond well to each other.
The results are drawn in the graphs of fig. B3a and B3b.

B.4. The field in ferroxdure 100 with actual $\mu_r$.

The initial magnetisation curve (the virginal) can be written by the following relation:

$$\underline{B} = \mu_o \mu_r \underline{H}$$

where $\mu_r$ depends on the magnitude of $\underline{H}$ only.
Calling $\mu_o \mu_r = \mu$

for short, div $\underline{B}$ = o yields

$$\text{div } (\mu \text{ grad } U_m) = 0$$

or in the rectangular coordinate system of fig. B3.

$$\frac{\partial}{\partial x}\left(\mu \frac{\partial U_m}{\partial x}\right) + \frac{\partial}{\partial y}\left(\mu \frac{\partial U_m}{\partial y}\right) = 0$$

The field that is defined by this equation can be found by the method indicated in appendix C.
The relation of B to H for the ceramic material has to be known for the execution of the calculation; the makers supplied the required curves, shown in figure B4a and B4b. They present the intrinsic induction $B_i$ in relation to the field-intensity H.
The well known features of this type of magnetic material are clearly shown.
Important is here also the virginal, as this is the "workline" during the process of magnetisation; it is an acceptable presupposition that the material after pressing to its final shape it is in a magnetically neutral condition, a condition comparable after being heated above the Curie temperature.

After completion of the calculations according to appendix C the scalar magnetic potential is known in a great number of grid-points spread over the picture of the magnetised material.
The field-intensity H can be derived from this scalar function and the local magnetisation follows from the virginal, or from its mathematical approximation.
After reduction of the excitation, then in the last stage of the process of magnetisation the material attains its state of remanence.
As the jig is considered to be ideal iron with a infinite permeability it is supposed that the magnetisation conserves its orientation, its value is indicated by the section of the hysteresis-curve where it cuts the M-axis, see figure B5. In spots where the field intensity was high enough to attain complete saturation the curve shown in figure B5 can serve, for lower values of H an inferior hysteresis loop has to be estimated.
Approximately one can suppose that inferior loops results in a residual magnetisation with relative the same value as for the main loop.

Thus

$$M_r = \left(\frac{M_r}{M\ max}\right)_{mainloop} \times M$$

In this way it is possible to find the $\underline{M}_r$ in each point of the ceramic material.
The sources of magnetisation are to be found from

$$\rho^* = -\nabla . \underline{M}_r \quad \text{and} \quad \sigma^* = \underline{M}_r . \underline{n}$$

Appendix C.

The numerical calculation of magnetic fields.

I. General.

The method of numerical calculation whith a digital computer has been dealt with by several authors (LC1),(LC2),(LC3),(LC4). It will therefore suffice to point out its general procedure and focus further the attention on the specefic difficulties that occured with the calculation of fields due to permanent magnetisation. For stationary fields the following relations apply,

$$\underline{B} = \mu_0(\underline{H} + \underline{M})$$

$$\text{div } \underline{B} = 0$$

$$\text{rot } \underline{B} = \mu_0 \text{ rot } \underline{H} + \mu_0 \text{rot } \underline{M}$$

in isotropic media $\underline{B} = \mu_0 \mu_r \underline{H}$

$$\text{rot } \underline{H} = \underline{J}$$

Sometimes it may be useful to introduce some auxiliary quantities such as

$J^* = \nabla \times \underline{M}$ = vector of bounded current distribution

$\rho^* = -\nabla . \underline{M}$ = a scalar of fictive magnetic „charge" analogous to the electrostatic charge

$\sigma^* = \underline{n} . \underline{M}$ a scalar of fictive magnetic surface charge

$\underline{A}$ = a vectorpotential function of the coordinates, such that

$$\nabla \times \underline{A} = \underline{B} \quad \text{and} \quad \nabla . \underline{A} = 0$$

U = a scalar potential function of the coordinates, such that

$$- \text{grad } U = \underline{H}$$

In electrical engineering the usual problem is to find the field quantities in some space when the currents, material properties and boundary conditions are given.

A great majority of electric machinery has a cylindrical shape, and its excitation is such that the field vectors lie in planes perpendicular to the shaft.
This has the advantage that the fields problems can be considered as two-dimensional.

## 2. Two-dimensional fields in electric machinery.

The most suitable coordinate-system is undoubtedly the system of cilindrical coordinates r, $\varphi$ , z, the last being directed parallel to the shaft.
Sometimes it is preferred to develop the machine into a linear arrangement, in that case r and $\varphi$ are transformed to x and y.

It is easily verified that the vector $\underline{B}$, $\underline{H}$ and $\underline{M}$ lie in the x,y plane, the vector of conduction current density $\underline{J}$ as well as its partner $\underline{J}^*$ are directed parallel to the z axis.
The vector potential $\underline{A}$, as can be shown, has only one component, $A_z\underline{k}$, which means a considerable simplification in further analysis.

There is electric machinery where the excitation coil is not cut by the plane under consideration, e.g. homopolar machines. In that case the field can be considered to be related to the scalar magnetic potential U.

## 3. Typical properties of the field problem of the stepping motor.

The stepping motor has such an outside excitation and therefore the problem will be treated for this particular case.
Because the field repeats periodically it suffices to investigate a section of a width of two pole pitches only.

The air-gap is small enough to warrant the use of a developed motor. The upper and lower boundaries of the area to be treated, are arbitrarily chosen lines parallel to the rotor surface at distances sufficiently remove to consider the field quantities there as constants. Figure C1 shows a typical arrangement of the active parts. The two stator teeth are considered to be equipotential planes; there are strong arguments to support this, and little reason to suppose that field lines would enter the teeth at one side and leave them at the other side in the x-y plane.
The potential of the teeth is due to the excitation and must be considered to take a value + U and - U respectively as the value zero potential must be attributed to the neutral parts of the machine, the shaft, shields etc.

The rotor has a distribution of a permanent magnetisation as shown in appendix B.
For a first approximation the permanent magnetisation is simplified as if it appeared only on the rotor surface as was shown in 3.3.
Before further details are considered, the method of calculation must be discussed.

## 4. The approximation of the field by way of difference equations.

The problem is to find U from the following basic equations.

$$\underline{B} = \mu_0(\underline{H} + \underline{M})$$

$$\underline{H} = -\nabla U$$

$$\nabla . \underline{B} = 0$$

and the appropriate boundary conditions.

It can be shown that the U can be approximated sufficiently accurate in a finite number of points by difference equations.

A grid is drawn over the area of fig C1, the mesh distances such that the number of grid points remain acceptable, considering computer time, and sufficient to warrant a proper representation of the domains where the field alters rapidly with the distance.
One grid-point and its surrounding is shown in fig.C2. It is indicated by $P_o$ and its closest neighbours are $P_1$, $P_2$, $P_3$, and $P_4$, the subscripts also to be used for the properties in these location, e.g. the potential in $P_1$ is called $U_1$ etc.

To replace differentials by difference equations the U is expresses in a Taylor series.

$$u_1 = u_o + h_1\left(\frac{\partial u}{\partial x}\right)_o + \frac{h_1^2}{2}\left(\frac{\partial^2 u}{\partial x^2}\right)_o + O(h_1^3)$$

When $O(h_1^3)$ indicates rest value of the series

and

$$u_3 = u_o - h_3\left(\frac{\partial u}{\partial x}\right)_o + \frac{h_3^2}{2}\left(\frac{\partial^2 u}{\partial x^2}\right)_o + O(h_3^3)$$

Elimination of the first order differentials leads to

$$\frac{h_1 h_3}{2}(h_1+h_3)\left(\frac{\partial^2 u}{\partial x^2}\right)_o = (u_1-u_o)h_3 + (u_3-u_o)h_1 + \text{----}$$

For the points 2 and 4 a companion relation leads to

$$\frac{h_2 h_4}{2}(h_2+h_4)\left(\frac{\partial^2 u}{\partial y^2}\right)_o = (u_2-u_o)h_4 + (u_4-u_o)h_2 + \text{---}$$

or

$$\left(\frac{\partial^2 u}{\partial x^2}\right)_o + \left(\frac{\partial^2 u}{\partial y^2}\right)_o = -(\alpha_1+\alpha_2+\alpha_3+\alpha_4)u_o + \alpha_1 u_1 + \alpha_2 u_2 + \alpha_3 u_3 + \alpha_4 u_4$$

with

$$\alpha_1 = \frac{2}{h_1(h_1+h_3)}, \quad \alpha_2 = \frac{2}{h_2(h_2+h_4)},$$

$$\alpha_3 = \frac{2}{h_3(h_1+h_3)}, \quad \alpha_4 = \frac{2}{h_4(h_2+h_4)}.$$

In domains containing no currents nor magnetic material

$$\nabla . \underline{B} = 0 = -\nabla . \nabla U \quad \text{or}$$

$$\frac{\partial^2 U}{\partial x^2} + \frac{\partial^2 U}{\partial y^2} = 0 \qquad \text{and therefore}$$

$$U_0 = \frac{\alpha_1 U_1 + \alpha_2 U_2 + \alpha_3 U_3 + \alpha_4 U_4}{\alpha_1 + \alpha_2 + \alpha_3 + \alpha_4}$$

The method of calculation is based on this relation. In the process of one iteration in all points of the grid the potential U is reevaluated; the values at the boundaries are the anchors from whom proper values of the potentials at inside points are approximated.

The first time all points are attributed with some arbitrary guessed potentials, after a few iterations, when some wild guess may result in extraordinary computed values, the process of gradual convergence starts resulting in a acceptable representation of the real field.

Inside magnetised material the situation is somewhat complicated.

Here applies

$$\underline{B} = \mu_0 (\underline{H} + \underline{M})$$

and from

$$\nabla . \underline{B} = 0$$

follows

$$\nabla . \underline{H} = -\nabla . \underline{M} = \rho^*$$

together with

$$\underline{H} = -\nabla U$$

it leads to the Poisson equation for the two-dimensional field

$$\frac{\partial^2 U}{\partial x^2} + \frac{\partial^2 U}{\partial y^2} = \rho^*$$

when this equation is expressed in the difference equation of the grid, the potential in any grid point is found from

$$U_0 \simeq \frac{\alpha_1 U_1 + \alpha_2 U_2 + \alpha_3 U_3 + \alpha_4 U_4 + \rho^*}{\alpha_1 + \alpha_2 + \alpha_3 + \alpha_4}$$

This equation can only be applied if everywhere inside the material the $\rho^*$ is known.
In the first approximation that is used in this paper, it is presupposed that the divergence of $\underline{M}$ inside the material may be disregarded, and that only the surface charge $\sigma^*$ is of real importance.

If the behaviour of ferromagnetic material is given by

$$\underline{B} = \mu_0 \mu_r \underline{H}$$

and

$$\mu_r = \mu_r(H)$$

then

$$\nabla . \mu \nabla U = 0$$

or

$$\frac{\partial}{\partial x}\left(\mu \frac{\partial U}{\partial x}\right) + \frac{\partial}{\partial y}\left(\mu \frac{\partial U}{\partial y}\right) = 0$$

here $\mu$ is a function of the local calue of H.
In the difference equation the $\mu$ value is separately to be calculated for the neighbourhood of each grid-point, as indicated at figure C2.

The value of the potential in a grid-point is now found from

$$U_0 = \frac{\alpha_1 \mu_1 U_1 + \alpha_2 \mu_2 U_2 + \alpha_3 \mu_3 U_3 + \alpha_4 \mu_4 U_4}{\alpha_1 \mu_1 + \alpha_2 \mu_2 + \alpha_3 \mu_3 + \alpha_4 \mu_4}$$

5. The boundary conditions.

As was stated before the boundary values at AB and CD were fixed U = 0.
At the surface of the teeth a value was steadfast held at $\pm$ U = $\frac{1}{2}$ m.m.f. of the coil.

More difficulties arise with the border lines AD and BC. Recourse was had to the consideration that due to periodicity the pattern of values of U on AD and BC must be equal, and also, but with changed sign, to that of EF. Now as the values of all grid points on EF are calculated from their neighbours and constitute a proper approximation, these values are inserted as boundary values at AD and BC after every iteration.

The last special boundary condition to be observes is the interface of magnetised material and air.

Here

$$\underline{B}_{n\ air} = \underline{B}_{n\ ferroxdure} \text{ and } \underline{H}_{t\ air} = \underline{H}_{t\ ferroxdure}$$

has to be satisfied.

With

$$\underline{B} = \mu_o(\underline{H} + \underline{M}) = \mu_o \mu_r \underline{H} + \mu_o \underline{M}_r$$

follows for the normal to the rotor surface

$$H_{air} = \mu_r H_{fxd} + M_r$$

or, in the difference equation for the grid points on the rotor surface

$$U_o = \beta_2 U_2 + \beta_4 U_4 \pm \beta_m M_r.$$

when $\beta_2 = \dfrac{h_4}{h_4 + h_2 \mu_r}$, $\beta_4 = \dfrac{\mu_r h_2}{h_4 + \mu_r h_2}$ and $\beta_m = \dfrac{h_2 h_4}{h_4 + \mu_r h_2}$

The above indicated process of calculation was properly translated into a ALGOL-program and put to work with the relevant parameters.
The results were given in chapter 5.

Appendix D.

The calculation of the m.m.f. on behalf of the iron parts of the stator.

The line-integral of the magnetic field-intensity $\int_s \underline{H}.d\underline{l}$ is approximated along a contour as shown in figure D1, that represents a cross-section through one half of the stator-iron.
The contour is drawn along an estimated average field-line, consisting of the parts indicated with $l_1, l_2, l_3$ and $l_4$.
The total length is therefore

$$l = l_1 + l_2 + l_3 + l_4$$

The extremely small gap between the stator halves may be ignored. The calculation is carried out under the supposition that the field may be considered to be homogeneous in the section 1 and 4, and that leakage fluxes may be considered non-exsistent.
If the flux through one tooth, indicated by $\Phi_1$, is known than

$$B_1 = \Phi_1 / A_1$$

The flux in the outside section 4 is the sum of the contributions of each tooth, therefore in this case

$$B_4 = 4\Phi_1 / A_4$$

The flux in the left and right flanges, sections 2 and 3, gives decreased induction from inside to outside.
For calculations with Simpson's rule (L1), the induction inside, outside and in the middle of the sections are to be calculated; so $B_{2_i} = 4\Phi / A_{2_i}$ etc.

To find the relevant values of the field-intensity the properties of the material are to be known; fig. D2 shows the permeability of the stator material as a function of the fieldintensity H in double logarithmic scale.

As

$$B = \mu H$$

and therefore

$$\log B = \log \mu + \log H$$

it is easy to establish B along a graphical method in the same diagram.
For every induction B the H can be traced and this value can be used in the final calculation of the m.m.f. stator-iron.

Thus

$$\int_S \underline{H}.d\underline{l} = H_1 l_1 + H_{2_{av}} l_2 + H_{3_{av}} l_3 + H_4 l_4 \qquad (2.19)$$

with

$$H_{2_{av}} = H_{3_{av}} = \frac{1}{6} (H_{2_i} + 4 H_{2m} + H_{2_o})$$

This calculation ought to be carried out for every rotor-position to find the proper correction to the potential of the stator-teeth.

The table D1 shows the relevant seizes of the stators to be used in the calculation.

Table D1

| length-element | length in mm | |
|---|---|---|
| $l_1 = l_4$ | 100 | |
| $l_2 = l_3$ | 34 | |
| **cross-section** | **surface in $mm^2$** | |
| $A_4$ | 4725 | |
| $A_{3_i} = A_{2_i}$ | 1761 | |
| $A_{3_m} = A_{2_m}$ | 3710 | |
| $A_{3_o} = A_{2_o}$ | 5660 | |
| $A_1$ | 272,3 | g/w= 1/40 |
| $A_1$ | 255,5 | g/w= 1/20 |
| $A_1$ | 221,0 | g/w= 1/10 |

References.

L 1 Samual Seely, Electromechanical Energy Conversion
Mac Graw Hill Book Company Inc.
New York.(1962)

L 2 J.A. Stratton, Electromagnetic Theory.
Mac Graw Hill Book Company Inc.
New York.(1941)

L 3 J.A. Schot, Elektromechanica 1.
Technological University of Twente.
Enschede(1967)

L 4 The design of permanent magnets, with particular reference to leakage coefficient.
Advance Information N° 418
Philips' Gloeilampenfabrieken te Eindhoven.(march 1963)

L 5 W.Baran Fangmagnetsysteme aus periodisch angeordneten Barium-ferrit-Dauermagneten ohne Eisenpolschuhe; Magnetfelder, Anziehungskräfte und Konstruktions-vorschriften.
Teil 1.
Technische Mitteilungen Krupp.
Forschungs-Berichte Band 22(1961)
Nr 4.

LA2 J.H.van Lint Wiskunde V
Syllabus van het college complexe functie theorie (1963)
Technische Hogeschool Eindhoven.

LB1 A.Rademakers and H.van Suchtelen. Magnetizing Permanent Magnets.
Matronics, no.12.
Philips. (April 1957)

LB2 A.J.C. Bakhuizen — De bepaling van het stationaire koppel van reluktantie stappenmotoren 1. Rapport EM 69-4. Technological University of Eindhoven. (1969)

LC1 E.A. Erdélyi, F.C, Trutt, R.F. Jackson. — The non-linear potential equation and its numerical solution for highly saturated electrical machines. IEEE Transactions on aerospace-support conference procedures.

LC2 E.A, Erdélyi, F.C. Trutt, R.E. Hopkins. — Flux *dis*tribution in saturated high-speed homopolar inductor alternators with purely reactive loads. IEEE Transactions on aerospace support conference procedures.

LC3 H. Braess, H.Weh, E.A. Erdélyi. — Numerische Berechnung Magnetischer Felder und Kräfte. Archiv für Elektrotechnik 52. Band Heft 5. (1969)

LC4 K. Reichert: — Ein numerisches Verfahren zur Berechnung magnetischer Felder, insbesondere in Anordnungen mit Permanentmagneten 52. Band Heft 5. (1968) *Archiv für Elektrotechnik*

LD1 Liwschitz. — Die Elektrischen Maschinen Band III. Verlag von B.G. Teubner Berlin (1934)

L6 E.M.H. Kamerbeek — *Elektromechanica. b.o. (unpublished)* *1966*

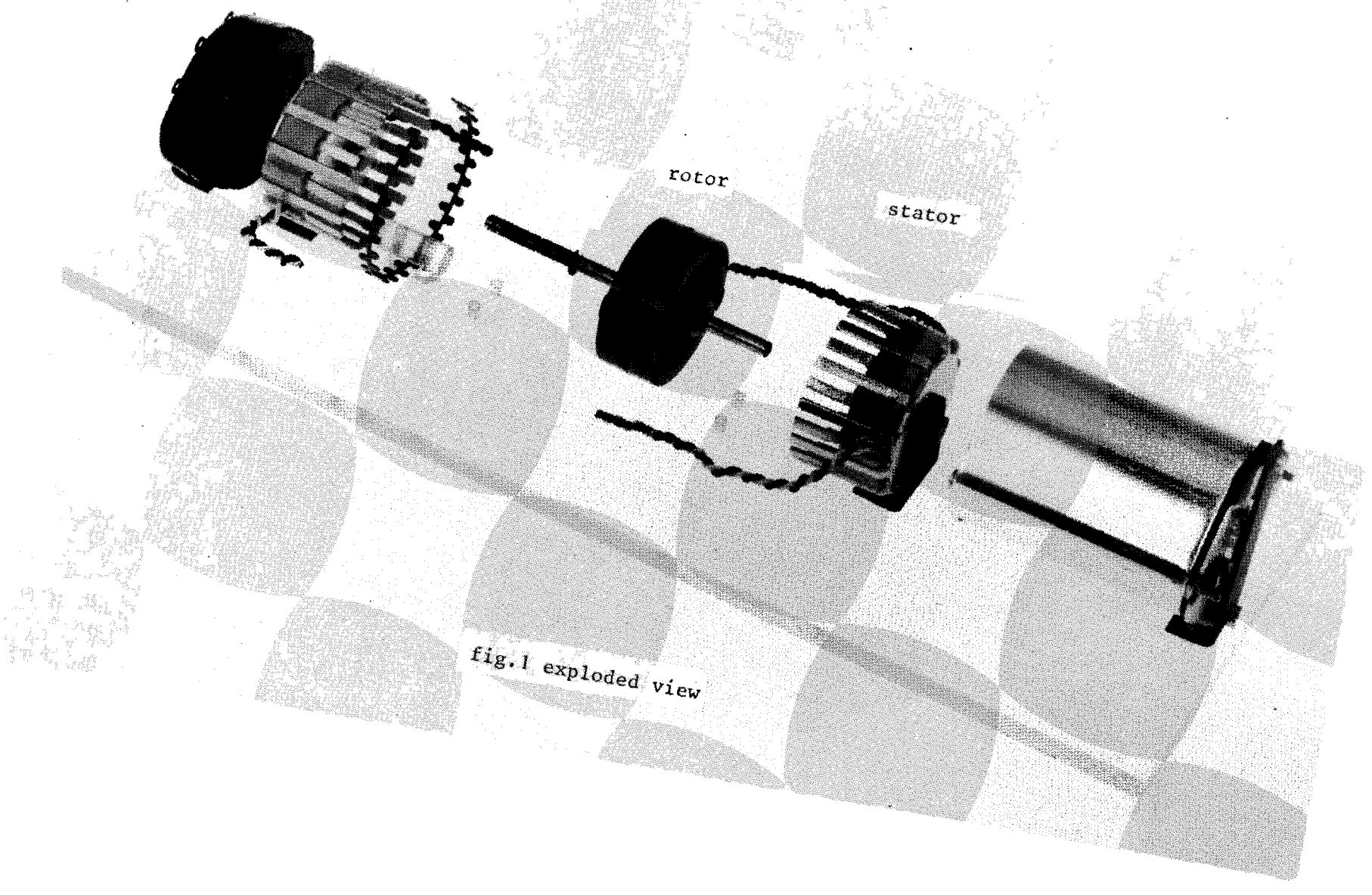


fig.1 exploded view

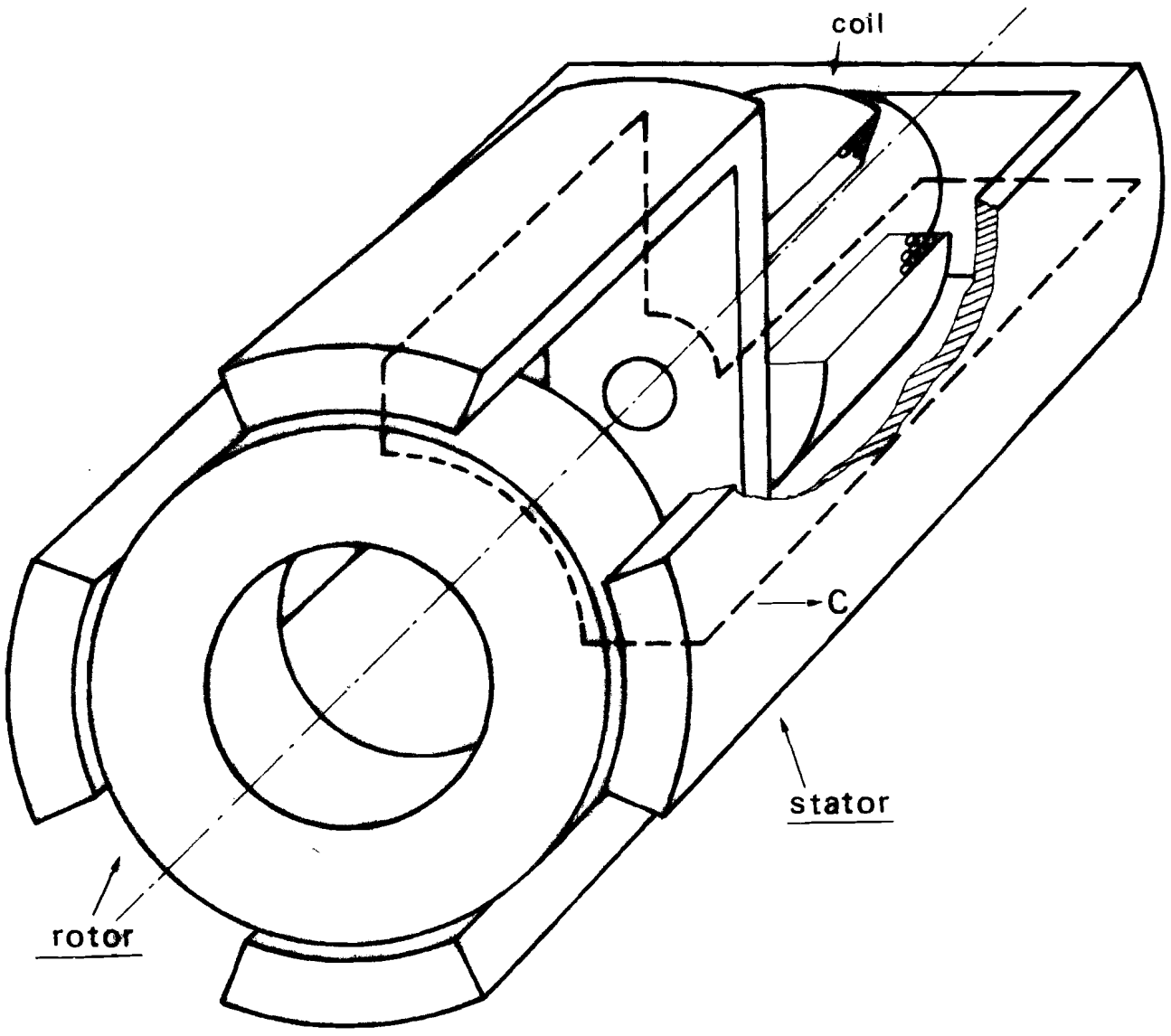


fig 2

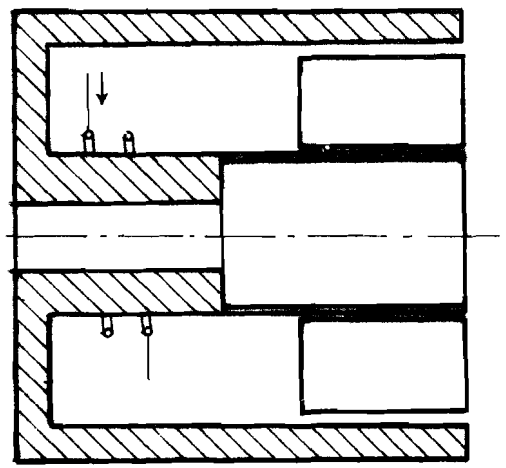

A—A

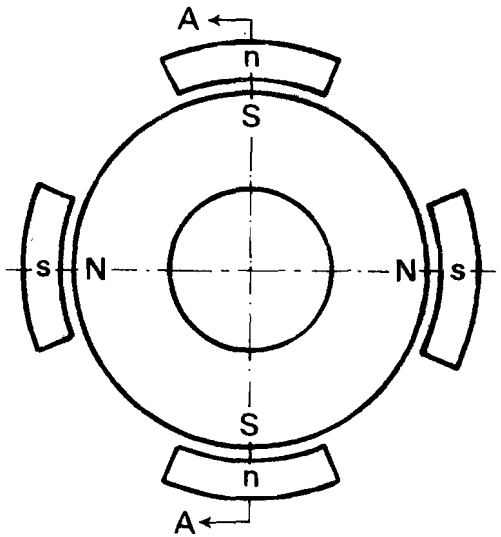


left

fig.3a

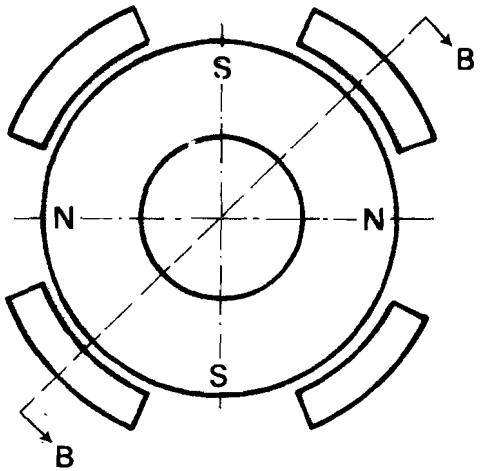


right

fig.3b

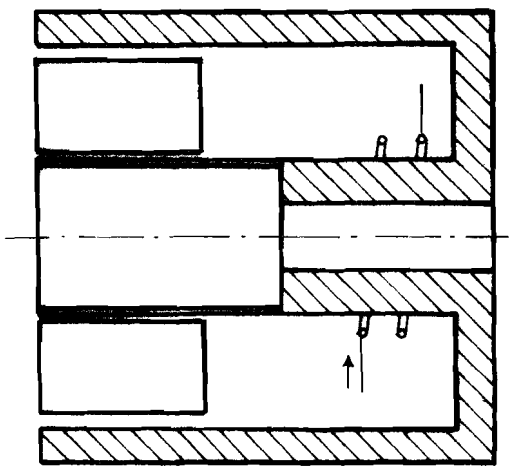

B—B

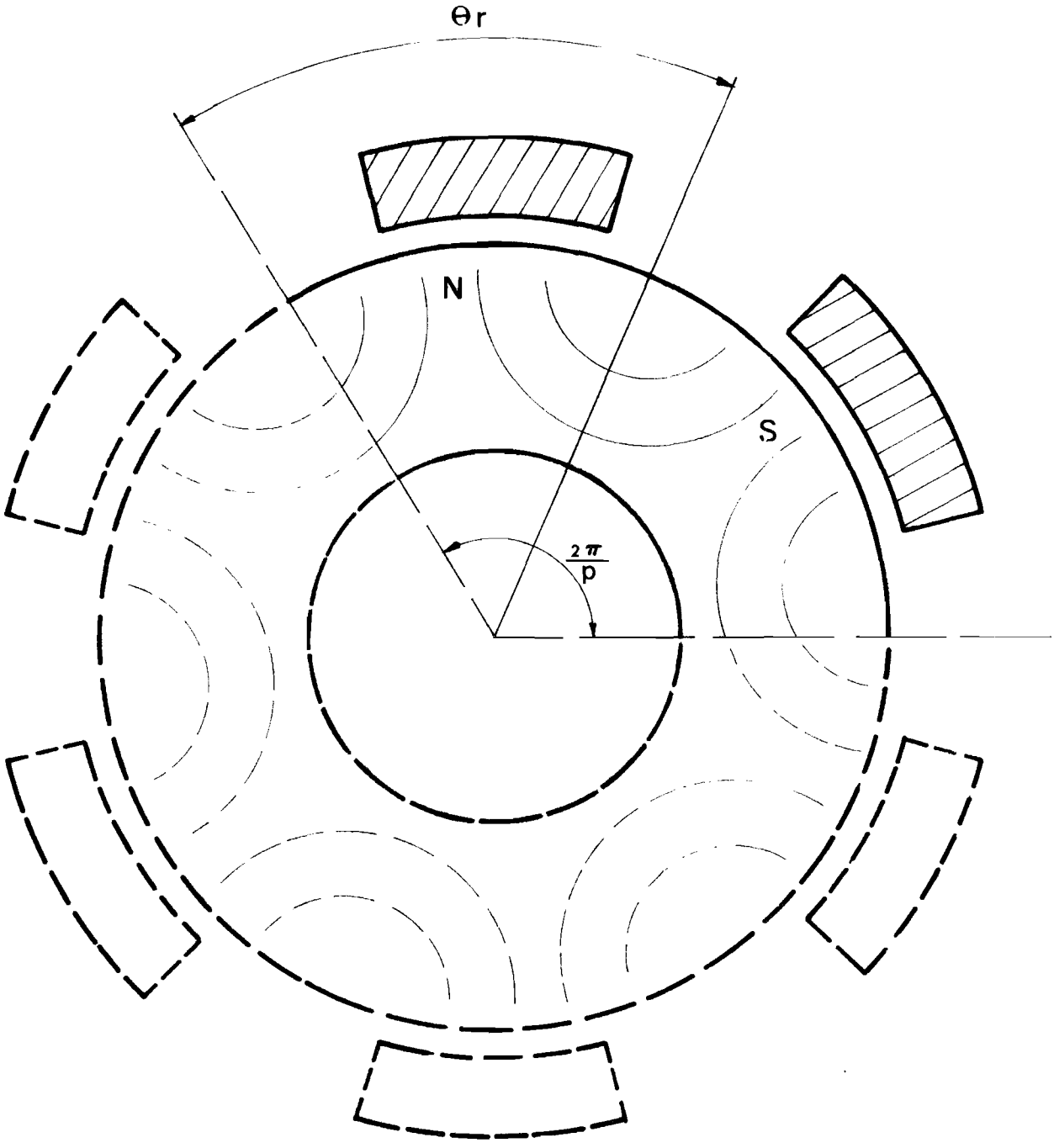


fig. 4

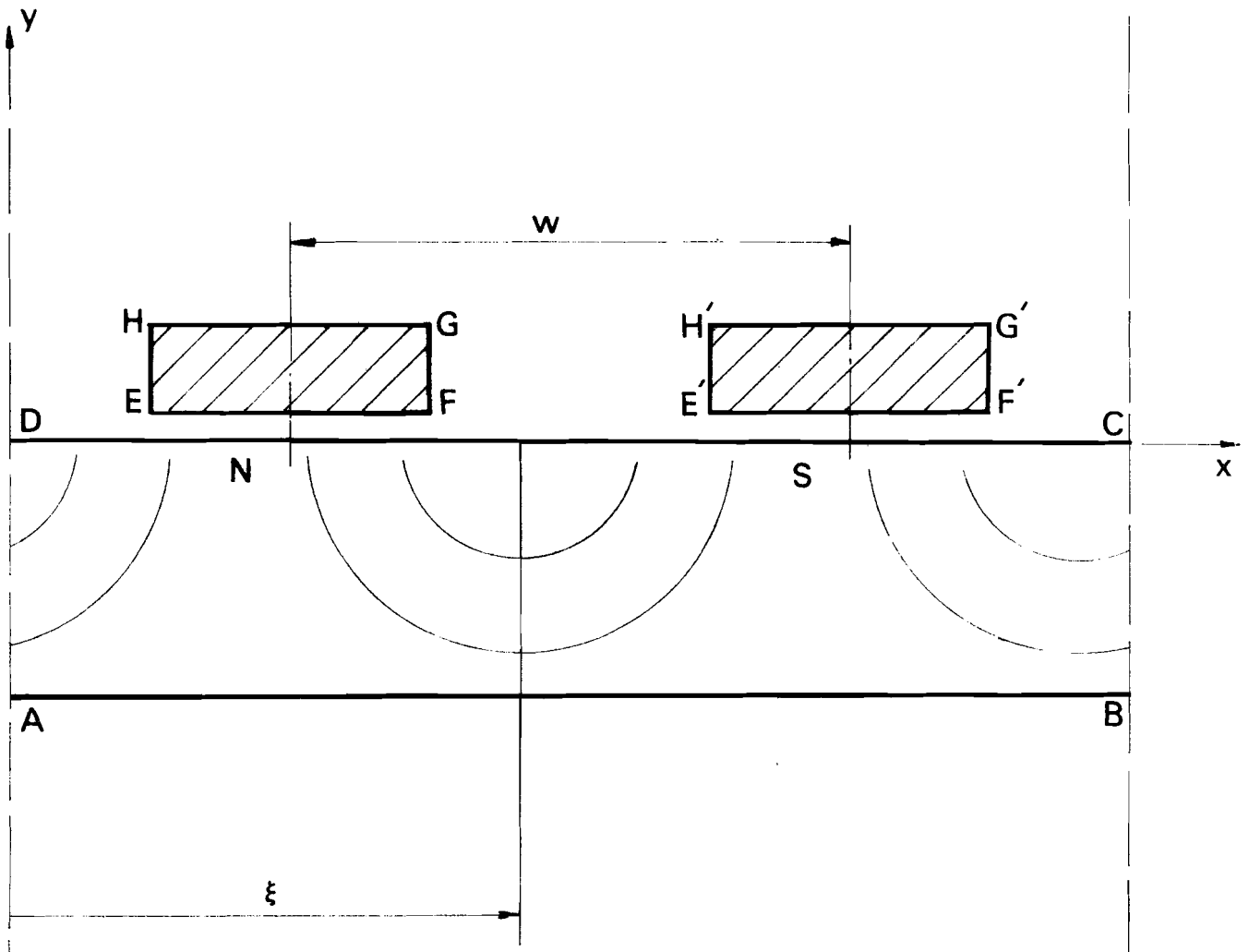


fig. 5

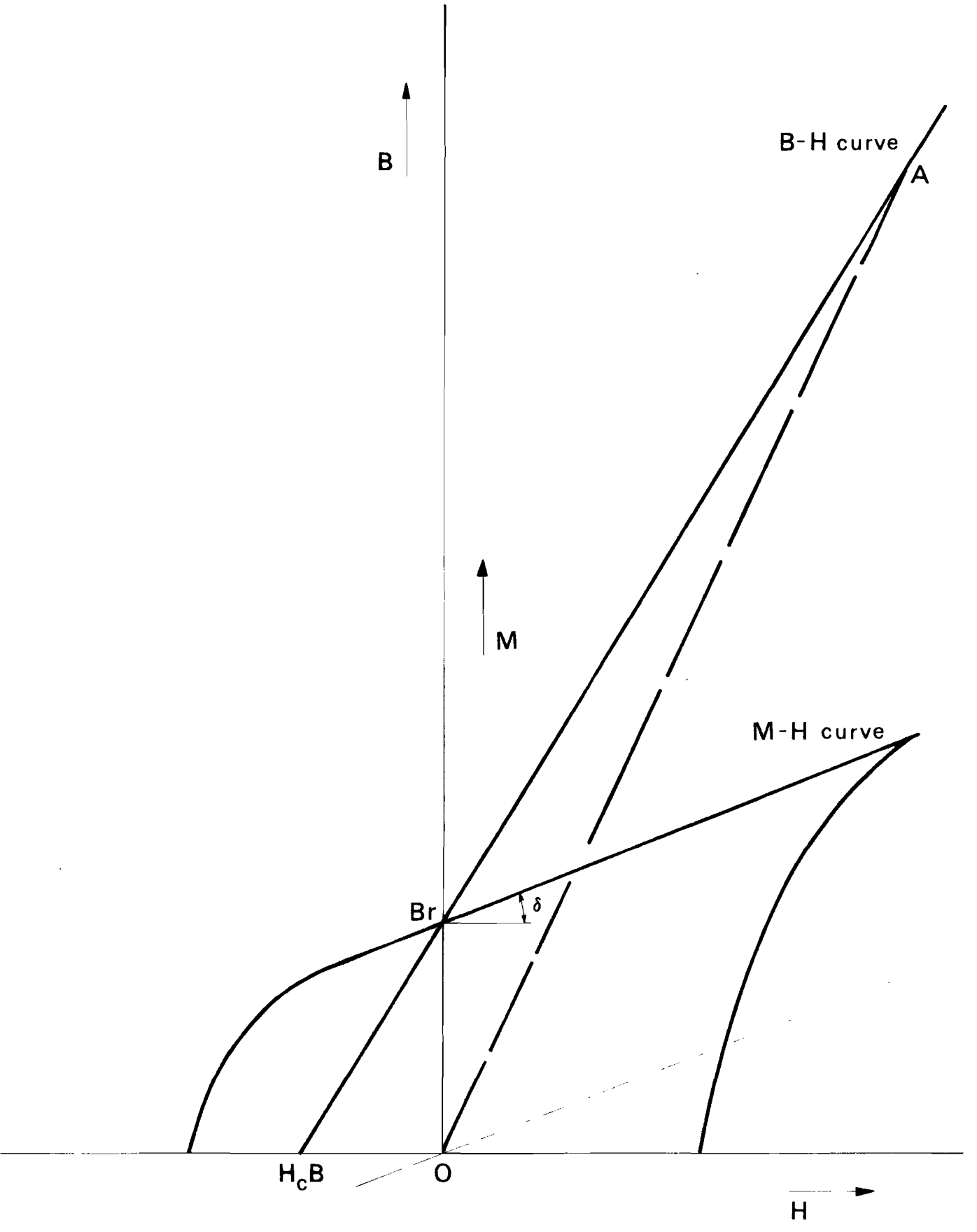


fig. 6

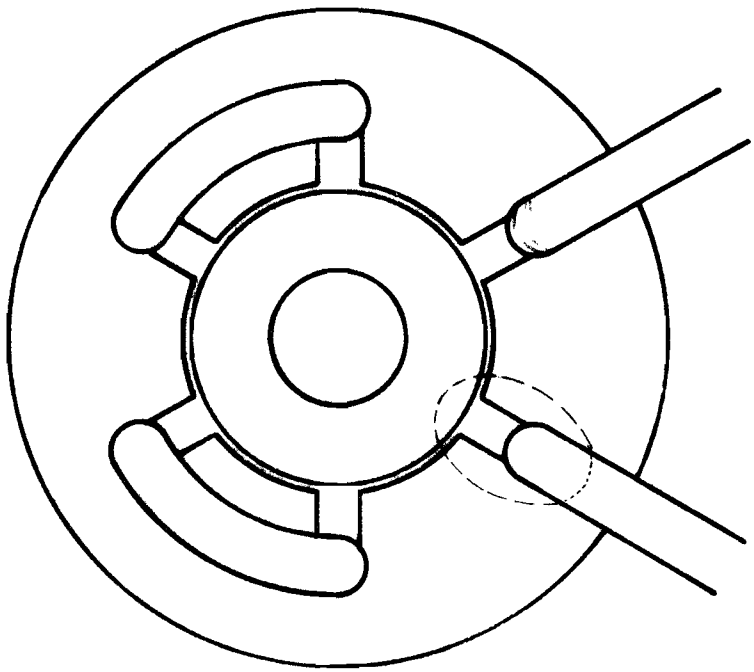

fig. 7

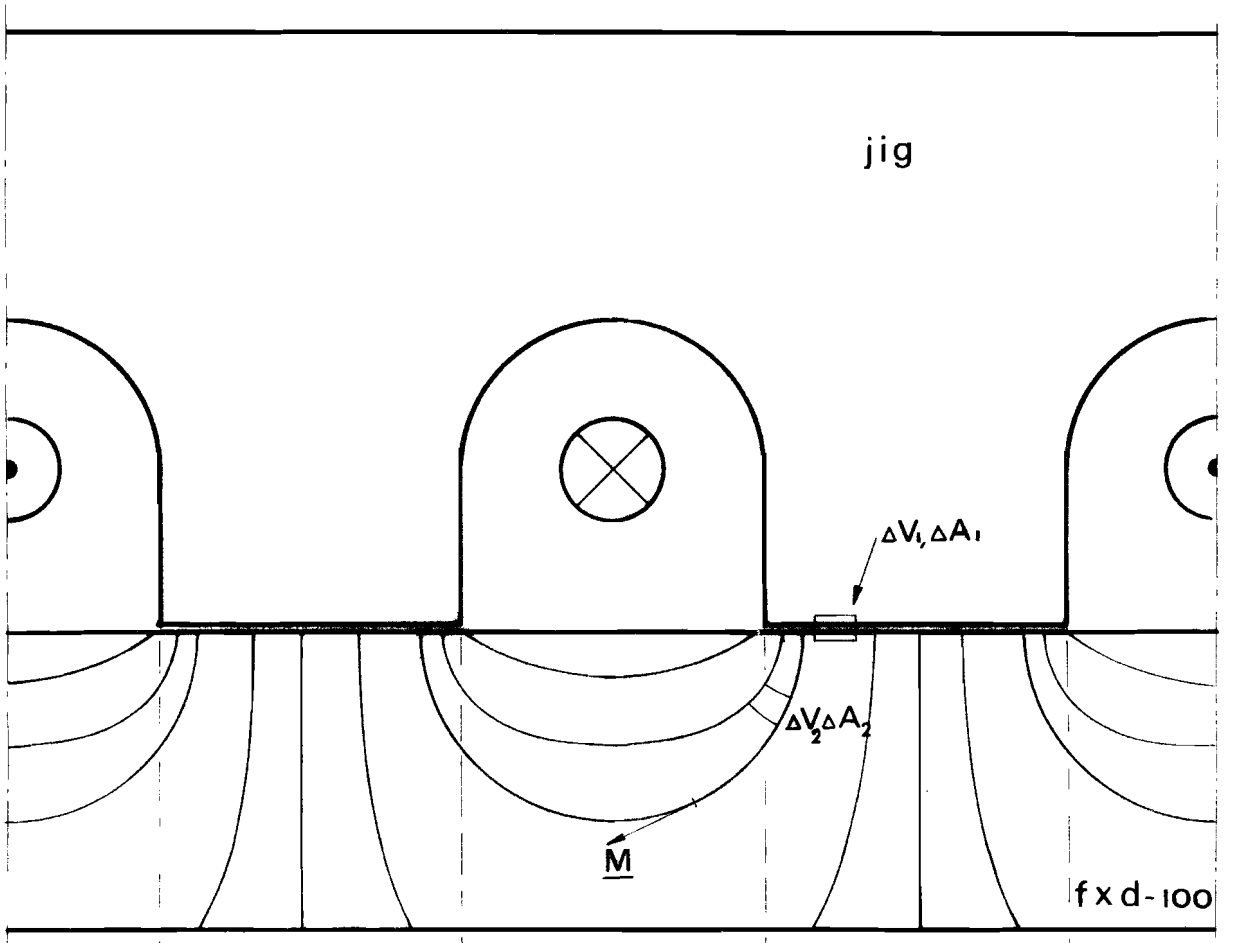


fig. 8 a

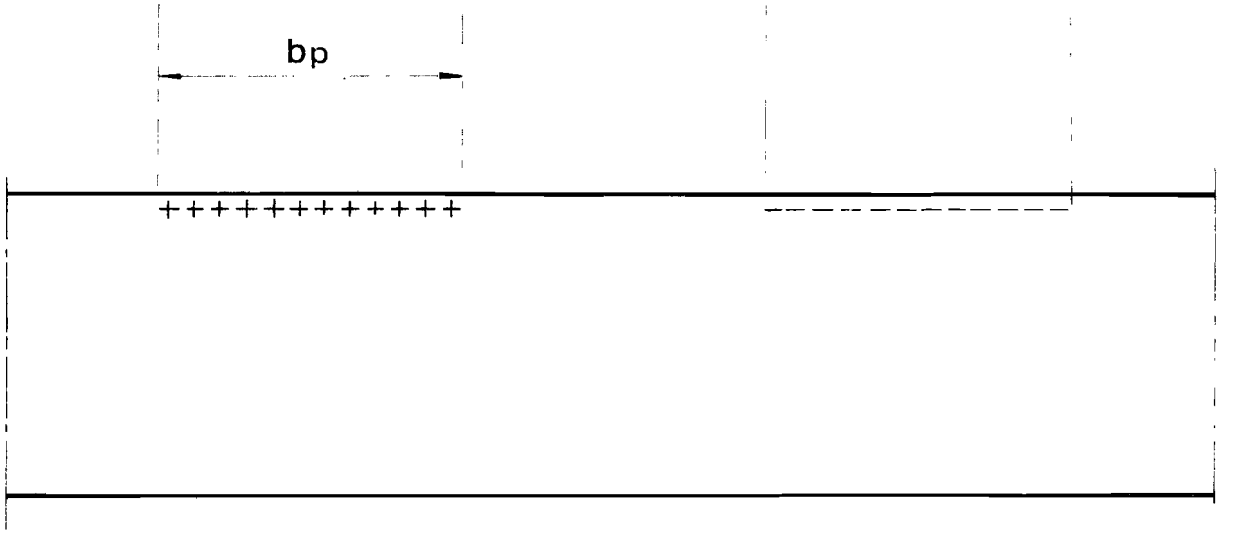


fig. 8 b

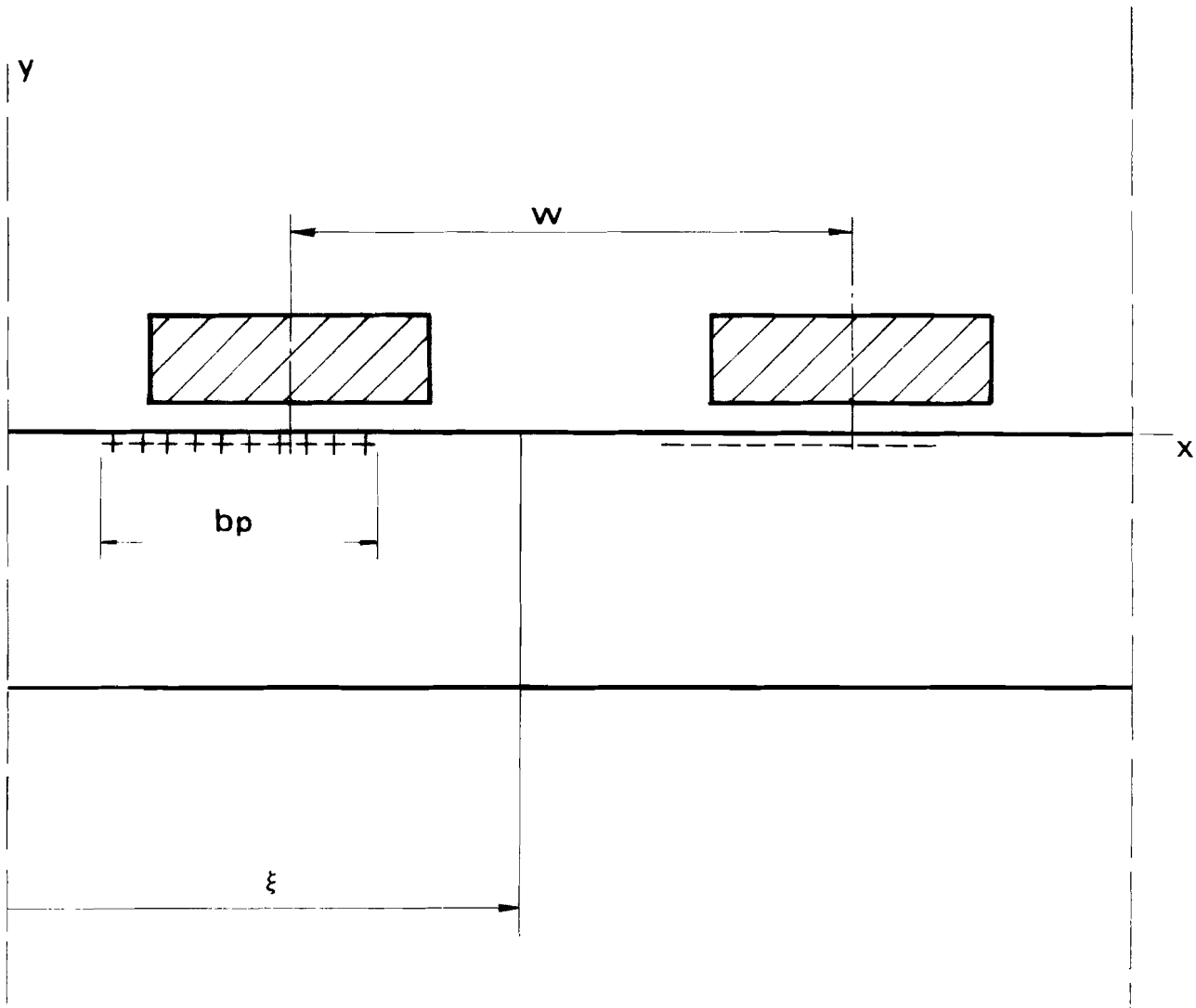


fig. 9

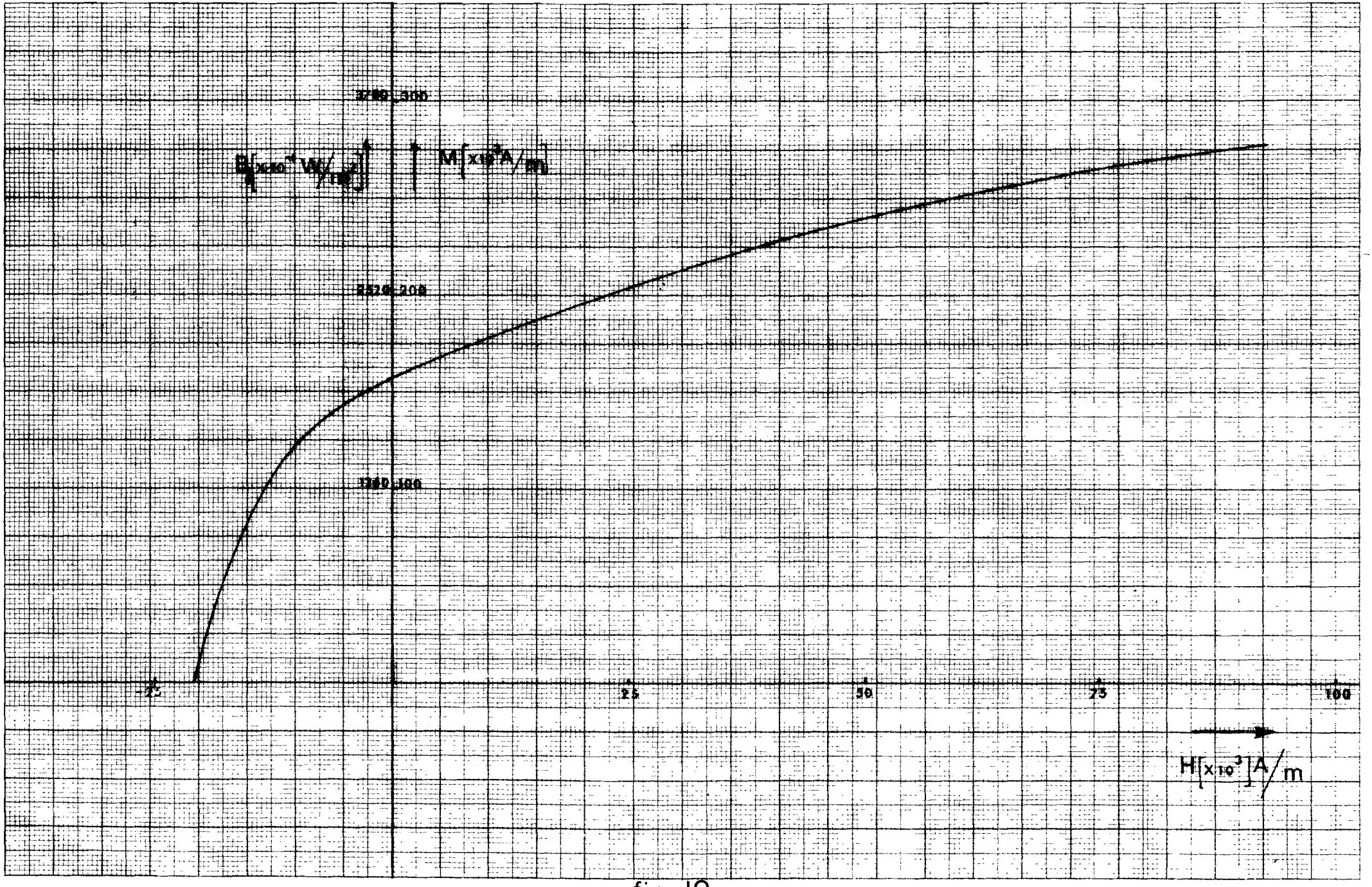


fig. 10

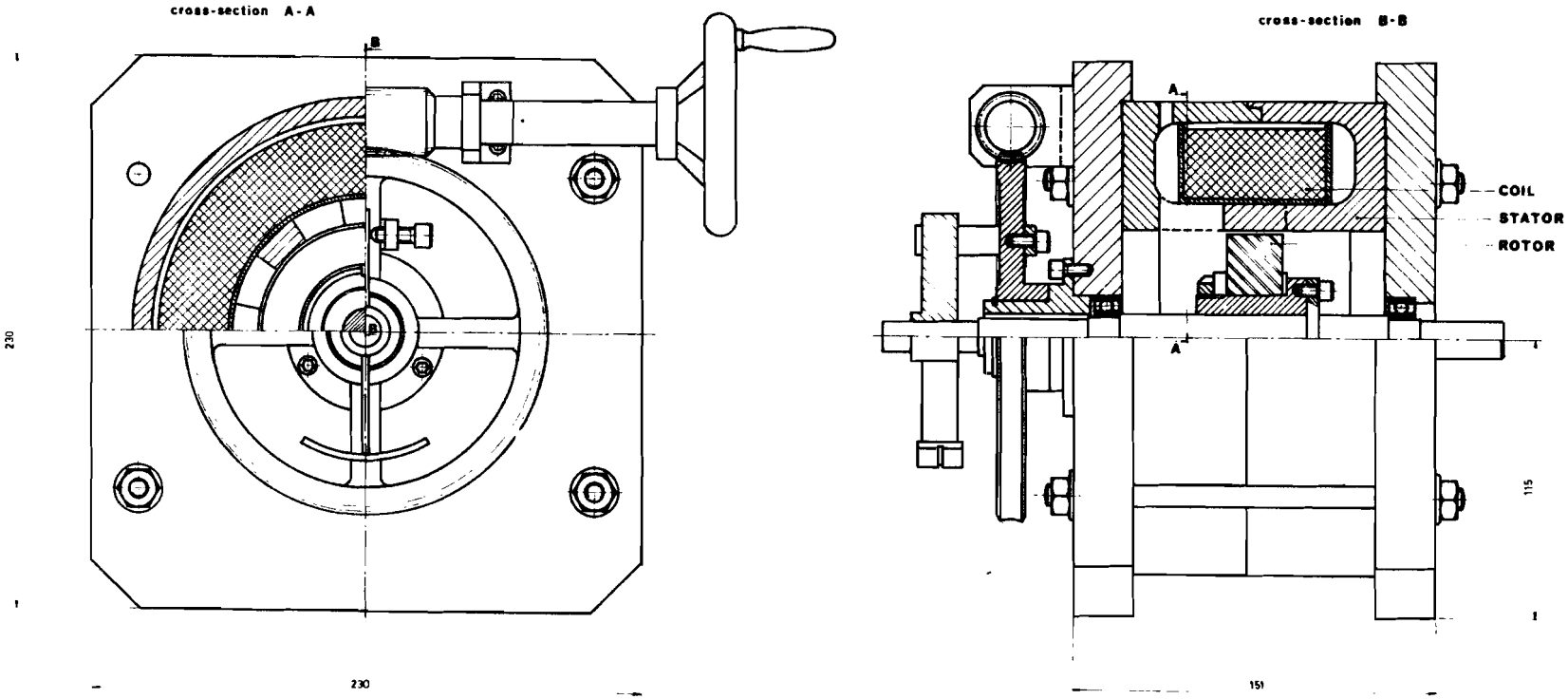
cross-section A-A
B
230
230
cross-section B-B
A
A
COIL
STATOR
ROTOR
115
151

fig 11

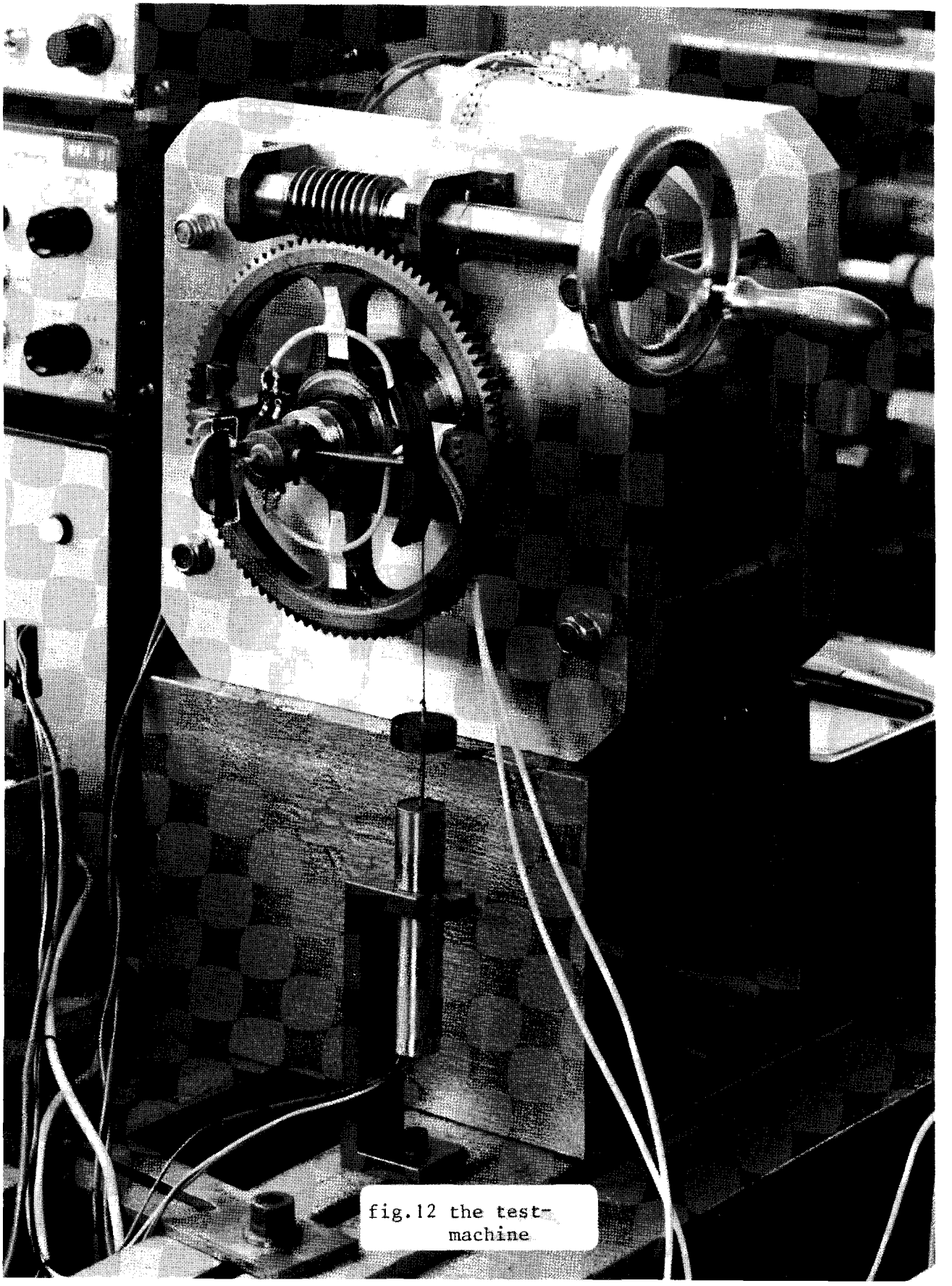

fig.12 the test-machine

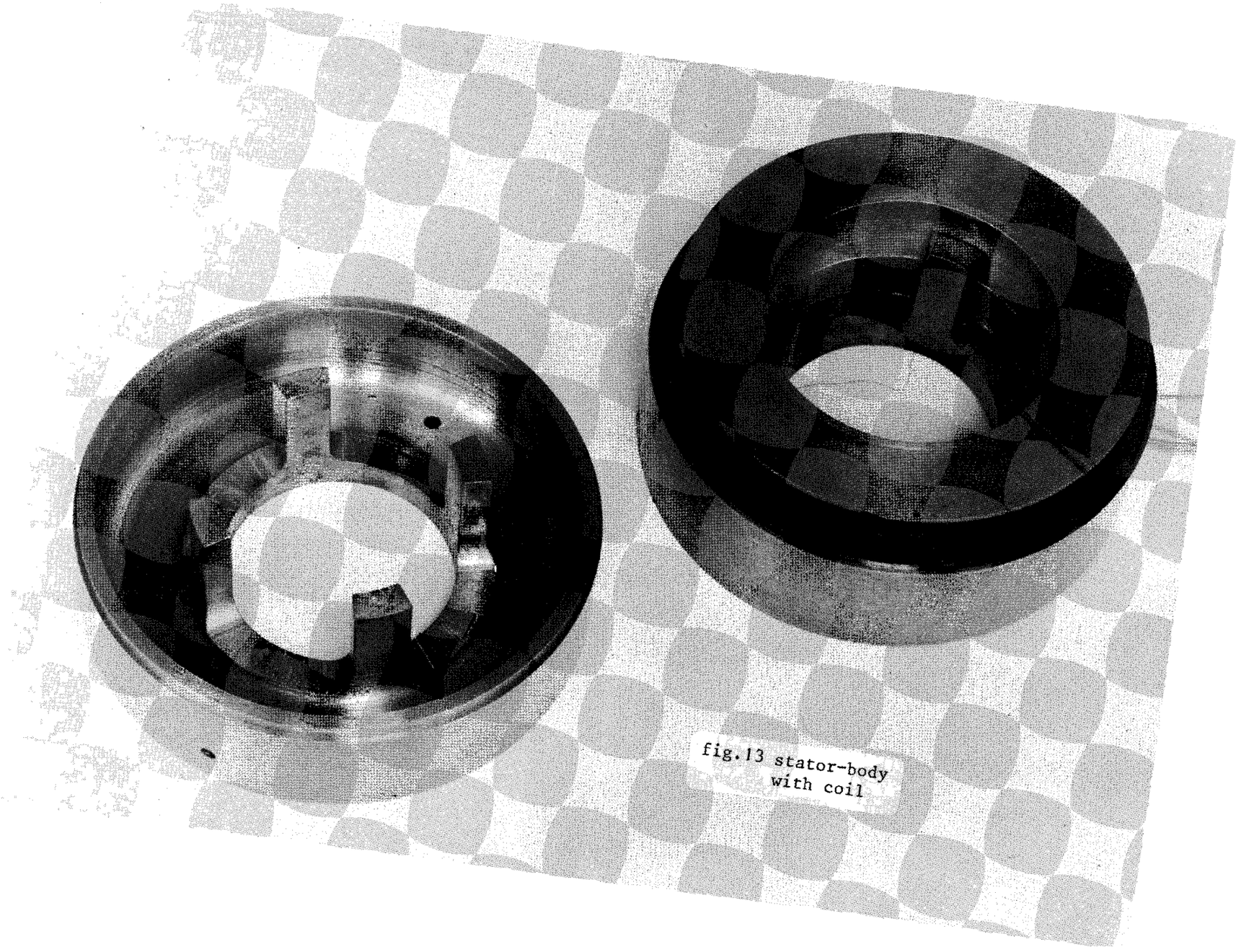

fig.13 stator-body
with coil

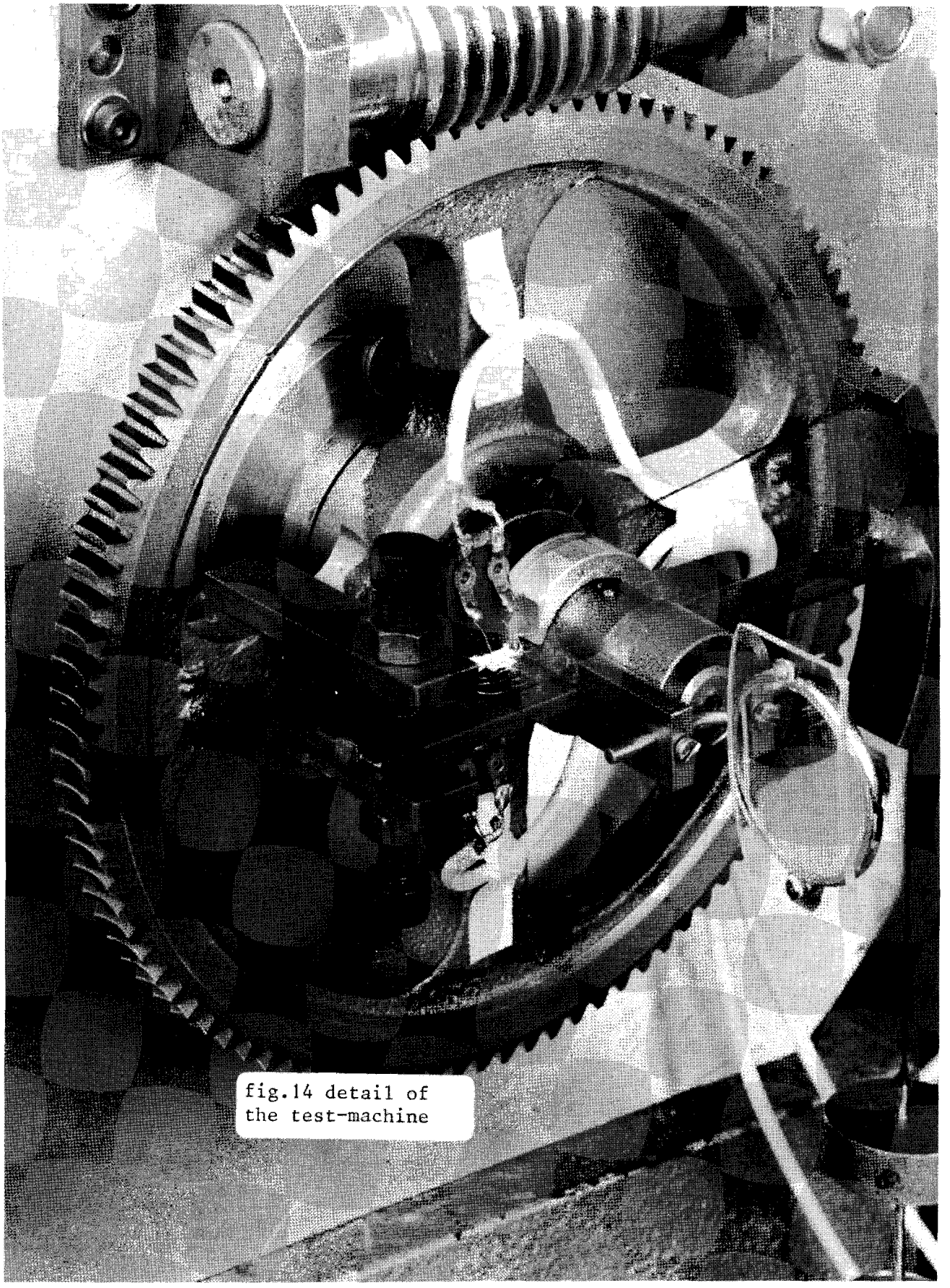

fig.14 detail of
the test-machine

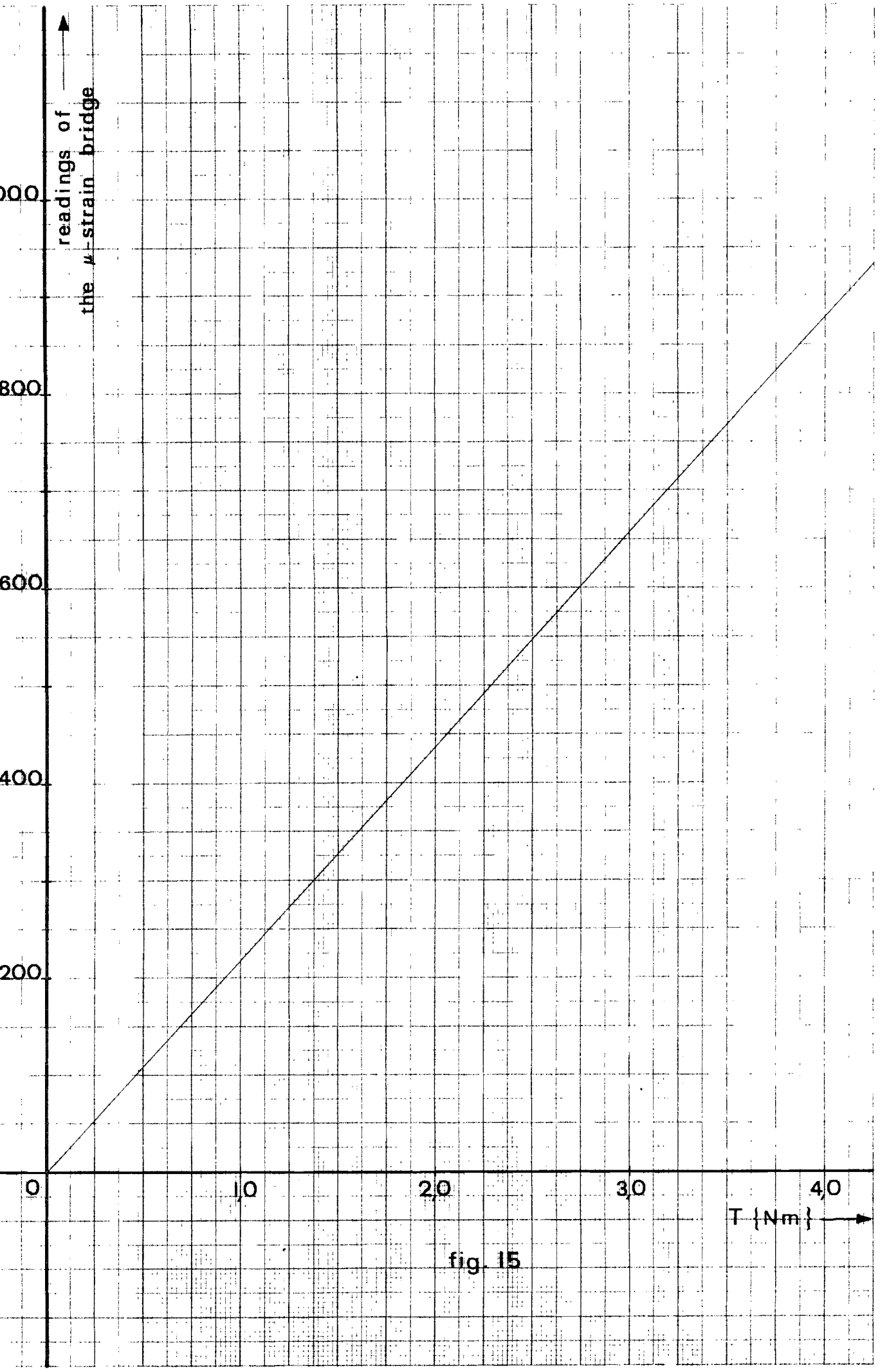
readings of
the μ-strain bridge
000
800
600
400
200
0
1,0
2,0
3,0
4,0
T {Nm}

fig. 15

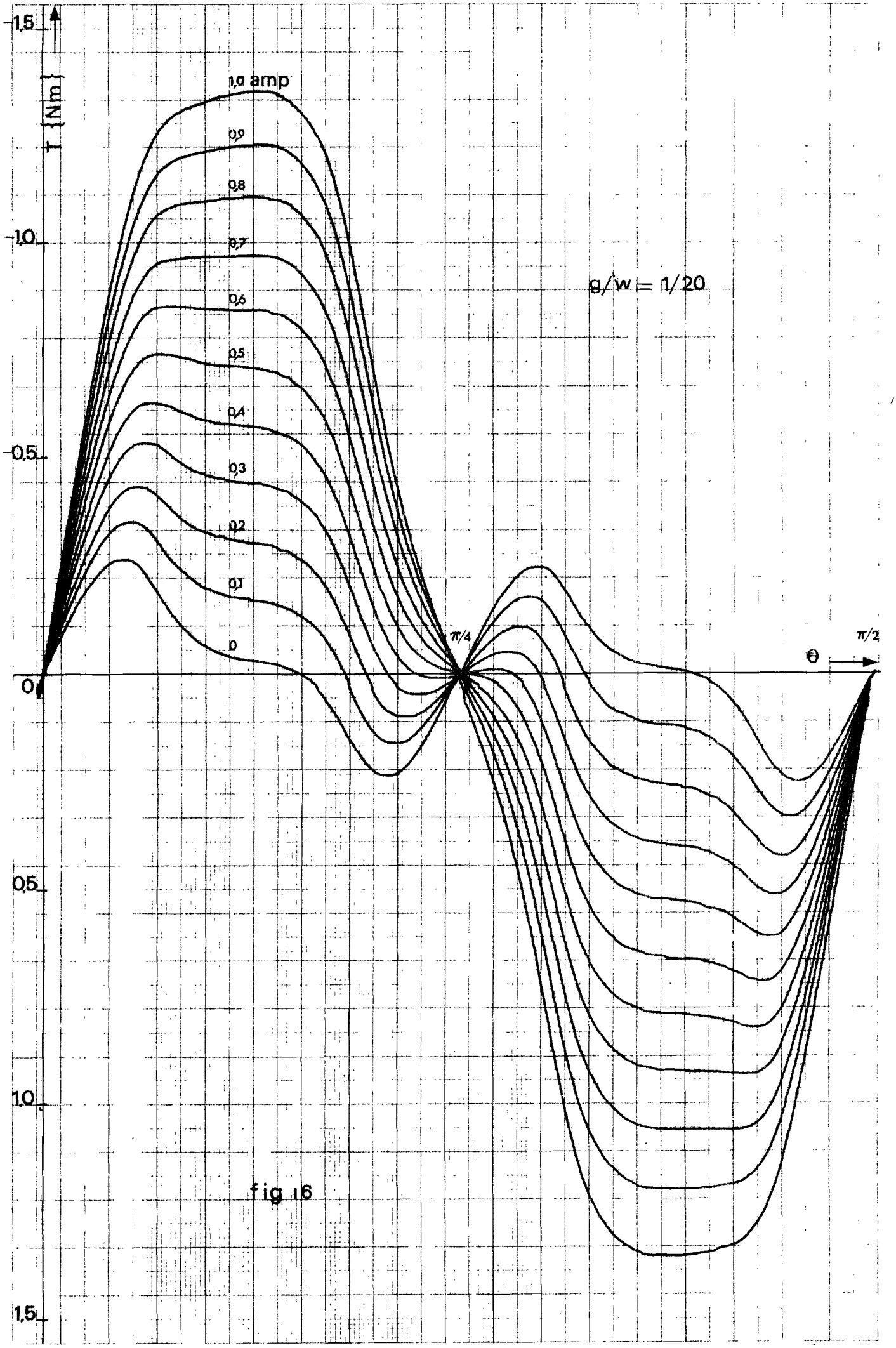
1,5
1,0
0,5
0
0,5
1,0
1,5
T {Nm}
1,0 amp
0,9
0,8
0,7
0,6
0,5
0,4
0,3
0,2
0,1
0
g/w = 1/20
π/4
π/2
θ

fig 16

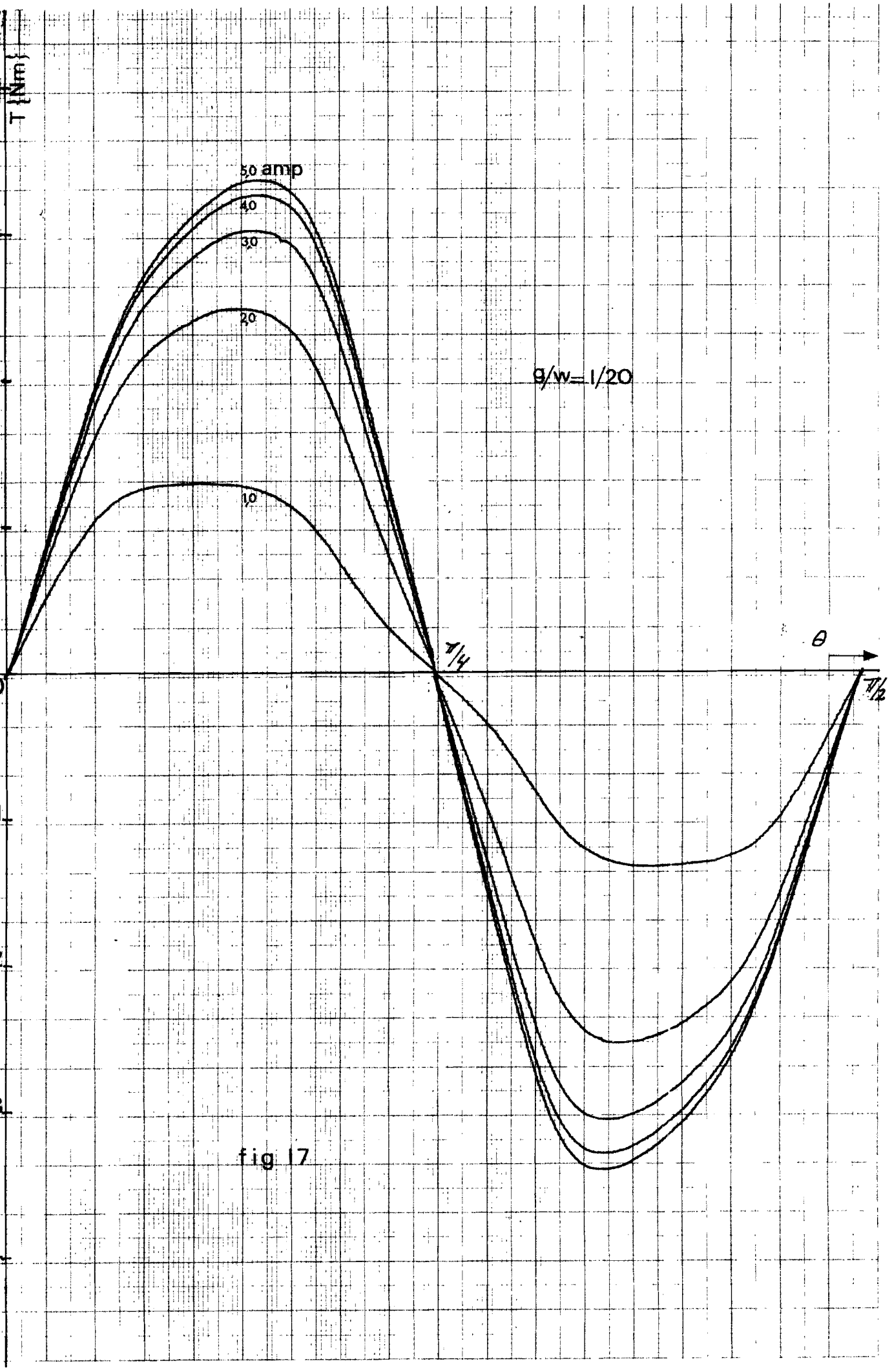


fig 17

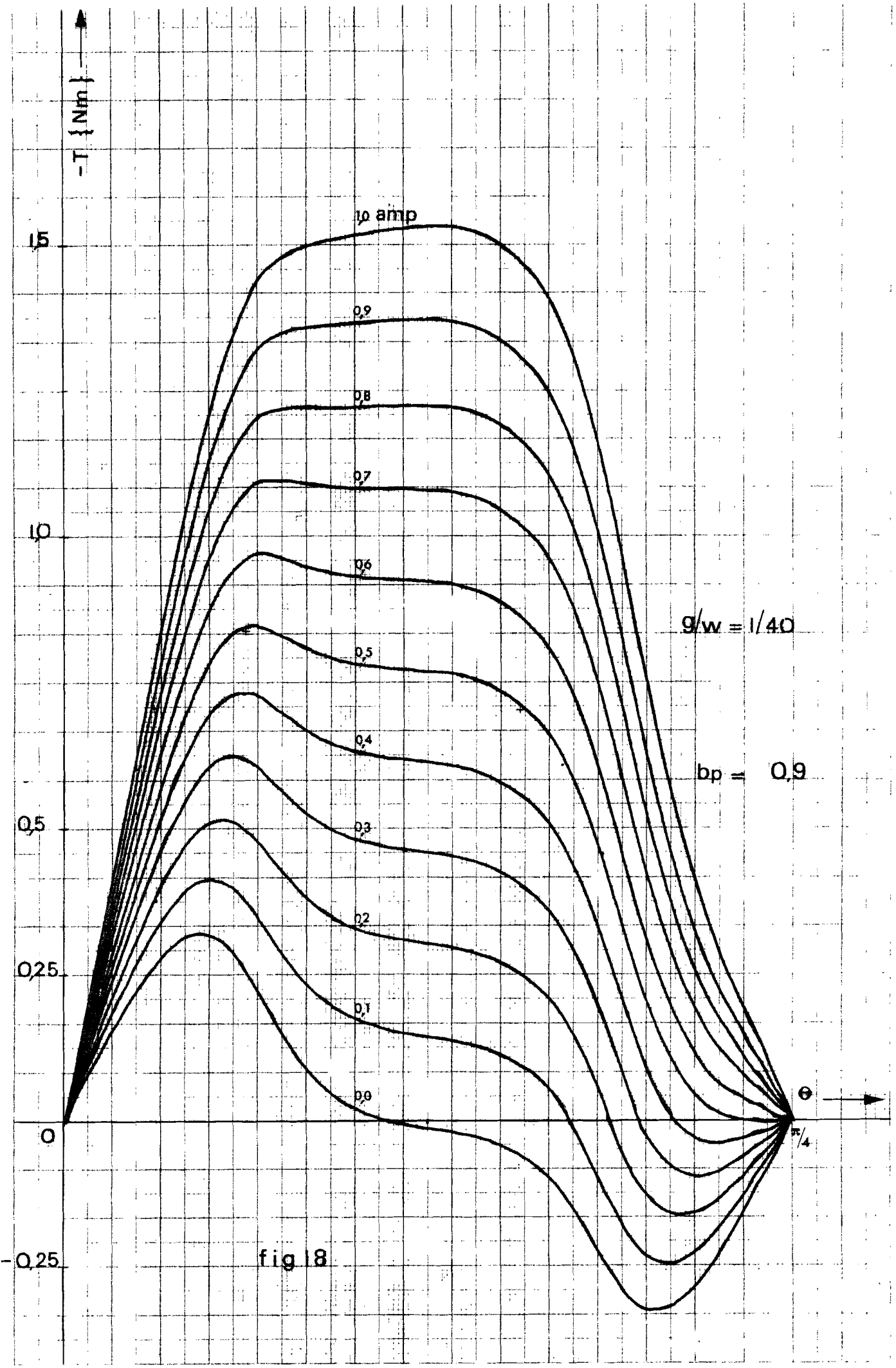
-T {Nm}
1,0 amp
0,9
0,8
0,7
0,6
0,5
0,4
0,3
0,2
0,1
0,0
1,5
1,0
0,5
0,25
0
-0,25
g/w = 1/40
bp = 0,9
θ
π/4

fig 18

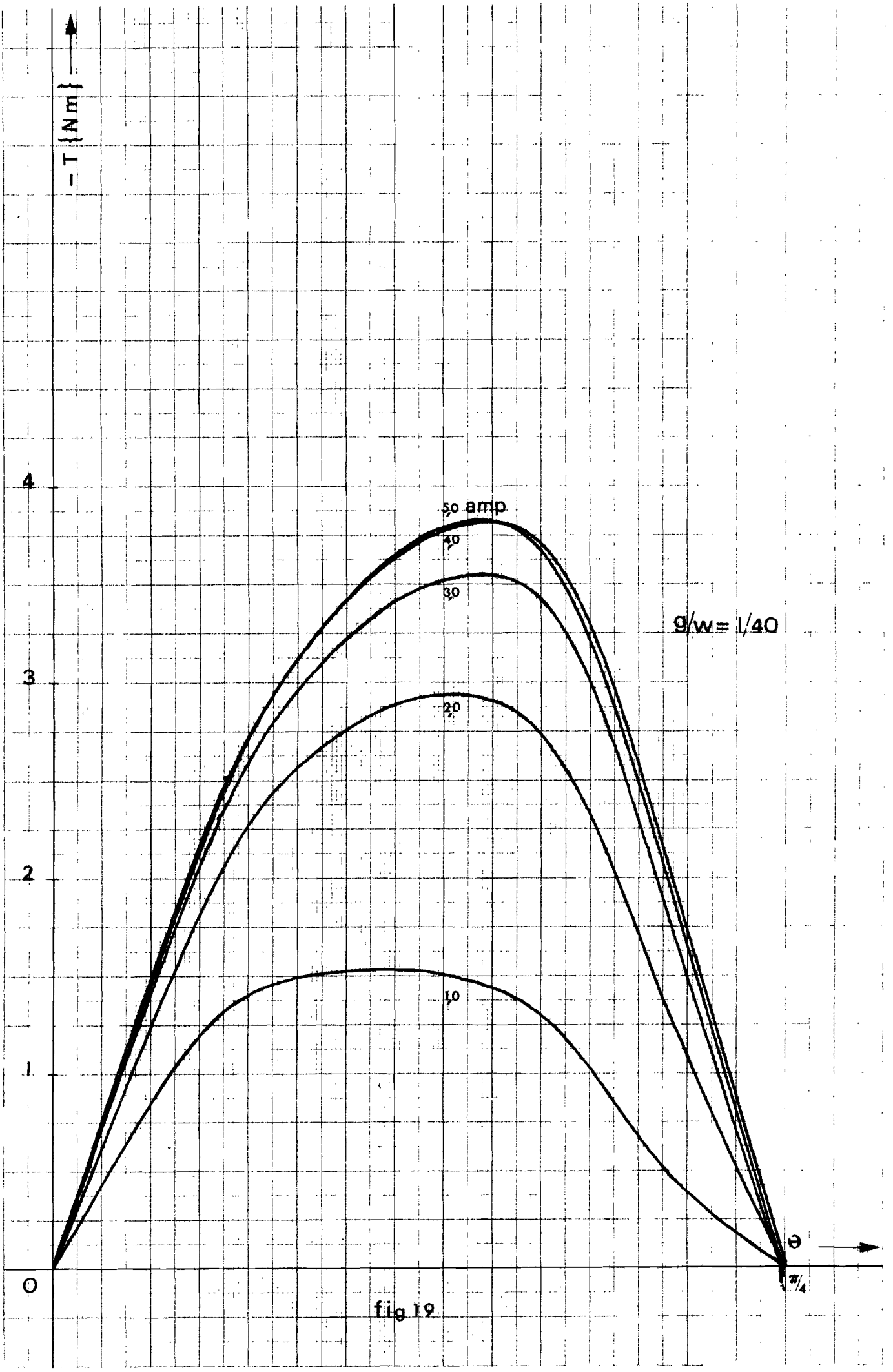


fig 19

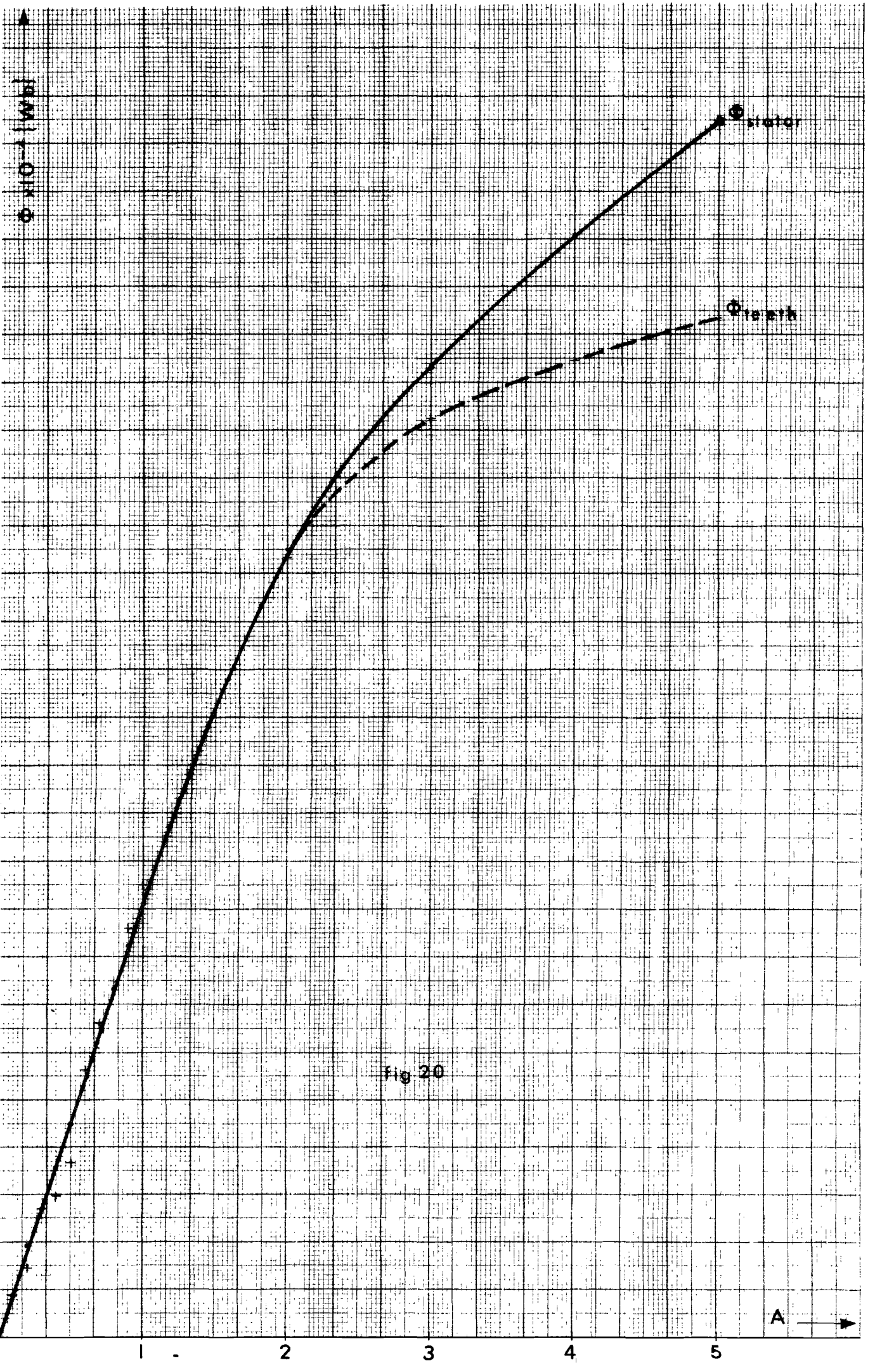


Fig 20

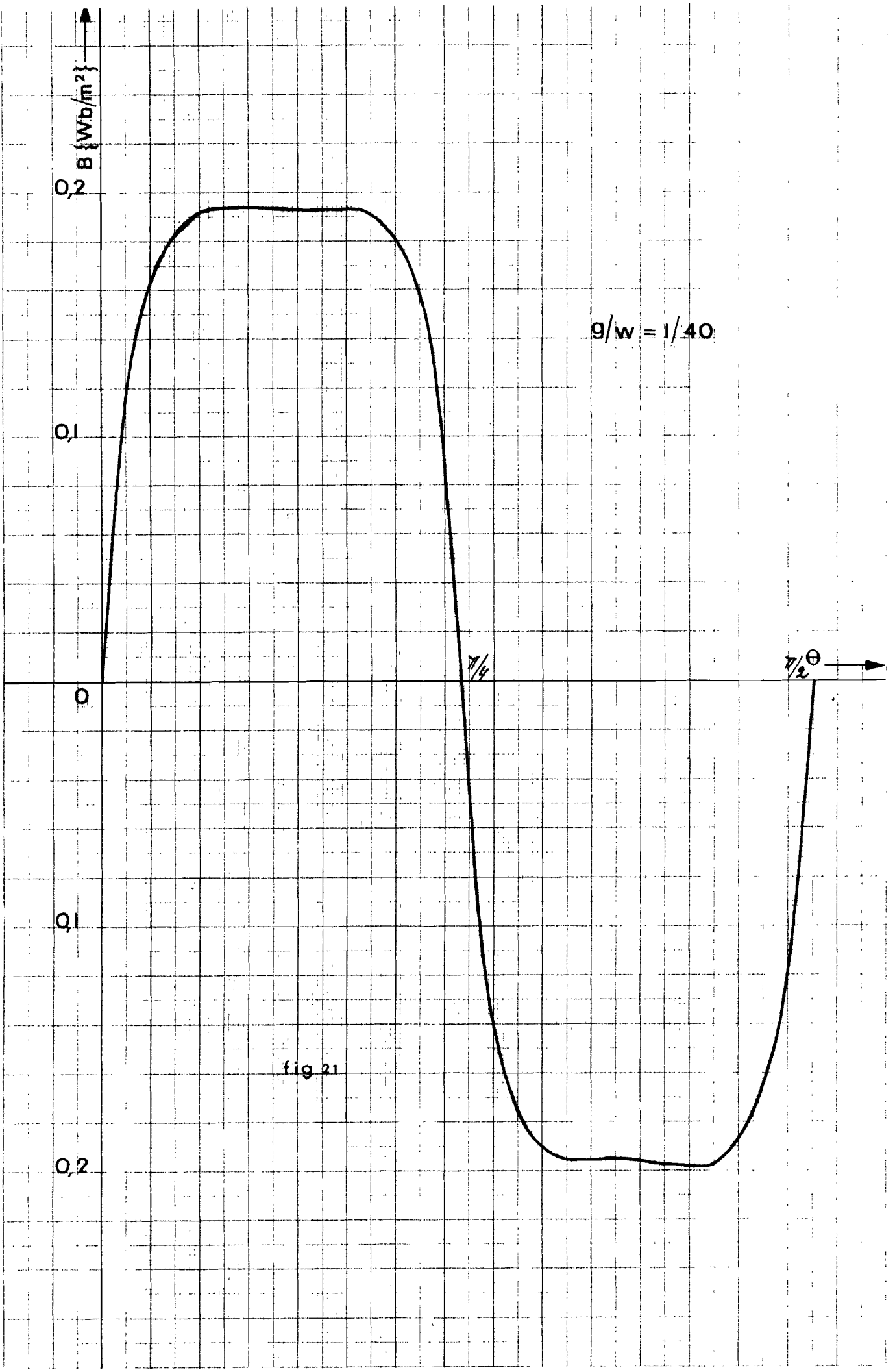


fig 21

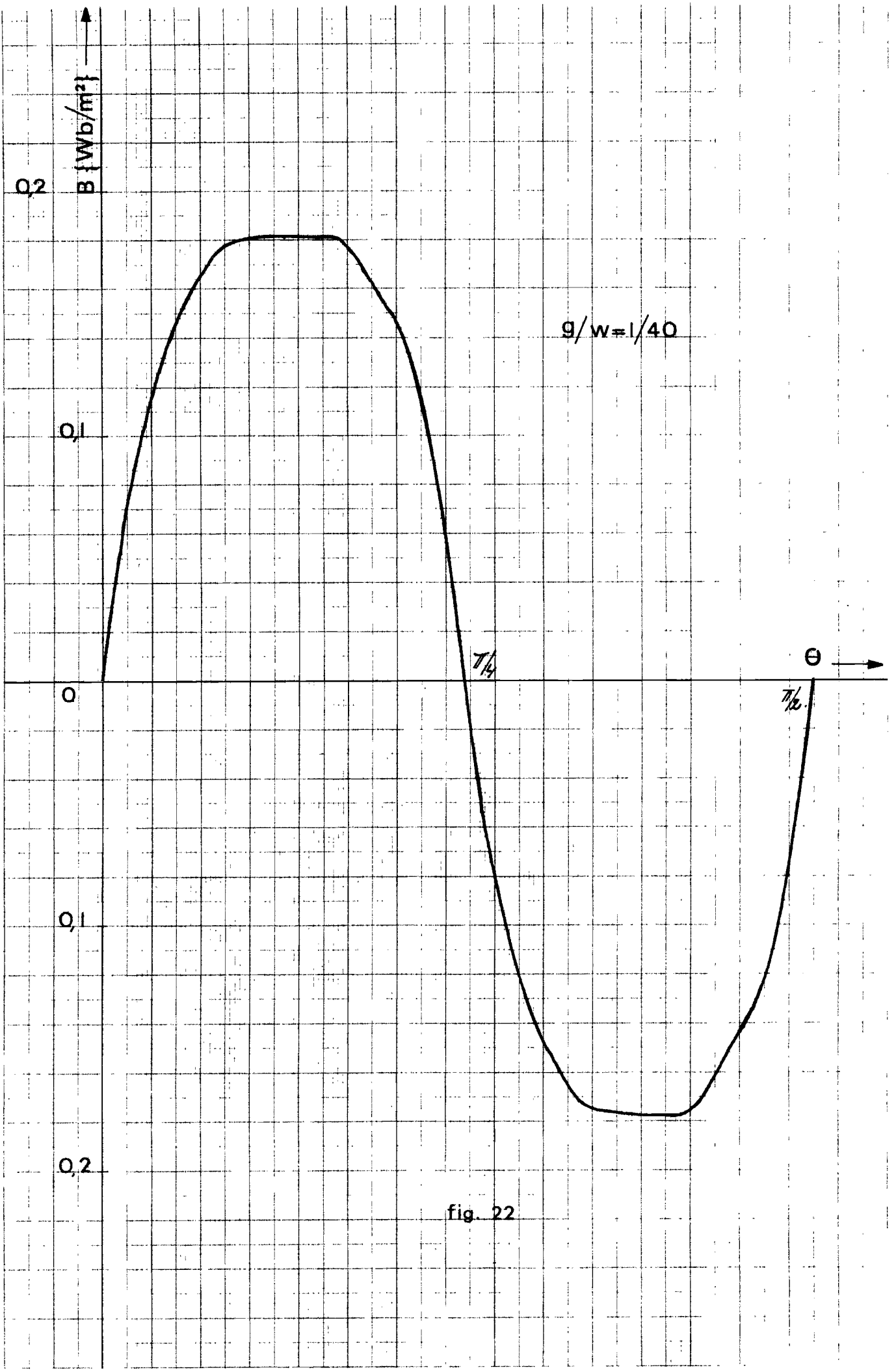


fig. 22

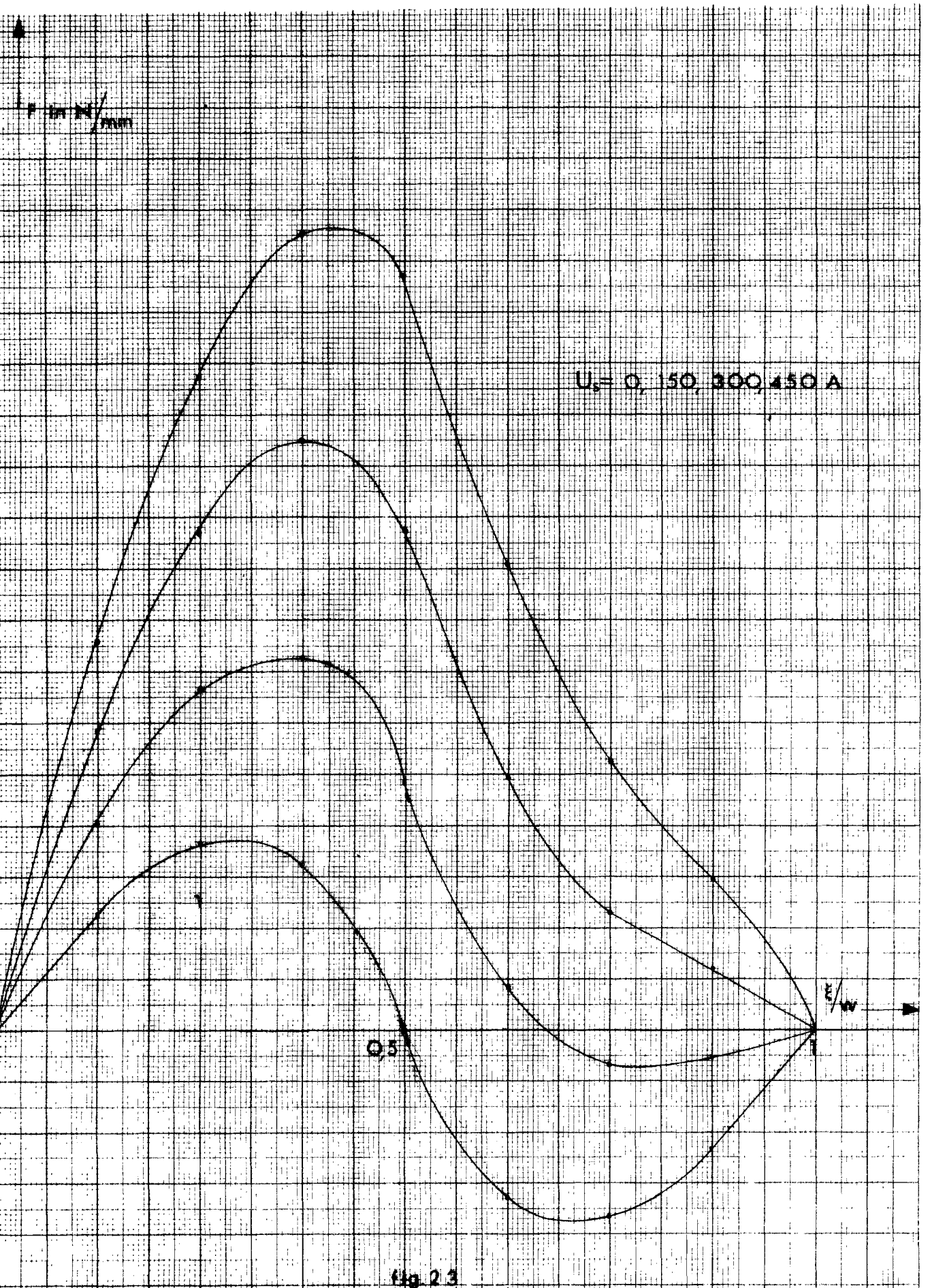


fig. 2 3

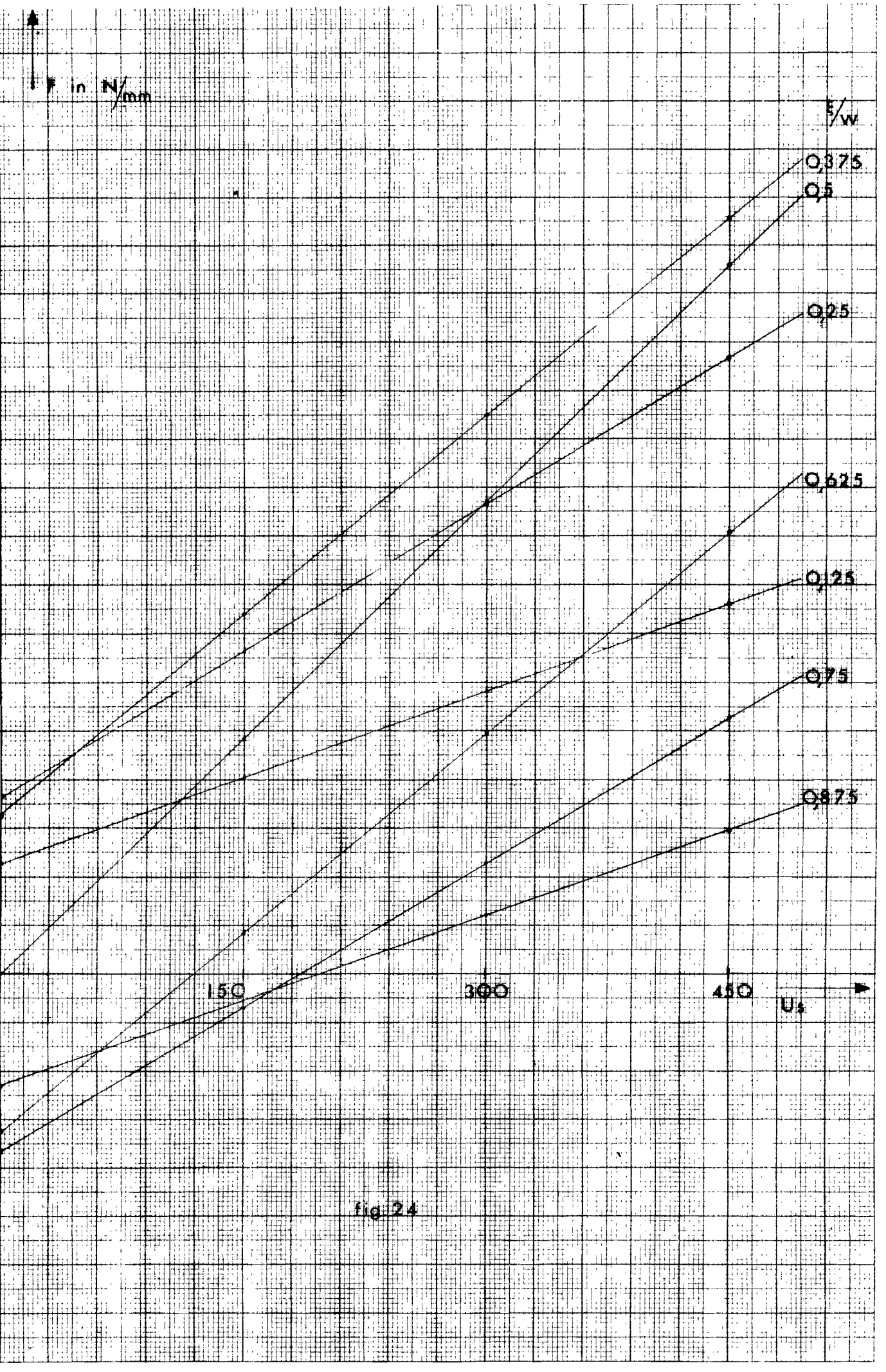


fig. 24

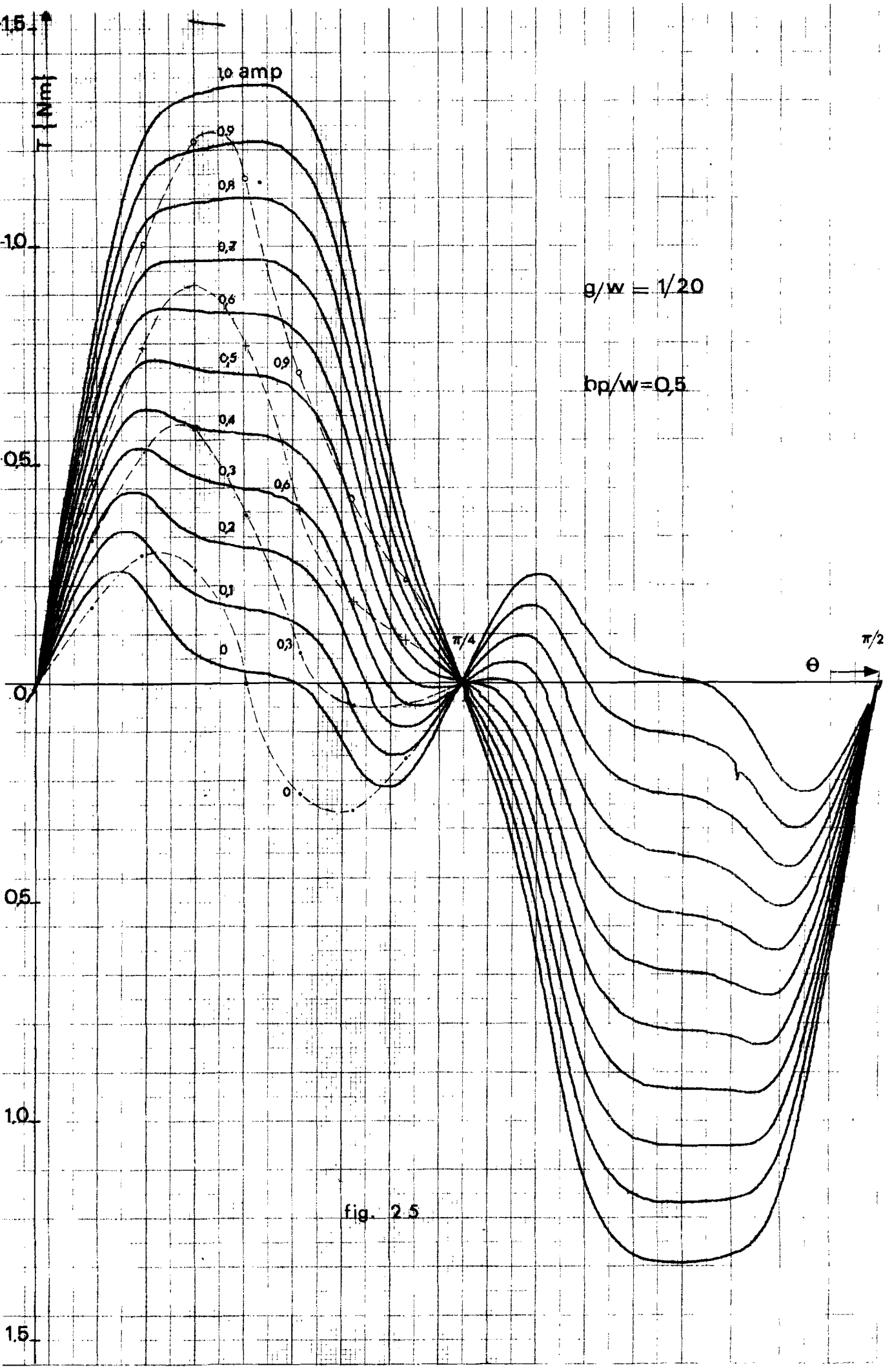
T (Nm)
1,5
1,0
0,5
0
0,5
1,0
1,5
1,0 amp
0,9
0,8
0,7
0,6
0,5
0,4
0,3
0,2
0,1
0
0,9
0,6
0,3
0
π/4
π/2
θ
g/w = 1/20
bp/w=0,5

fig. 2.5

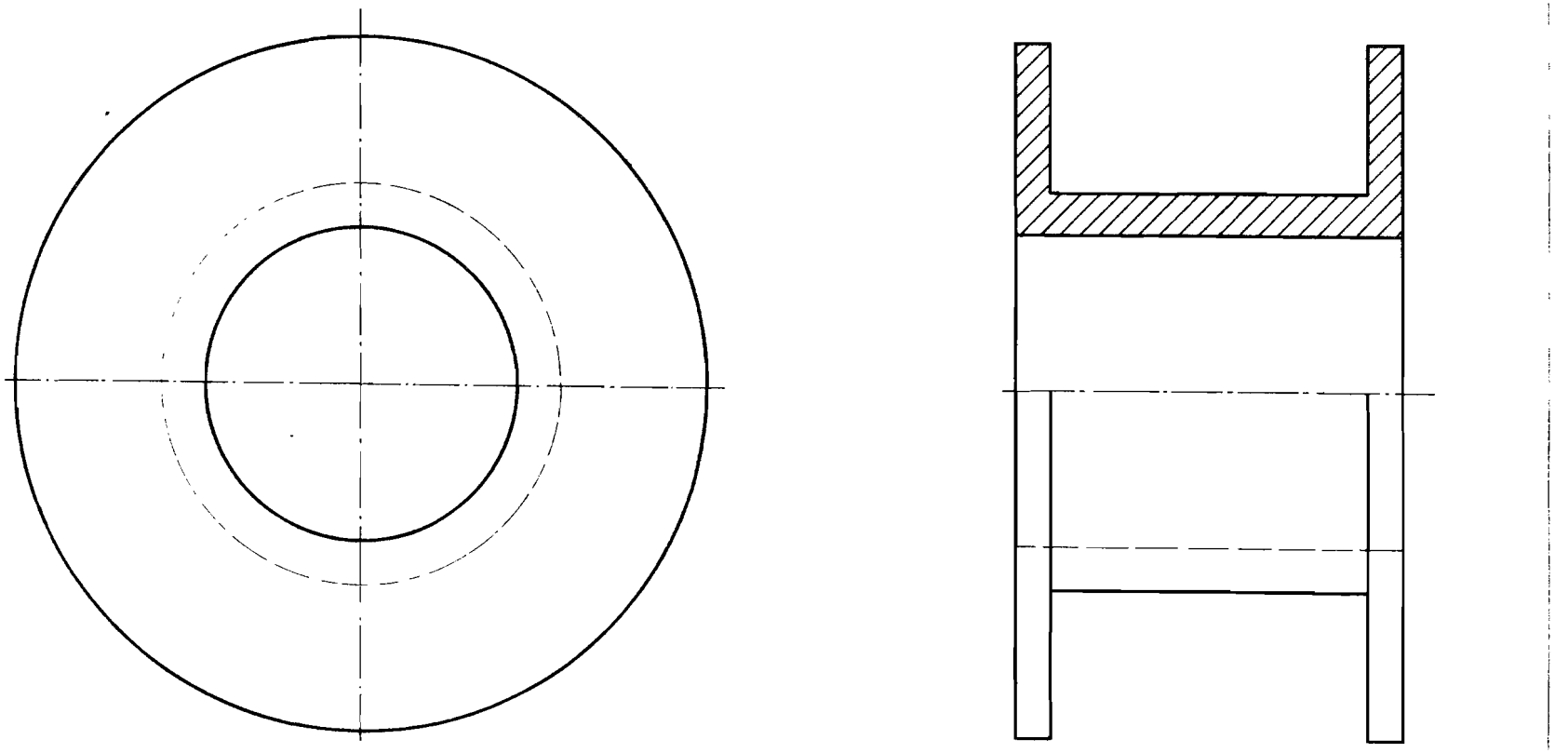

fig 26

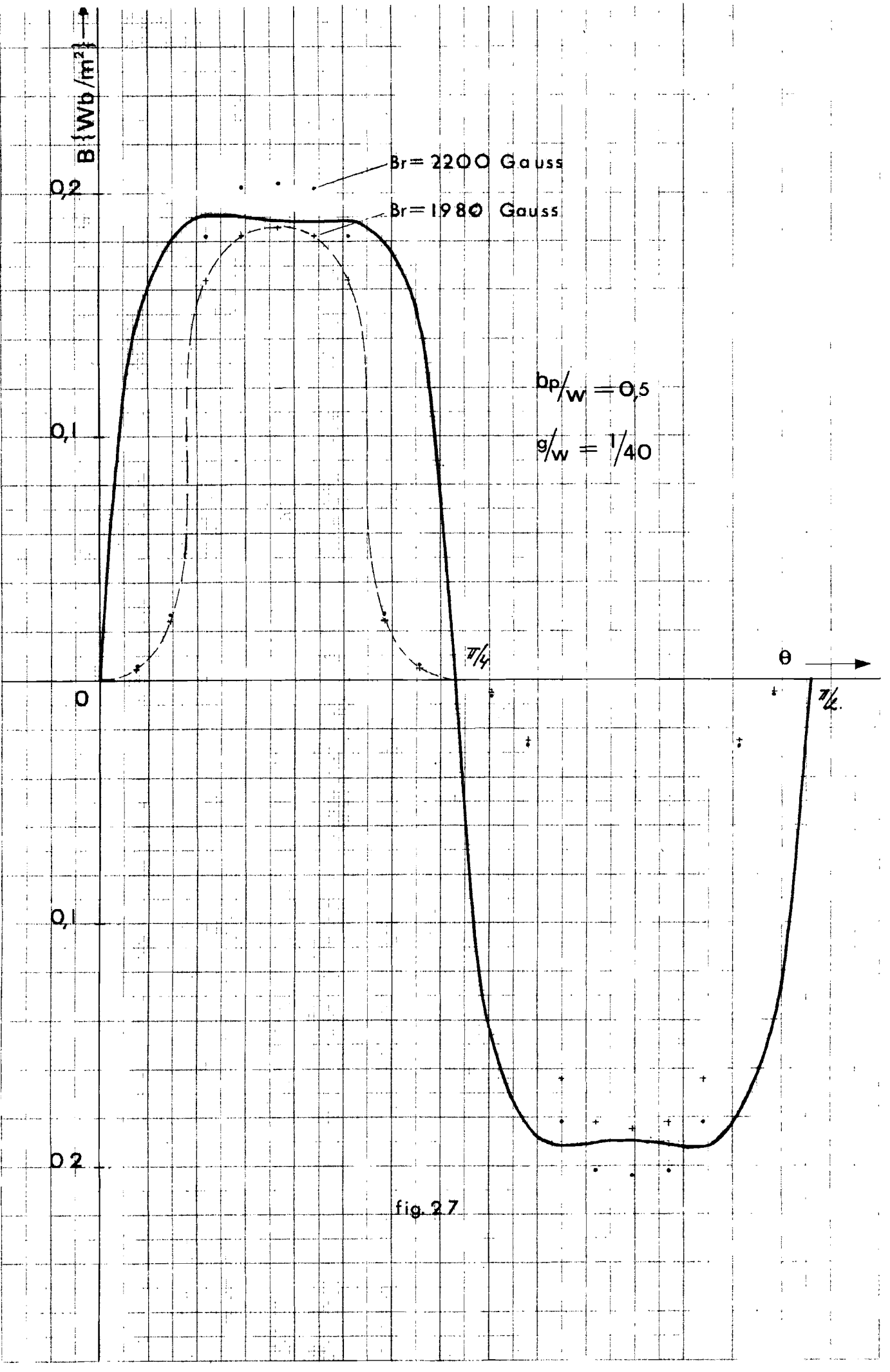
B [Wb/m²]
0,2
0,1
0
0,1
0,2
Br = 2200 Gauss
Br = 1980 Gauss
bp/w = 0,5
g/w = 1/40
π/4
θ
π/2

fig. 27

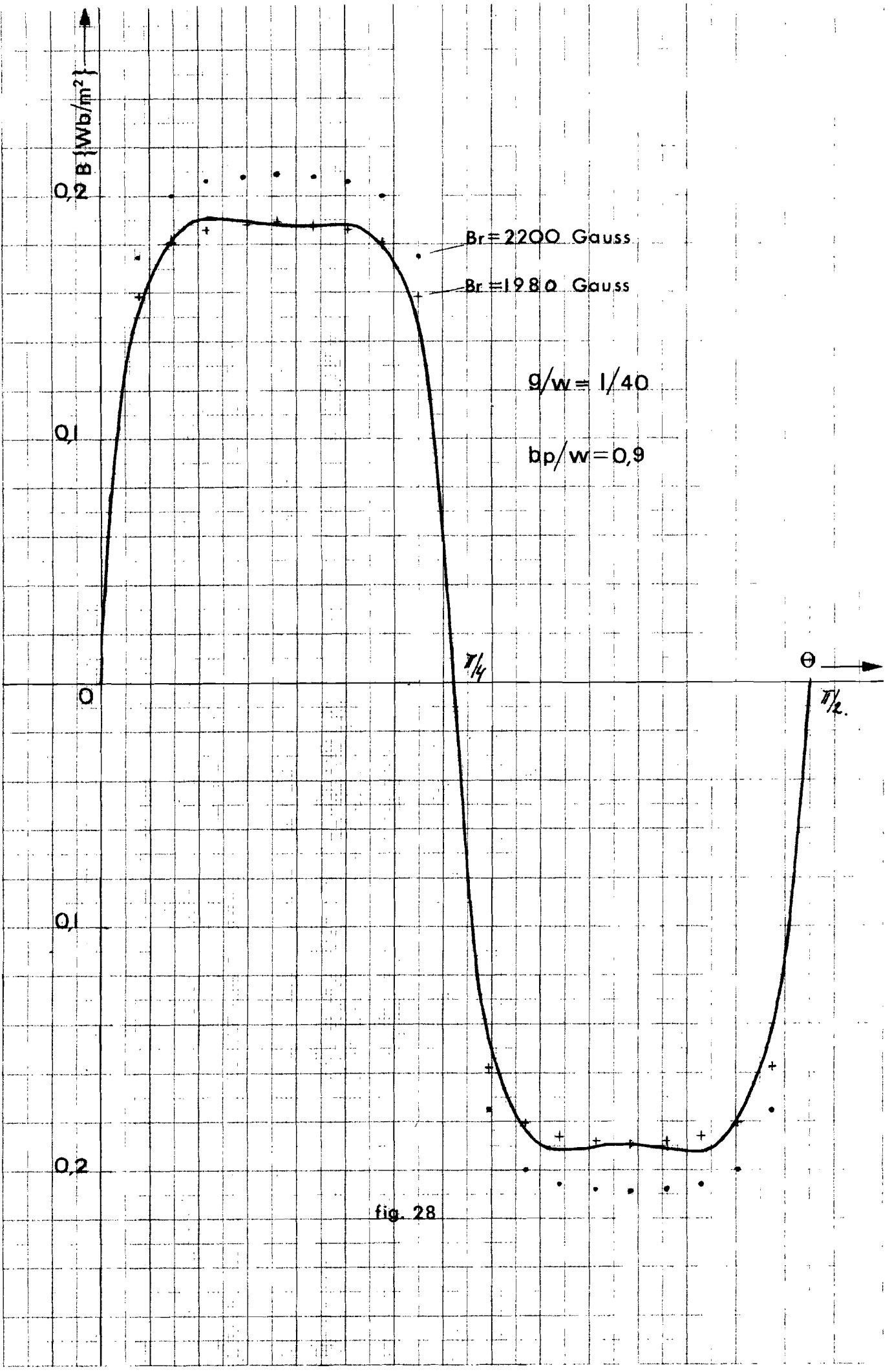
B {Wb/m²}
0,2
0,1
0
0,1
0,2
Br = 2200 Gauss
Br = 1980 Gauss
g/w = 1/40
bp/w = 0,9
π/4
θ
π/2.

fig. 28

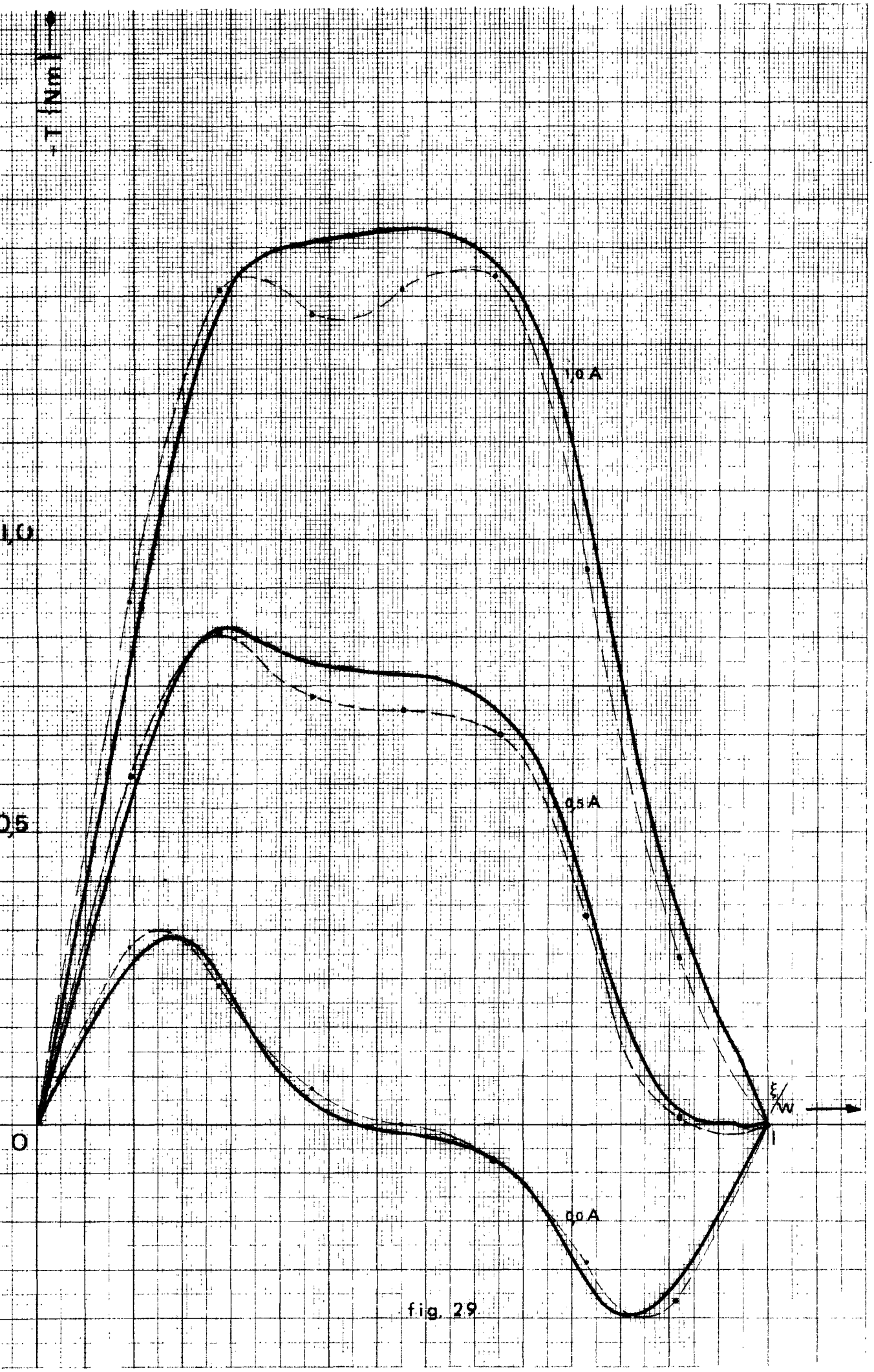


fig. 29

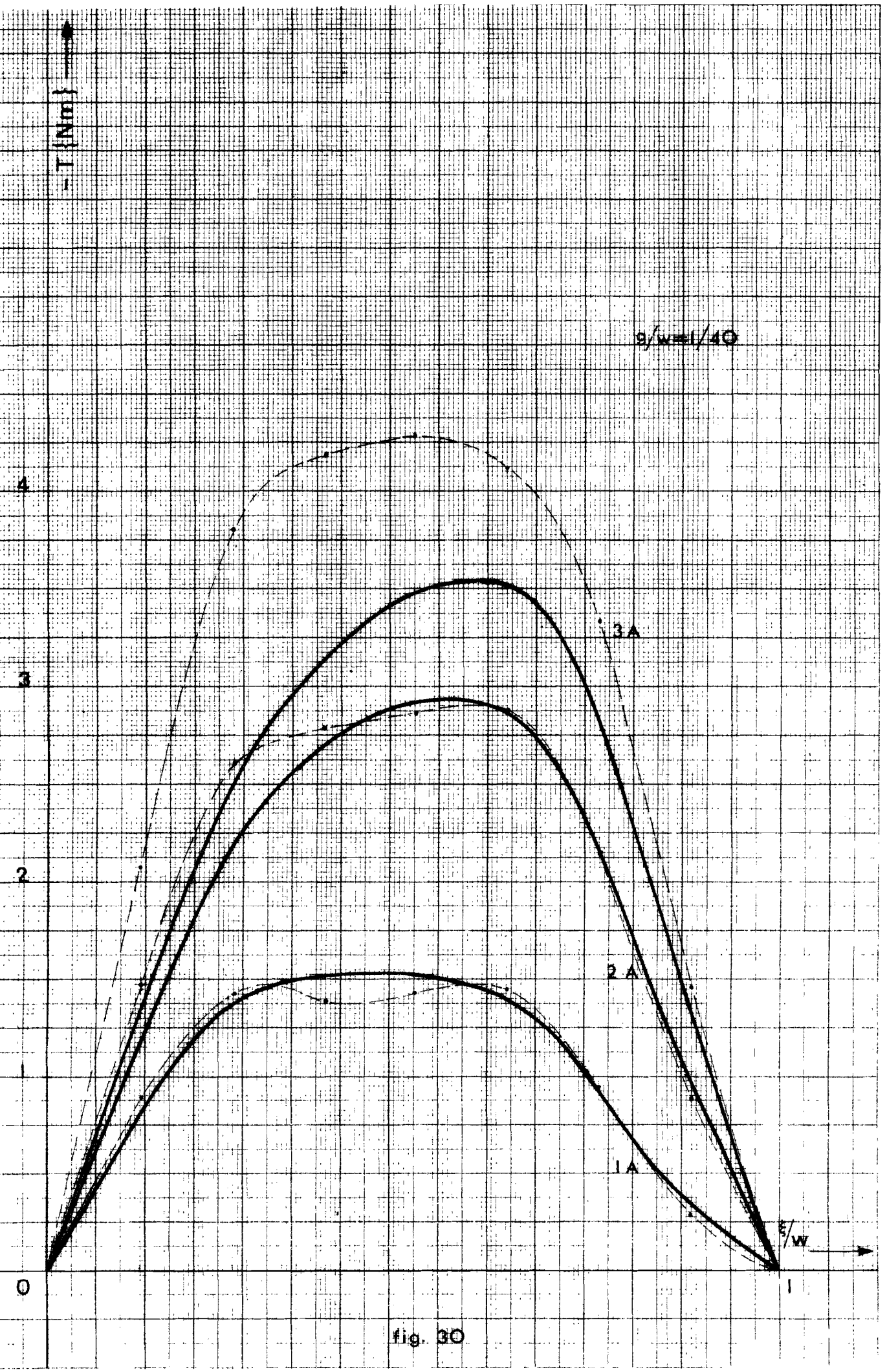


fig. 30

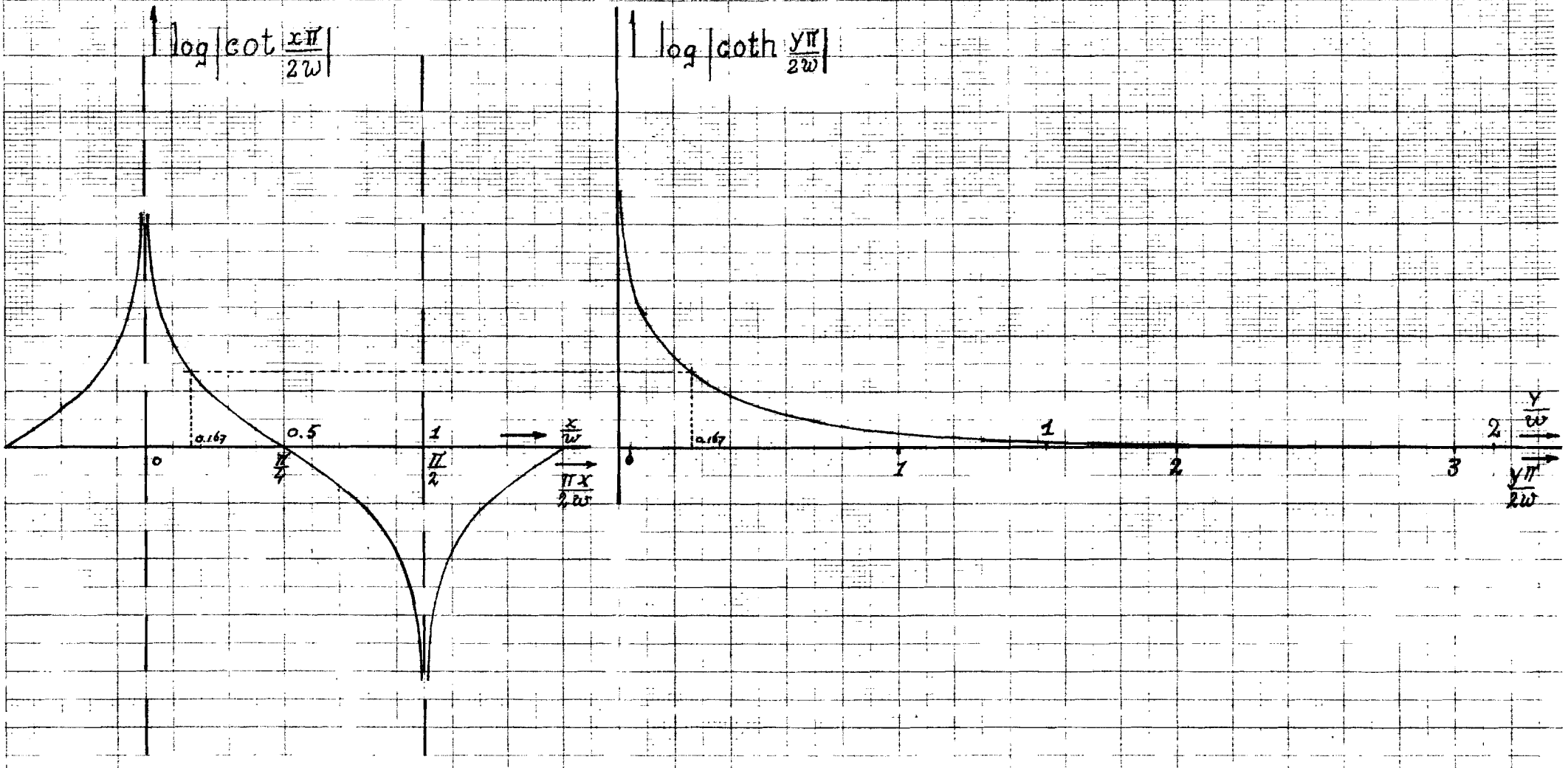


graph. A1a

graph. A1b

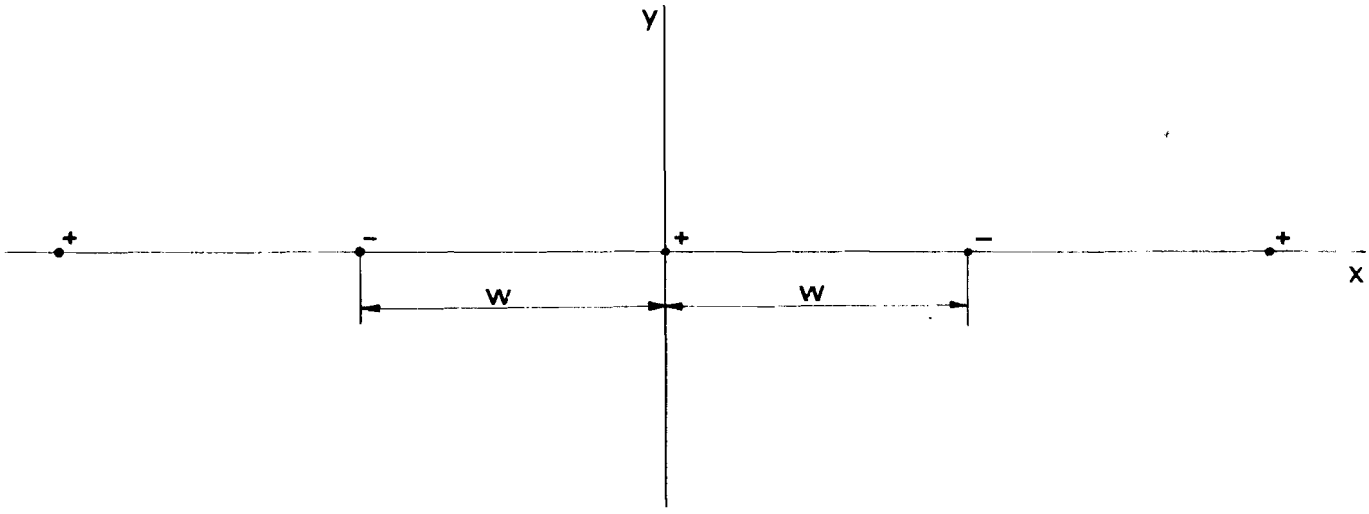


fig. A I a

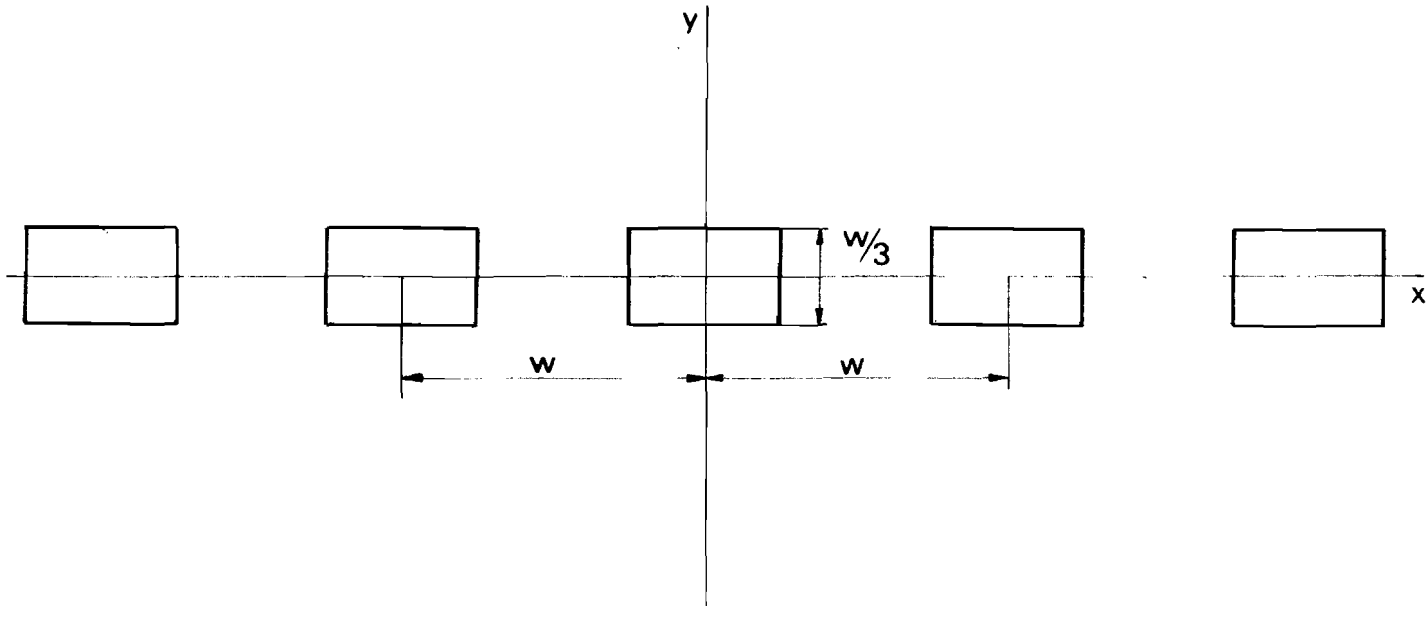


fig. A I b

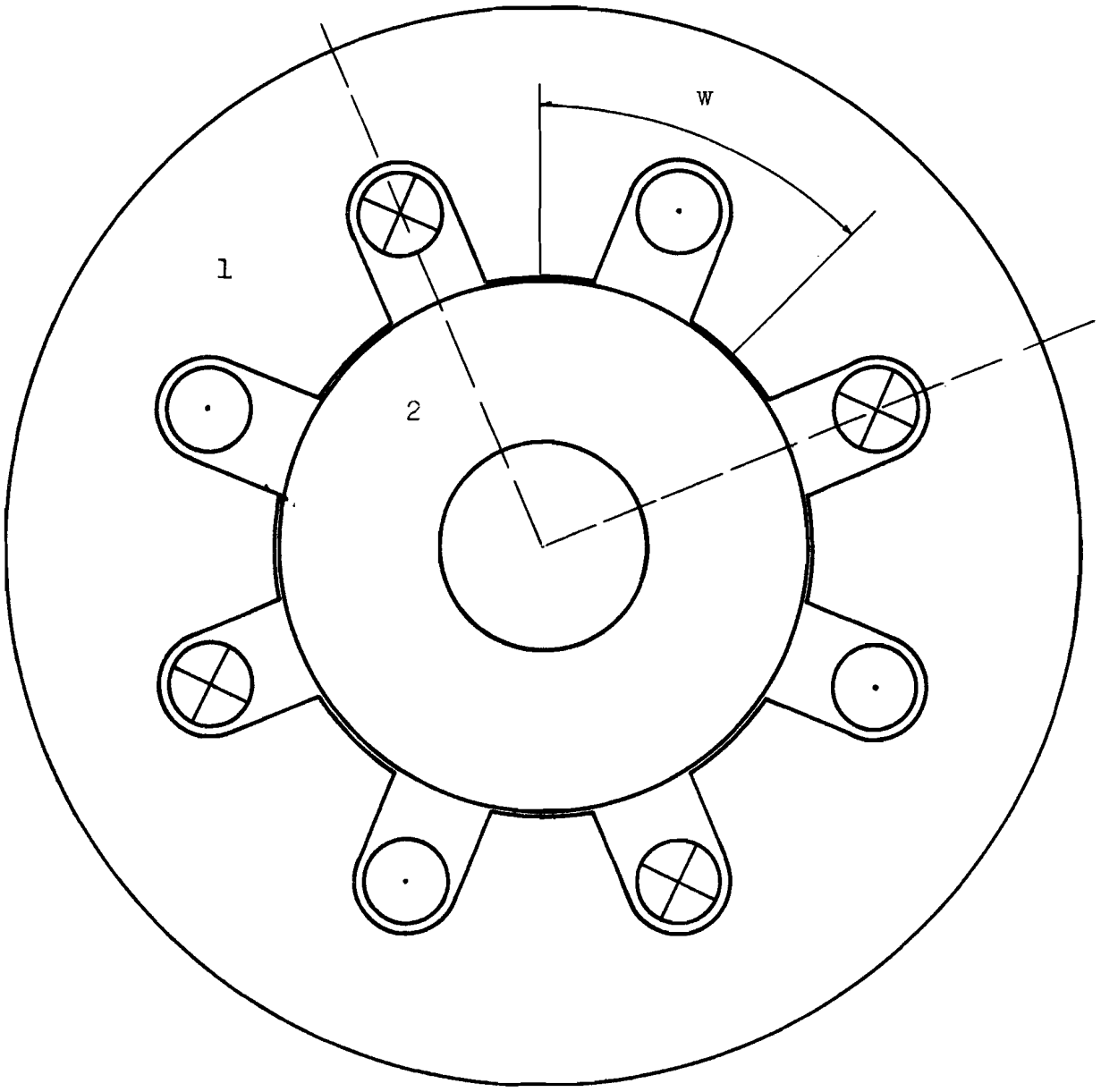


1. Laminated soft iron.

2. Ferroxdure 100.

fig. B 1.

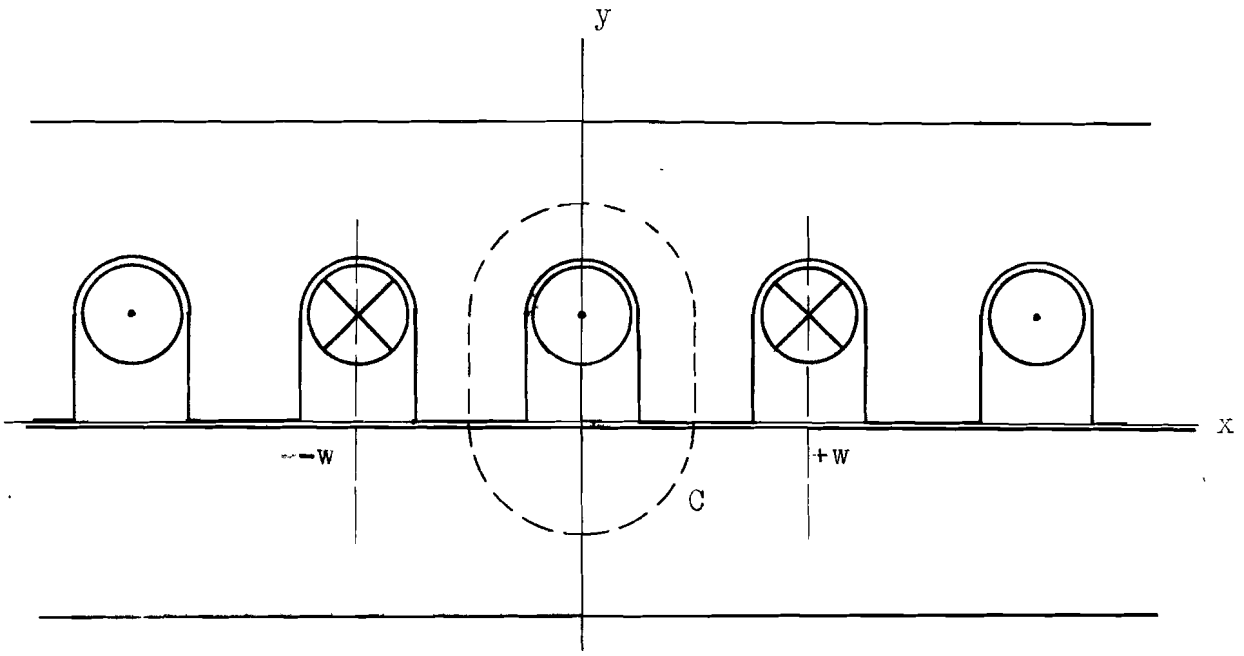


fig. 2.

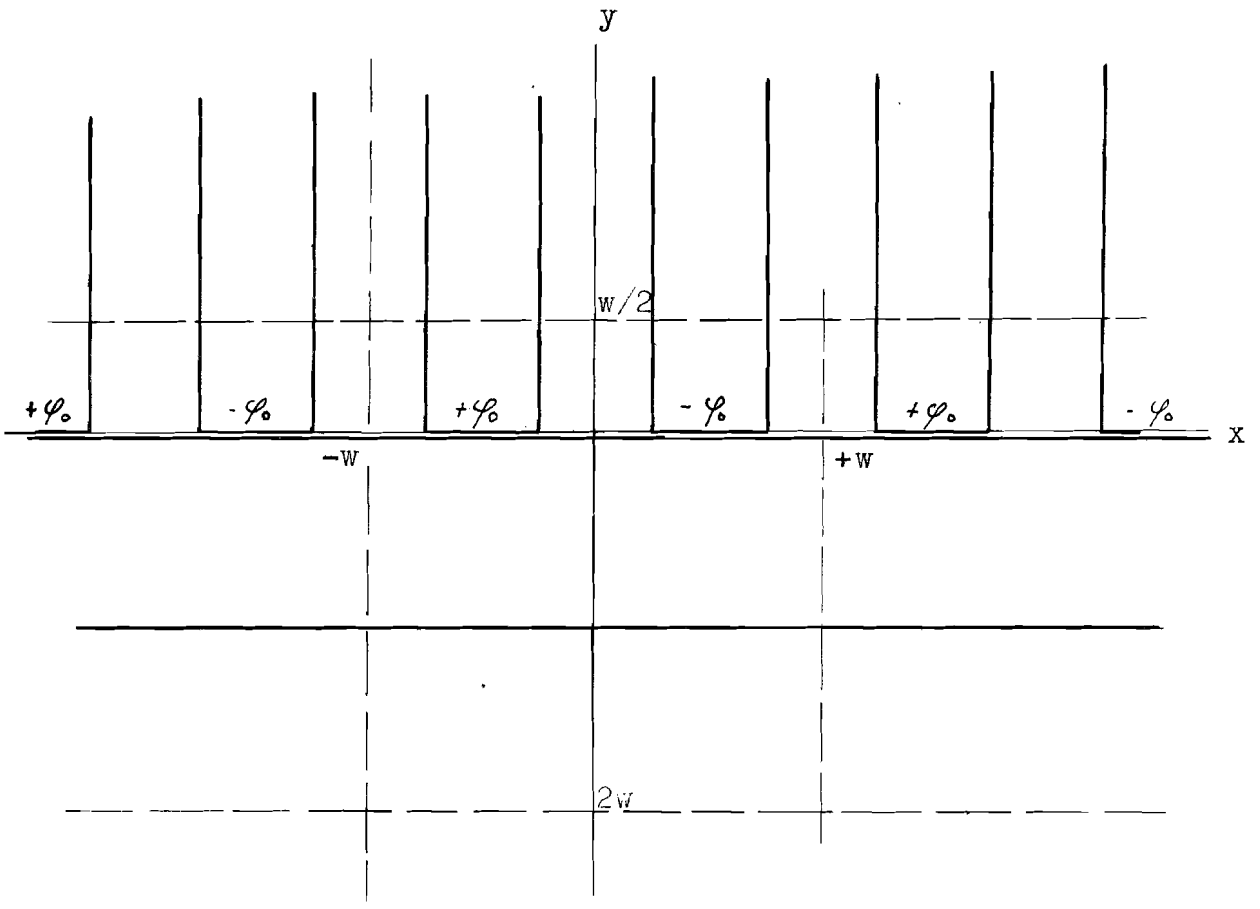


fig. B 3.

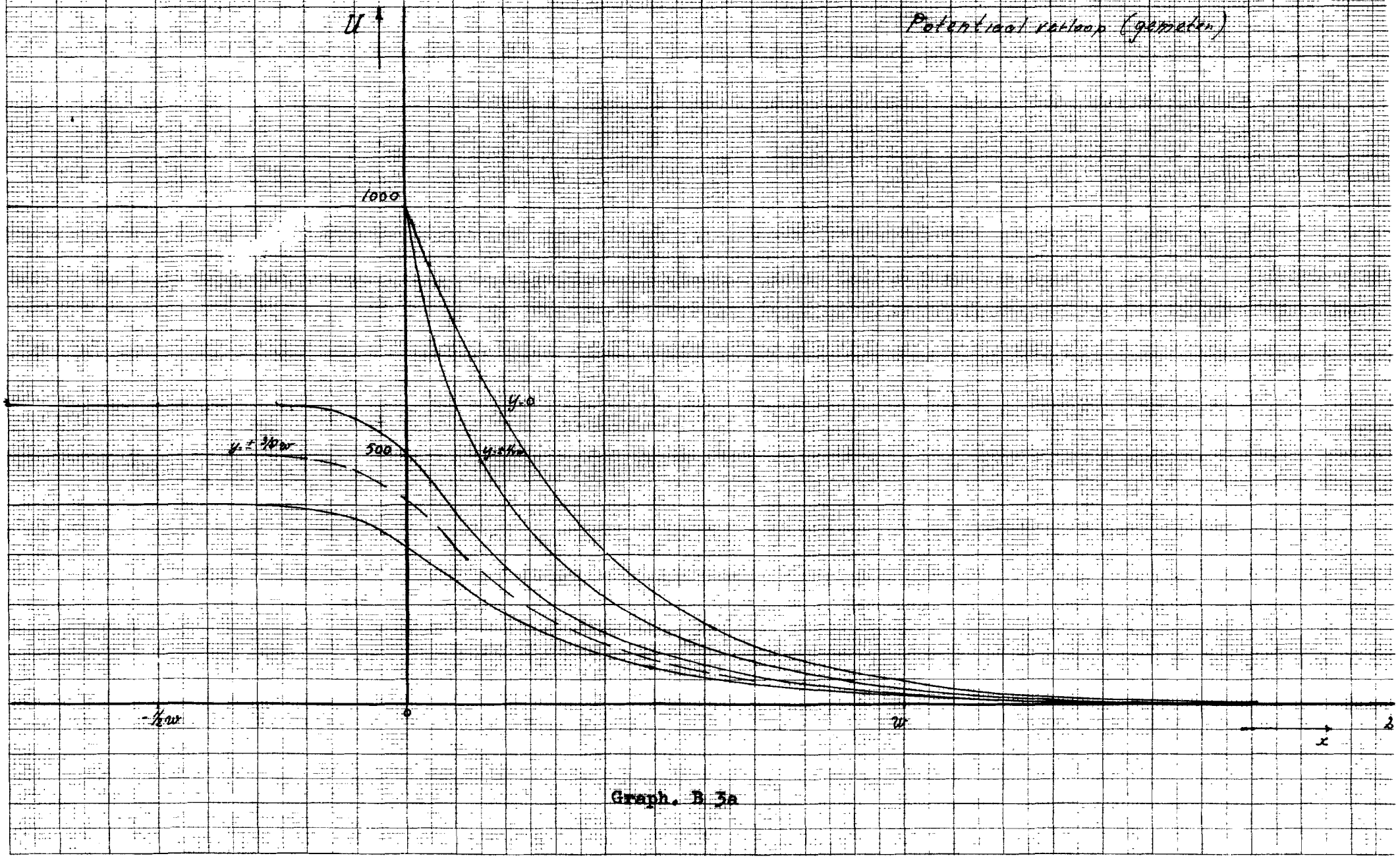


Graph. B 3a

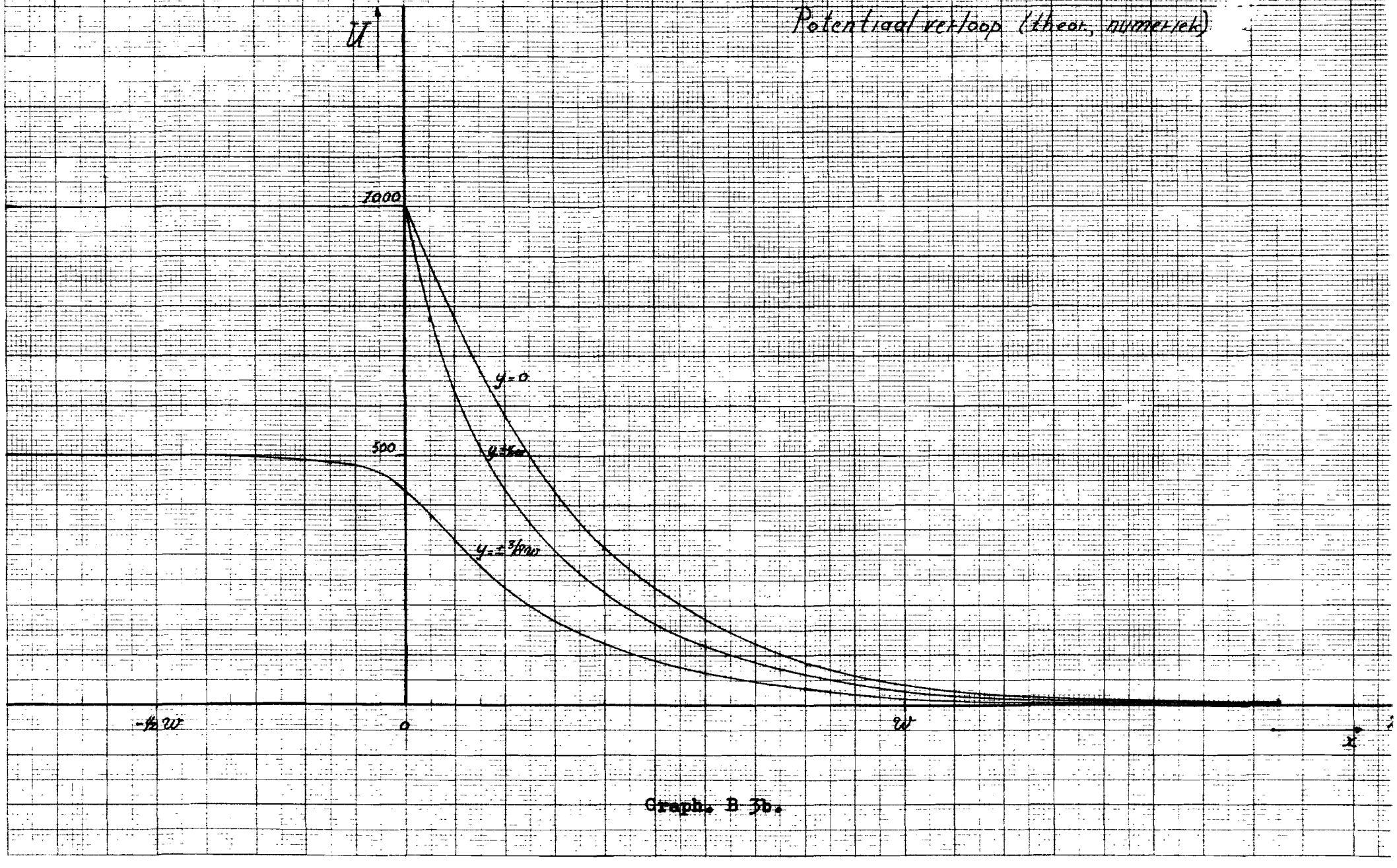


Graph. B 3b.

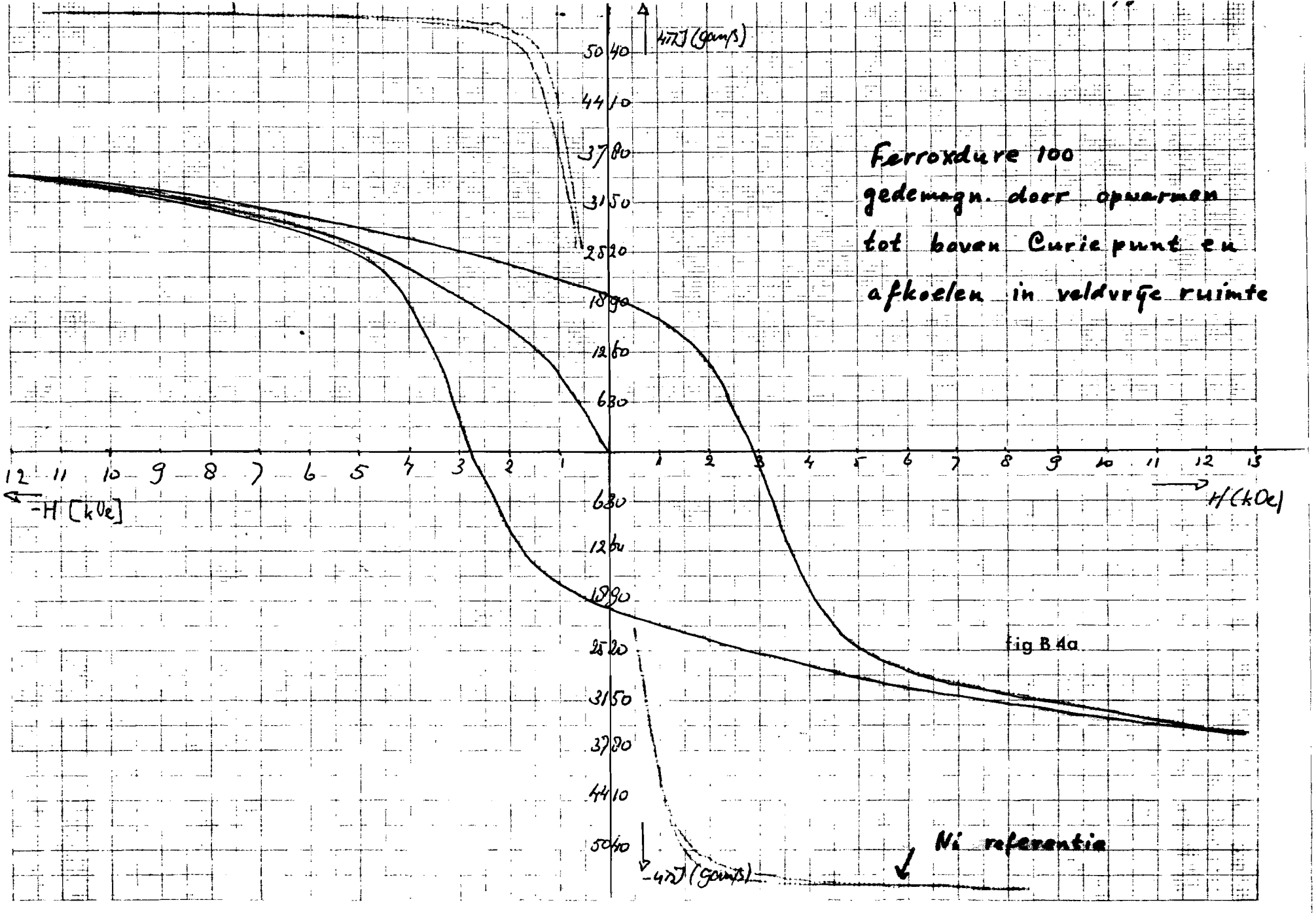
Ferroxdure 100
gedemagn. door opwarmen
tot boven Curie punt en
afkoelen in veldvrije ruimte
-H [kOe]
H (kOe)
4πJ (gauss)
-4πJ (gauss)
Ni referentie

fig B 4a

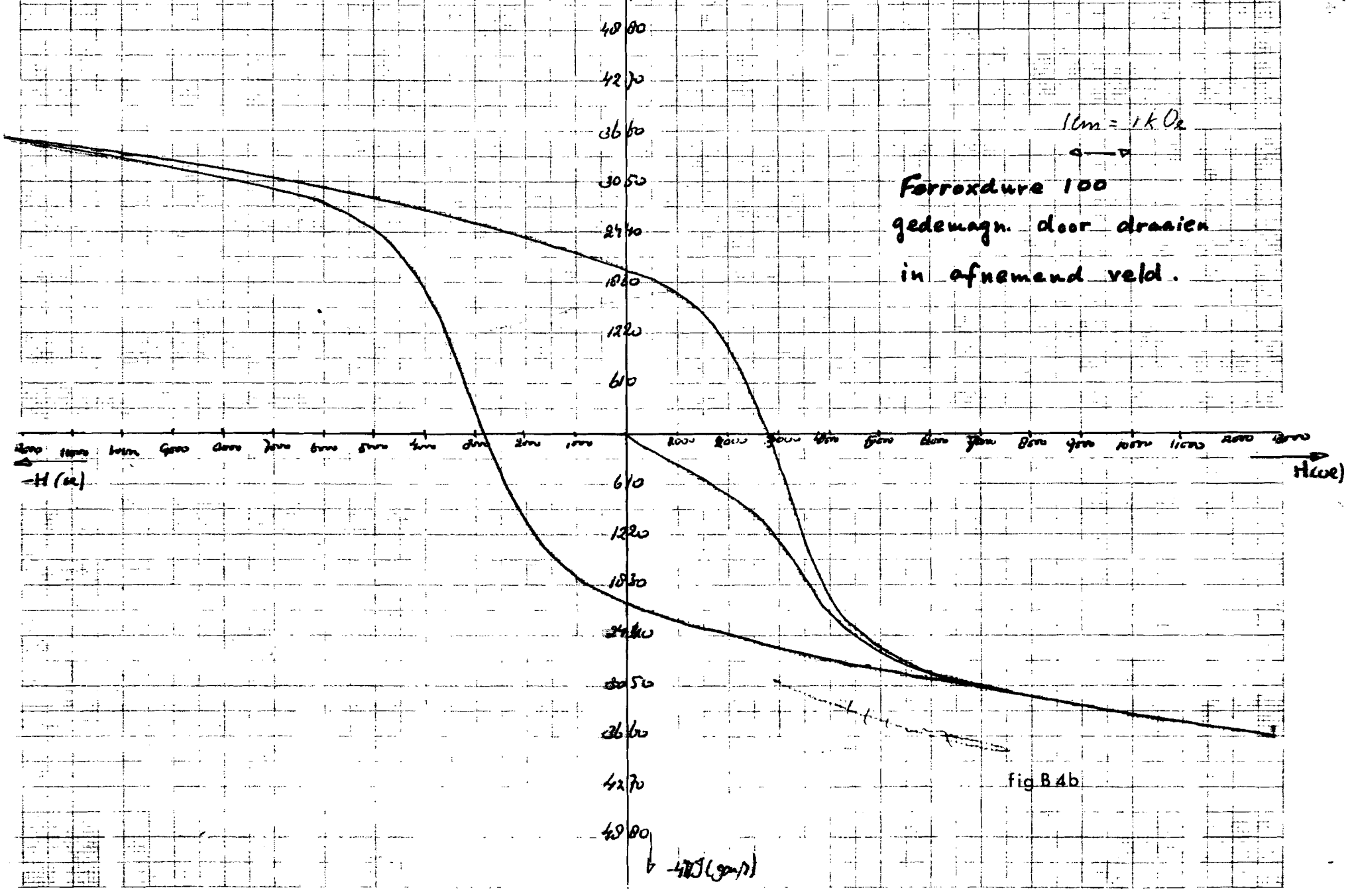
1 cm = 1 kOe
Ferroxdure 100
gedemagn. door draaien
in afnemend veld.
-H (Oe)
H (Oe)
-4πJ (gauss)

fig B 4b

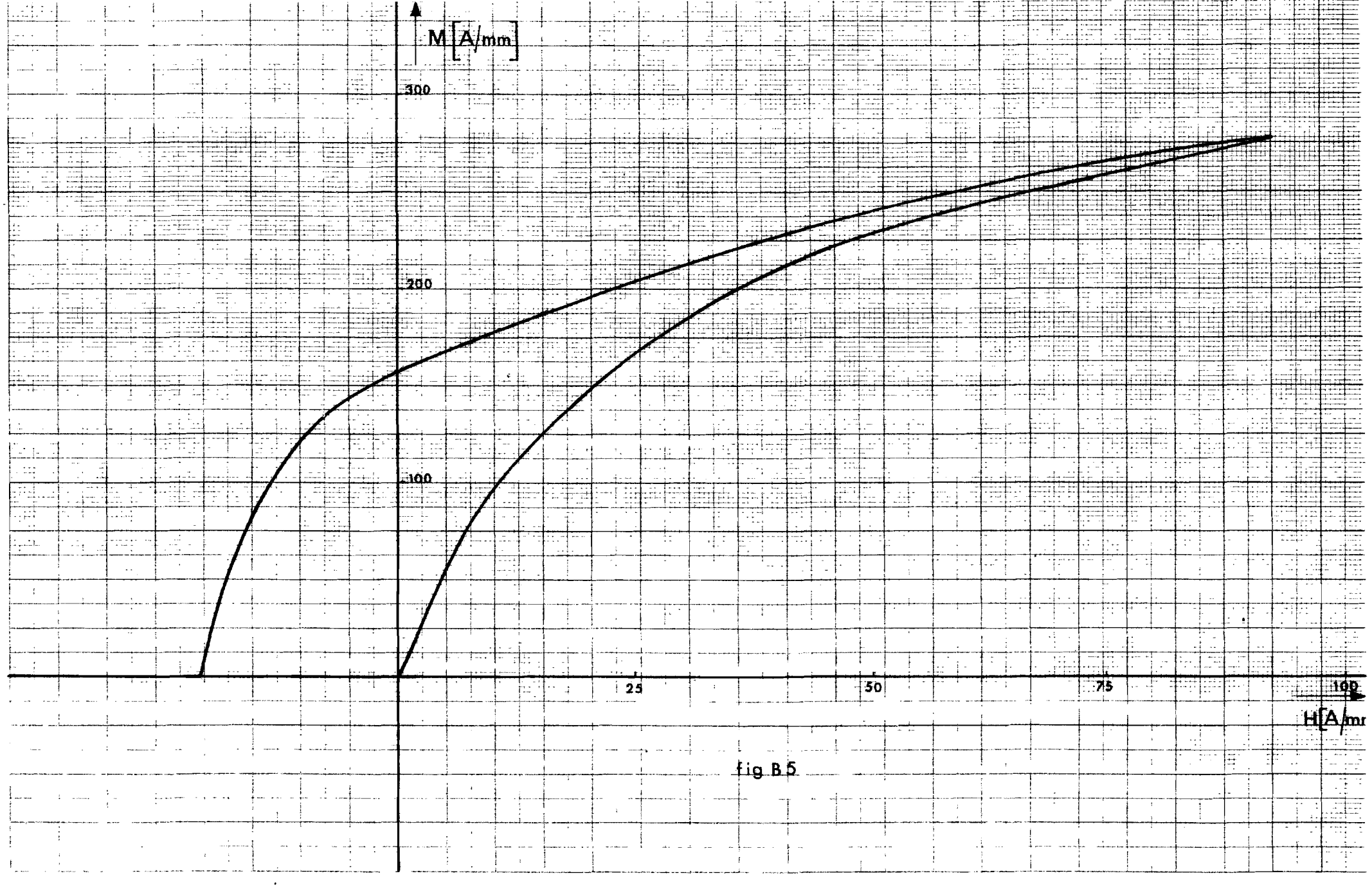


fig B 5

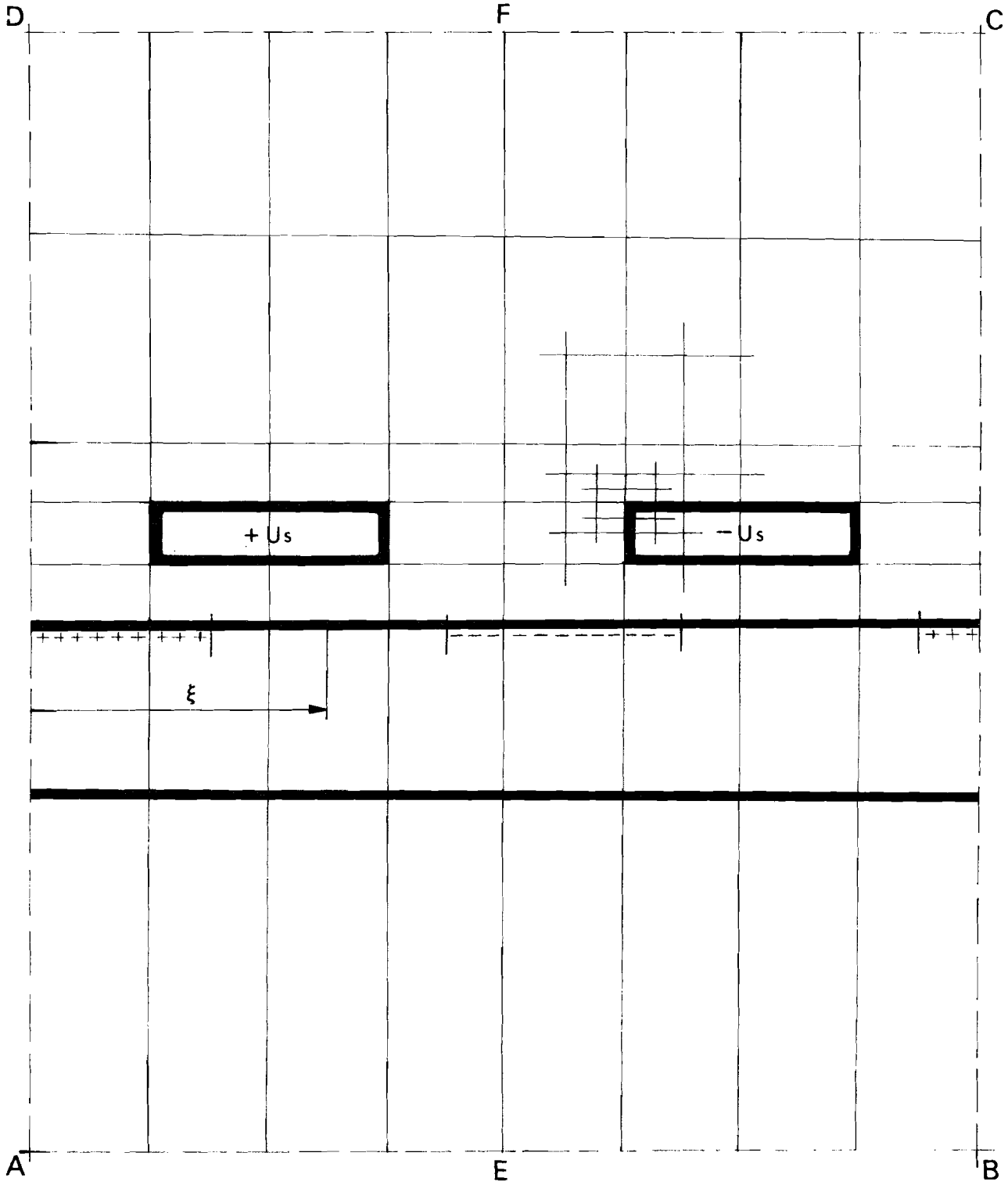


fig. 1c

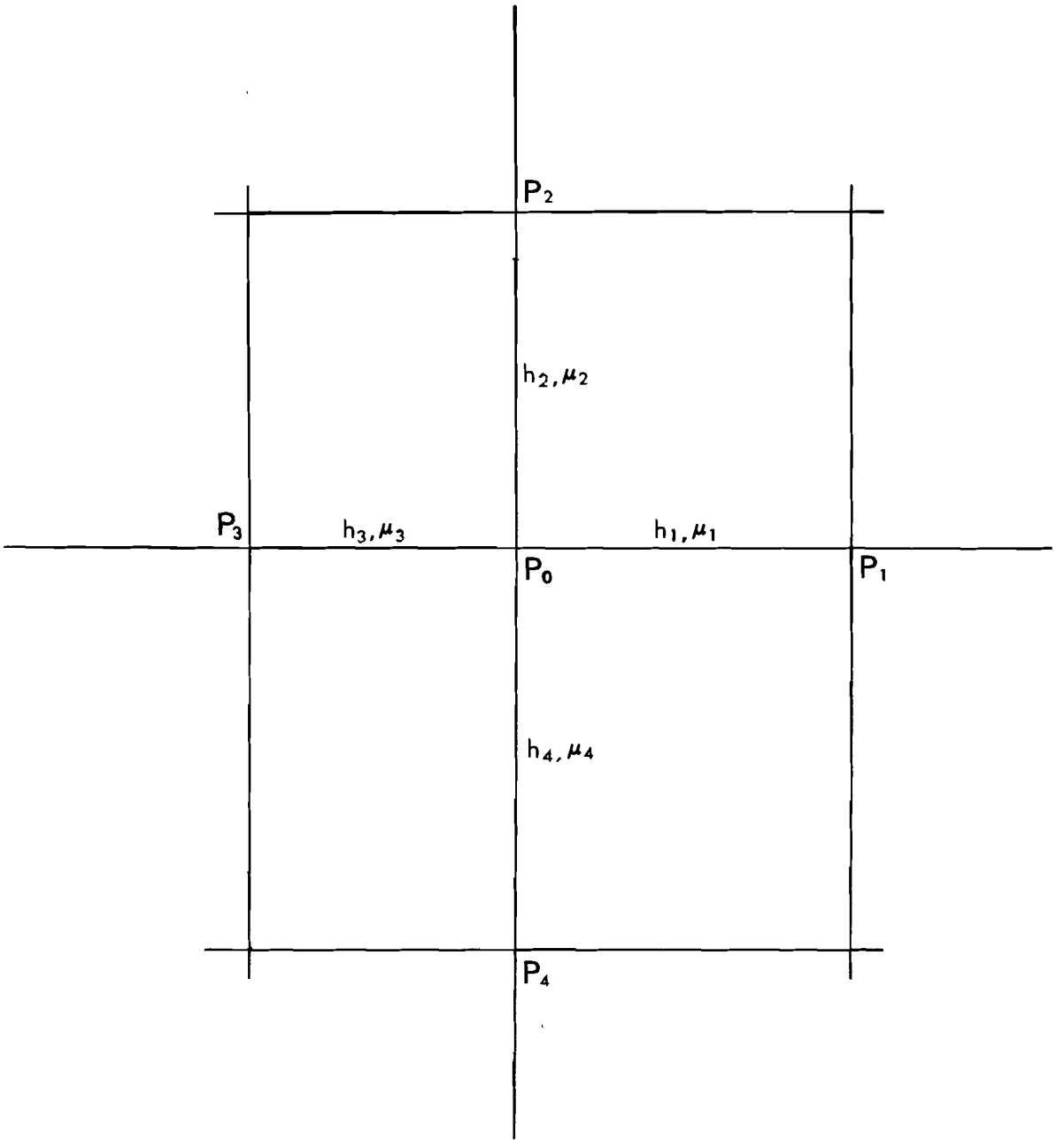


fig 2 c

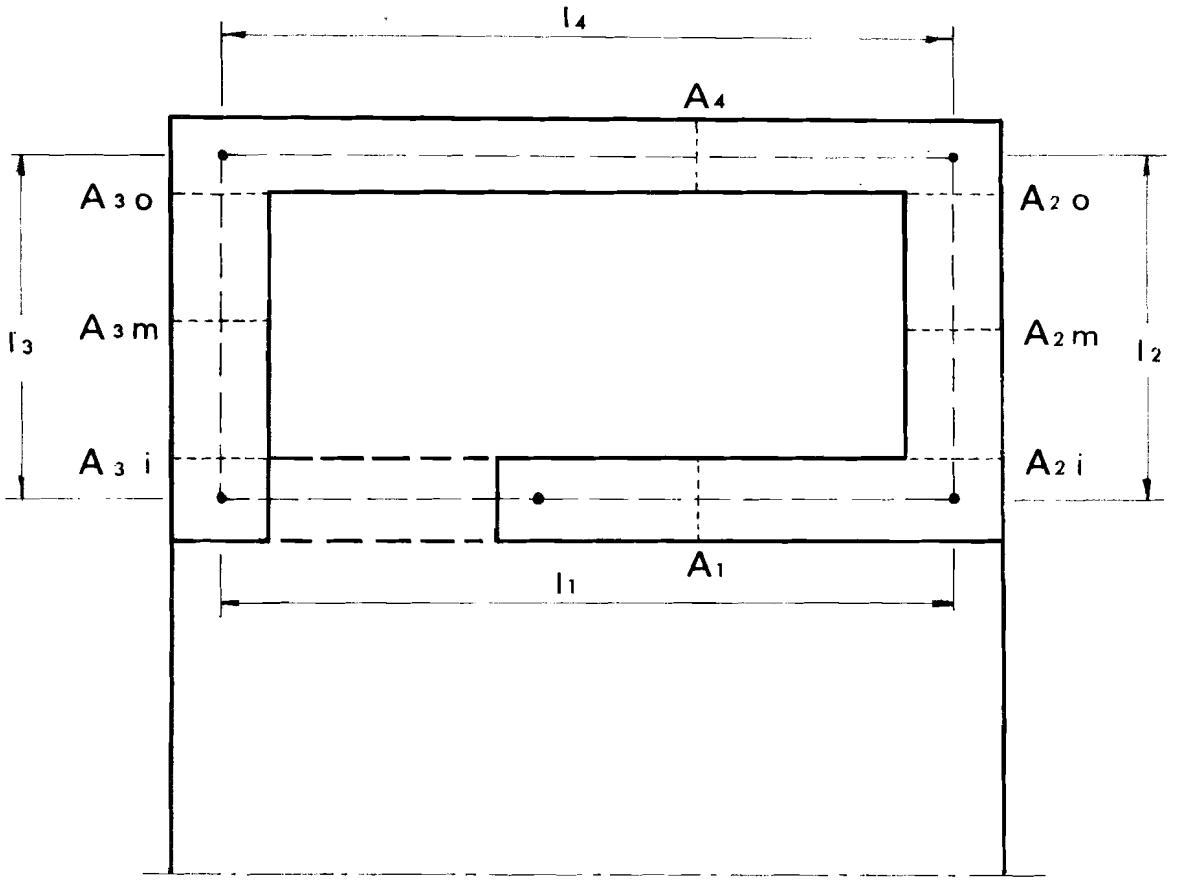


fig. D.1

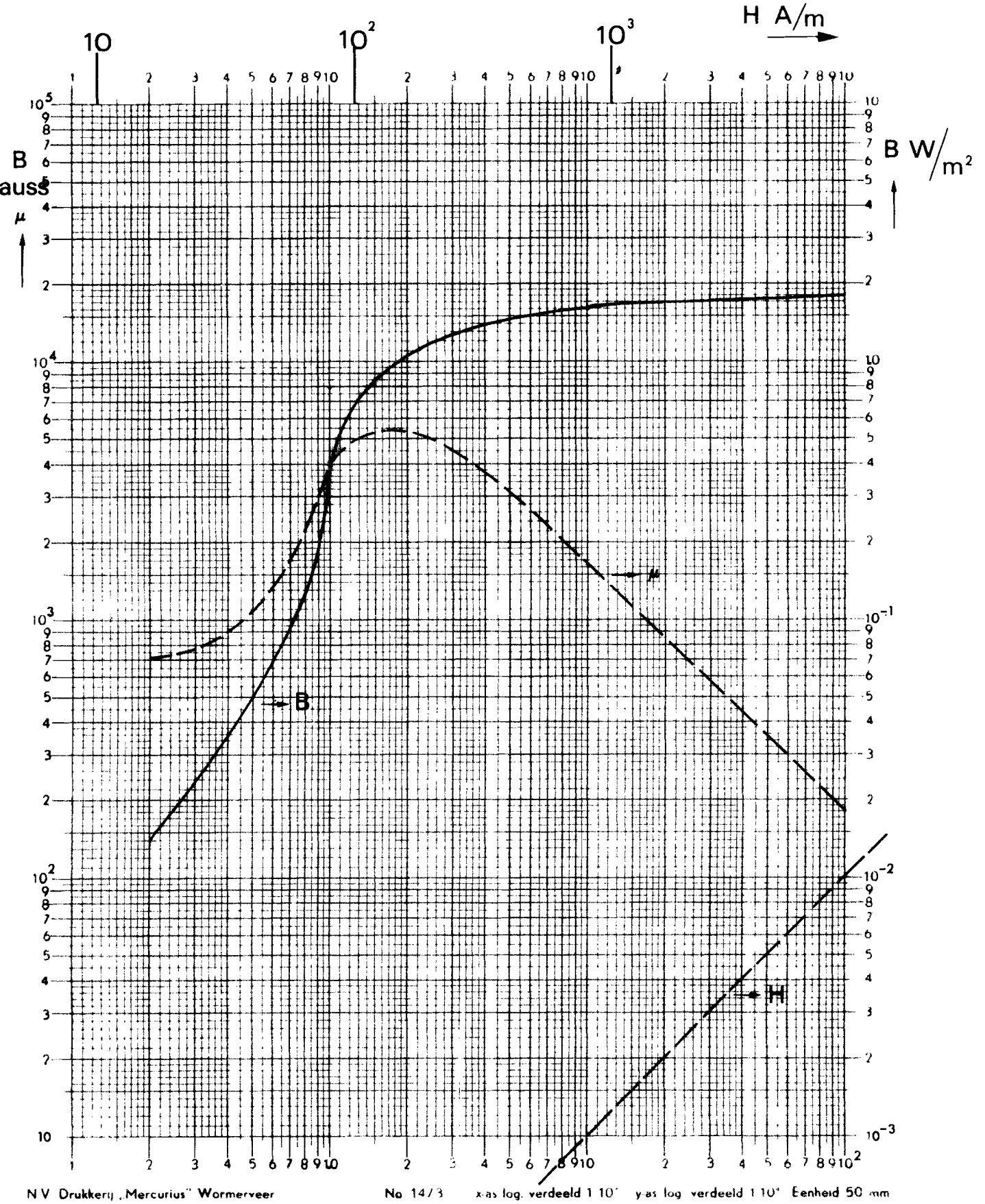


N V Drukkerij „Mercurius" Wormerveer No 14/3 x-as log. verdeeld 1 10¹ y-as log. verdeeld 1 10⁴ Eenheid 50 mm

fig D 2